Transformation Behavior in Near-Equiatomic Ti-Pd Shape Memory Alloys

(等原子比近傍のTi-Pd形状記憶合金の相変態)

March 2002

Virgil Constantin SOLOMON

Graduate School of Science and Technology
KUMAMOTO UNIVERSITY

Summary

Ti-Pd alloys are well known as high-temperature shape memory material since they undergo a B2 to B19 thermoelastic martensitic transformation around 800 K upon cooling. It is known that for understanding the transformations that take place in a material under the changing conditions of temperature, composition and pressure, a clear phase diagram is important. A well-established phase diagram is also essential in practical application of the shape memory alloys where a small changing of the composition can lead to a large variation of transformation temperatures. However, for Ti-Pd alloys, the present available knowledge seems to be not enough for a complete understanding of the equilibrium phase diagram especially in the near-equiatomic region that are the most important for practical applications of these materials as high temperature shape memory alloys. Moreover, in near-equatomic Ti-rich Ti-Pd alloys the full understanding of the mechanism of martensitic transformation is still under development. In the present thesis transformation behavior, phase equilibrium and connected phenomena in near-equiatomic Ti-Pd alloys was discussed based on Differential Scanning Calorimetry (DSC) measurements and Transmission Electron Microscopy (TEM) observations.

In Ti-rich alloys martensitic transformation was found to take place in two successive steps, while in Pd-rich alloy martensitic transformation occurs in only one step as indicated by the pairs of endothermic-exothermic peaks on DSC curves of those alloys. The successive martensitic transformation behavior is closely related to the nucleation and growth of fine Ti_2Pd precipitates ($C11_b$-type structure) and its mechanism could be explained as follows. The first step represents the reverse martensitic transformation of the TiPd matrix and the second one is due to the reverse martensitic transformation in the local neighboring areas of the precipitates where Pd concentration is higher than that in matrix.

Transformation behavior is greatly affected by aging conditions. Successive transformation takes place in the Ti-47at.%Pd alloy after short time aging irrespective of aging temperature. On the other contrary, after relatively prolonged aging period only the specimen aged above 1073 K shows successive transformation. From the obtained experimental data the homogeneity range of the TiPd

compound in Ti-rich side was estimated to extends from the near-equiatomic composition of about 50.4 at.%Ti at around 873 K to about 51.8 at.%Ti at 1073 K.

Three Ti_2Pd precipitate variants with the apparent habit planes of $(101)_{B19}$, $(10\bar{1})_{B19}$ and $(010)_{B19}$ nucleated and grew in the B2 parent phase of the aged Ti-47at.%Pd alloy. On the other hand, only one or two variants were observed when precipitates nucleated in martensitic state. Since the difference between the lattice spacing $(010)_{B19}$ and $(001)/3_{C11b}$ is about 20%, the nucleation of the third variant in martensite matrix is energetically unfavorable.

The influence of long aging time (3600 ks) in martensitic state on the precipitate variant selection in the case of undeformed and deformed specimens was also studied. The morphology and the habit plane of the precipitates were found to be different from those of the precipitates observed in solution treated specimens. However, in the case the deformed specimens the martensite was found to have a 4H structure, which is different from the 2H structure of martensite in quenched Ti-Pd alloy. The reverse transformation temperatures in deformed specimens were found to increase with tensile strain.

The morphology of B19 martensite in near-equiatomic Ti-rich Ti-Pd alloys drastically changes with the precipitates size and density. The main factor affecting martensite morphology seems to be the precipitate density. Due to the high density of precipitates the martensite must accommodate in a small volume by the formation of very narrow twins.

Table of Contents

Symbols and Abbreviations

Symbol	Unit	Definition
a, b, c	nm	Lattice parameters
A*	K	Reverse transformation peak temperature upon heating
A_f	K	Reverse transformation finish temperature upon heating
A_s	K	Reverse transformation start temperature upon heating
B2		Crystallographic notation for parent phase
B19		Crystallographic notation for martensitic phase
$C11_b$		Crystallographic notation for Ti_2Pd phase
c', c_{11}, c_{12}		Shear modulus
C_p	J/gK	Specific heat capacity
$d_{(hkl)}$	nm	Interplanar spacing
(hkl)		Miller's indices for crystallographic planes
$\Delta_f H$	J/g atom	Enthalpy of formation
K_f		Calibration factor
K_1		Twinning plane, or the first undistorted plane
K_2		The second undistorted plane
M*	K	Martensite peak temperature upon cooling
M_f	K	Martensite finish temperature upon cooling
M_s	K	Martensite start temperature upon cooling
M_s/T_m		Reduced martensitic transformation temperature
s		Twinning shear
t	ks	Time
T_m	K	Melting point
ΔT		Differential temperature
x	nm	Twin width
ε	%	Tensile strain
ε_{SME}	%	Strain recovered by shape memory effect

η_1		Twinning shear direction
η_2		Intersection of the plane of shear with K_2
Φ	mJ/s or mW	Heat flux
Φ_m		Measured heat flow rate
σ	MPa	Tensile stress

Abbreviation	**Definition**
at.%	Atomic percentage
BCC	Body-Centered Cubic
BF	Bright Field (image)
CPH	Closed-Packed Hexagonal
DF	Dark Field (image)
DSC	Differential Scanning Calorimetry
EDP	Electron Diffraction Pattern
FCC	Face-Centered Cubic
FCT	Face-Centered Tetragonal
HRTEM	High Resolution Transmission Electron Microscopy
HTSMA	High Temperature Shape Memory Alloy
IC	Incommensurate Phase
LIS	Lattice Invariant Shear
M	Matrix
MT	Matrensitic Transformation
RLB	Rubber-Like Behavior
SAEDP	Selected Area Electron Diffraction Pattern
SC-SRO	Symmetry-Conforming Short Range Order Principle
SMA	Shape Memory Alloy
SME	Shape Memory Effect
T	Twin
TEM	Transmission Electron Microscopy

Chapter 1

General Background of the Present Research

The achievement of advanced materials is an essential condition for continuous technological development in the world. Nowadays, the tendency in development of materials is not only to improve, generally speaking, classical mechanical properties (structural properties), but also to create materials with new intrinsic functions that allow a specific behavior in a given situation (functional properties). By definition, structural materials are those materials that are mainly characterized by their mechanical strength and are generally employed in load-bearing situations. Structural characteristics may include all mechanical and corrosion properties. Those materials whose principal functional characteristics are exploited rather than the structural properties of the material are denoted as functional materials. Functional characteristics may include piezoelectricity, photoconductivity, photoelectricity, pyroelectricity, shape memory and viscoelasticity properties[1]. Examples of functional materials are permanent magnets, superconductors, high permeability materials and shape memory materials[2].

The technological progress imply the discovering and using of advanced materials that allows the design of simple, miniaturized, self-regulating mechanical systems that posses previously unthinkable characteristics. These materials must combine both functional characteristics and good structural properties. Shape memory alloys (SMA's) are such a category of advanced materials. The term of shape memory alloys designate a group of metallic materials that once deformed show the ability to return to original shape when subjected to appropriate thermal processes. The deformation may be of any kind such as tension, compression or bending etc. This behavior is known as one-way shape memory effect (SME), as shown in Fig. 1.1. At a relatively low temperature a ring made

of SMA can be plastically deformed. Upon heating at a higher temperature the ring will return to the initial shape before to the deformation. The material "memorized" its original shape and thus exhibits a "shape memory" function.

The origin of shape memory effect on metallic materials is based on the possibility of a martensitic (or displacive) transformation (MT) to be reversible. The martensitic transformation is a difusionless phase transformation in solids, in which atoms move cooperatively, and often by a shear-like mechanism[3, 4]. From the thermodynamic point of view MT's are classified into two categories, thermoelastic and non-thermoelastic[5-7]. As a rule, SME occurs in the alloys that exhibit thermoelastic martensitic transformation. However, in some ferrous SMA's such as Fe-Ni-C and Fe-Mn-Si-(Cr) the origin of SME is associated with the non-thermoelastic martensitic transformation[8]. At a microscopic scale the SME requires a crystallographic reversible movement of martensite variant and twin boundary in the deformed material, without any contribution from normal slip.

The history of SME start in 1951 when Chang and Read[9] observed the reversibility of the transformation in a bent bar of the Au-47.5at.%Cd alloy. Later, the behavior was also observed in other alloys such as In-Tl[10, 11], Cu-Zn[12] and Cu-Al-Ni[13]. However, the bloom in researching field of the SMA's is considered to begin in 1962 when Buehler *et al.*[14] discovered the SME in equiatomic Ti-Ni alloy. So far, the Ti-Ni alloys are most important SMA's for practical applications and therefore they are most actively investigated. The importance of Ti-Ni alloys lie in their ability to experience large, reproducible shape recovery at temperatures closed to the room temperature. Since then many other SMA's have been discovered as for example Au-Cu-Zn[15], Cu-Sn[16-18], Ti-Ni-Cu, Cu-Au-Zn, In-Cd, Mn-Cd, Fe-based alloys etc.[8, 19]

Among the above-mentioned SMA's several have been used to develop different commercial products in various areas such as: (1) mechanical engineering, (2) electronic engineering, (3) safety technology, (4) sensors, actuators and ventilating engineering, (5) domestic

appliance industry, (6) aircraft and space exploration industry, (7) automobile industry, (8) composite materials, (9) medical applications and (10) arts, toys and gadgets[20]. Typical SMA's applications are couplings and fasteners, actuators and robots, air conditioners, damping devices, orthopedic and scoliosis correction devices and SMA reinforced composites[21-31].

Current commercial SMA's have the transformation temperatures below 473 K[32]. However, if SMA's with martensitic transformation temperatures above 573 K are developed, it will became possible that applications of these materials to be much widened such as in automobiles engines, rocket engines, air planes turbines, fire protection, safety control of high temperature chemical reactions, nuclear reactor environments etc. There are few metallic materials that might be used as high temperature shape memory alloys (HTSMA's): Cu-Al-Ni-Mn[33, 34], Ni-Al (Fe, Mn)[35-38], Ti-Ni (Zr, Hf)[39-41], Zr-Cu (Ni, Co)[42, 43], Ni-Mn (Ti, Al)[44], Nb-Ru, Ta-Ru[32, 45, 46] and Ti-noble metals (Au, Pt, Pd)[35, 47-49] alloys. Among them Ti-Pd alloy system is expected to be a hopeful candidate for HTSMA's. Crystal structures, transformation temperatures and shape memory characteristics of the presently known HTSMA's are introduced in the Appendix.

For understanding of the transformations that take place in the material structure under the changing conditions of temperature, composition and pressure, a clear phase diagram is important. A well-established phase diagram is also essential in practical application of SMA's where a small changing of the composition can lead to a large variation of transformation temperatures. For Ti-Pd alloys, the present available knowledge seems to be not enough for a complete understanding of the equilibrium phase diagram especially in the near-equiatomic region that are the most important for Ti-Pd HTSMA's[55-57]. Moreover, in near-equatomic Ti-rich Ti-Pd alloys the full understanding of the mechanism of MT is still under development. In the present thesis transformation behavior and phase equilibrium in near-equiatomic Ti-Pd alloys are discussed. This work is presented as follows:

Chapter 2 gives a survey of the fundamental aspects and recent progress in the knowledge of the Ti-Pd alloys: phase diagram, crystallographic aspects of the martensitic transformation, shape memory effect, ternary Ti-Pd-X alloys and applications of Ti-Pd alloys. On these bases, the objectives of the present thesis will be introduced and explained.

Chapter 3 discusses the experimental procedures, including materials, specimen preparation, transformation analysis and microstructure observations.

Chapter 4 presents the martensitic transformation behavior of the near-equiatomic Ti-Pd alloys.

Chapter 5 discusses the mechanism of successive transformation in the near-equiatomic Ti-rich Ti-Pd shape memory alloys.

In Chapter 6 the effect of aging on successive martensitic transformation in near-equiatomic Ti-rich Ti-Pd shape memory alloys is detailed discussed.

Chapter 7 discusses the morphologic and crystallographic aspects of Ti_2Pd (C11b-type structure) precipitates nucleated in martensitic and parent phase matrices in aged Ti-Rich Ti-Pd alloys, including precipitate variants selection and their influence on martensite morphology.

General conclusions drawn from the present work are given in Chapter 8.

References

1. M.V. Gandhi and B.S. Thompson: *Smart Materials and Structures*, Chapman & Hall, London, 1992.
2. G. Sauthoff: *Intermetallics*, VCH Verlagsgesellschaft, Weinheim, 1995.
3. Z. Nishiyama: *Martensitic Transformation*, ed. M. Fine, M. Meshii and C. M. Wayman, Academic Press, New York, San Francisco, London (1978).
4. K. Otsuka and C. M. Wayman: *Shape Memory Materials*, ed. K. Otsuka and C. M. Wayman, Cambridge University Press, 1998, 1.
5. G. V. Kurdjumov and L. G. Khandros: *Dokl. Nauk SSSR*, **66** (1949) 211.
6. H. Kessler and W. Pitsch: *Acta Metall.*, **15** (1967) 401.
7. K. Otsuka and K. Shimidzu: *Scr. Metall.*, **4** (1970) 467.
8. T. Maki: *Shape Memory Materials*, ed. K. Otsuka and C. M. Wayman, Cambridge University Press, 1998, 117.
9. L. C. Chang and T. A. Read: *Trans. AIME*, **189** (1951) 47.
10. M. W. Burkart and T. A. Read: *Trans. AIME*, **197** (1953) 1516.
11. Z. S. Basinski and J. W. Christian: *Acta Metall.*, **2** (1954) 101.
12. E. Hornbogen and G. Wasserman: *Z. Metallkd.*, **47** (1954) 427.
13. C. W. Chen: *J. Metals*, (Oct., 1957) 1202.
14. W. J. Buehler, J. W. Gilfrich and R. C. Wiley: *J. Appl. Phys.*, **34** (1963) 1475.
15. S. Miura, S. Maeda and N. Nakanishi: *Philos. Mag.*, **30** (1974) 565.
16. S. Miura, Y. Morita and N. Nakanishi: *Shape Memory Effect in Alloys*, Plenum Press, New York (1976) 389.
17. H. Kato and S. Miura: *Acta Metall. Mater.*, **43** (1995) 351.
18. H. Kato, N. Hirata and S. Miura: *Acta Metall. Mater.*, **43** (1995) 361.

19. K. Otsuka and C. M. Wayman: *Shape Memory Materials,* ed. K. Otsuka and C. M. Wayman, Cambridge University Press, 1998, 27.
20. J. van Humbeeck: *Shape-memory Materials and Phenomena-Fundamental Aspects and Applications,* ed. C.T. Liu *et al.,* MRS, Pittsburgh **246** (1992) 377.
21. K. N. Melton: *Shape Memory Materials,* ed. K. Otsuka and C. M. Wayman, Cambridge University Press, 1998, 220.
22. I. Ohkata and Y. Suzuki: *Shape Memory Materials,* ed. K. Otsuka and C. M. Wayman, Cambridge University Press, 1998, 240.
23. S. Miyazaky: *Shape Memory Materials,* ed. K. Otsuka and C. M. Wayman, Cambridge University Press, 1998, 267.
24. K. Otsuka and K. Shimizu: *Int. Met. Reviews,* **31** (1986) 93.
25. L. McD. Schetky: *Shape Memory Materials, Proc. Int. Symp. on Shape Memory Materials, Kanazawa, Japan, 1999,* ed. T. Saburi, Trans Tech Publications, 2000, 9.
26. M. Asai and Y. Suzuki: *Shape Memory Materials, Proc. Int. Symp. on Shape Memory Materials, Kanazawa, Japan, 1999,* ed. T. Saburi, Trans Tech Publications, 2000, 17.
27. Y. Adachi, S. Unjoh and M. Kondoh: *Shape Memory Materials, Proc. Int. Symp. on Shape Memory Materials, Kanazawa, Japan, 1999,* ed. T. Saburi, Trans Tech Publications, 2000, 31.
28. M.T. Yeh, H.P. Kao and S.E. Hsu: *Proc. of the Inter. Sym. on Shape Memory Materials,* ed. Y. Chu and H. Tu, International Scholar Press, Beijing, 1994, 561.
29. Y. Chu, K. Dai, M. Zhu and X. Mi: *Shape Memory Materials, Proc. Int. Symp. on Shape Memory Materials, Kanazawa, Japan, 1999,* ed. T. Saburi, Trans Tech Publications, 2000, 55.
30. G. Jun and C.T. Sun,: *J. Mater. Sci.*, **30** (1995) 5750.
31. P. Filip, J. Musialek, K. Michalek, M. Yen and K. Mazanek, *Mater. Sci. Eng. A,* **273-275** (1999) 769.
32. R. W. Fonda and H. N. Jones: *Mat. Sci. Eng A,* **273-275** (1999) 275.
33. T. Tadaki: *Shape Memory Materials,* ed. K. Otsuka and C. M. Wayman, Cambridge University Press, 1998, 97.
34. K. Sugimoto, K. Kamei and M. Nakaniwa: *Engineering Aspects of Shape Memory Alloys,* ed. T. W. Duering *et al.*, Butterworth-Heinemann, 1990, 89.
35. K. Otsuka and D. Golberg: *Intelligent Materials and Systems,* ed. P. Vicenzini, Techna Srl, 1995, 55.
36. P. L. Potapov, N. A. Poliakova and V. A. Udovenko: *Scr. Mater.,* **35** (1996) 423.
37. K. Ishida, R. Kaniuma, N. Ueno and T. Nishizawa: *Metall. Trans. A,* **22A** (1991) 441.
38. R. Kaniuma, H. Nakano, K. Oikawa, K. Ishida and T. Nishizawa: *Mat. Res. Symp. Proc.,* **246** (1992) 403.
39. J. H. Mulder, J. H. Maas and J. Beyer: *Proc. ICOMAT-92, Monterey,* 1992, 869.
40. K. N. Wu, Z. Pu, H. Tseng and F. Biancaniello: *Proc. Shape Memory and Superelastic Technologies,* ed. A. Pelton, D. Hodgson, and T. Duerig, 1994, 61.
41. A. V. Shelyakov, A. A. Gulyaev, P. L. Potapov, E. L. Svistunova, N. M. Mateeva, D. Hodgson and J. Cederstrom: *Proc. Shape Memory and Superelastic Technologies,* ed. A. Pelton, D. Hodgson, S. Russell, and T. Duerig, 1997, 89.
42. Y. N. Koval, G. S. Firstov, J. van Humbeeck, L. Delaey and W. Y. Yang: *J. Phys. IV,* **5** (1995) C8-1103.
43. G. S. Firstov, Y. N. Koval and J. van Humbeeck: *J. Phys. IV,* 7 (1997) C5-549.
44. P. L. Potapov, N. A. Poliakova, V. A. Udovenko and E. L. Svistunova: *Z. Metallk.,* **87** (1997) 33.
45. R. W. Fonda and R. A. Vandermeer: *Philos. Mag. A.,* **76** (1997) 119.
46. R. W. Fonda, H. N. Jones and R. A. Vandermeer: *Scr. Mater.,* **39** (1998) 1031.
47. K. Otsuka and X. Ren: *Intermetallics,* 7 (1999) 511.
48. H. C. Donkersloot and J. H. N. Van Vucht: J. Less-Common Met. **20** (1970) 83.
49. H. C. Yi and J. J. Moore: *Materials Science Forum,* Trans Tech Publications, **56-58** (1990) 735.
50. J. L. Smialek and R. F. Hchemann: *Met. Trans.,* 4 (1973) 1571.
51. R. Kaniuma, H. Nakano and K. Ishida: *Metall. Mater. Trans. A,* **27A** (1996) 4153.
52. P. G. Lindquist and C. M. Wayman: *Engineering Aspects of Shape Memory Alloys,* ed. T. W. Duering *et al.*, Butterworth-Heinemann, 1990, 58.
53. K. Enami, Y. Kitano and K. Horii: *Proc. MRS International Meeting on Advanced Materials,* **9** (1989) 117.
54. K. Enami, K. Morota, M. Hisa and K. Inoue: *Shape Memory Materials, Proc. Int. Symp. on Shape Memory Materials, Kanazawa, Japan, 1999,* ed. T. Saburi, Trans Tech Publications, 2000, 287.
55. *Phase Diagram of Binary Titanium Alloys*, ed. J. L. Murray, ASM International, 1987, 239.
56. Y. Shugo and T. Honma: *Bulletin of the Research Institute of Mineral Dressing and Metallurgy, Tohoku University* **43** (1987) 128.
57. *Binary Alloy Phase Diagrams,* ed. T. B. Massalski, ASM Int., Metals Park, OH, 1990, 181.

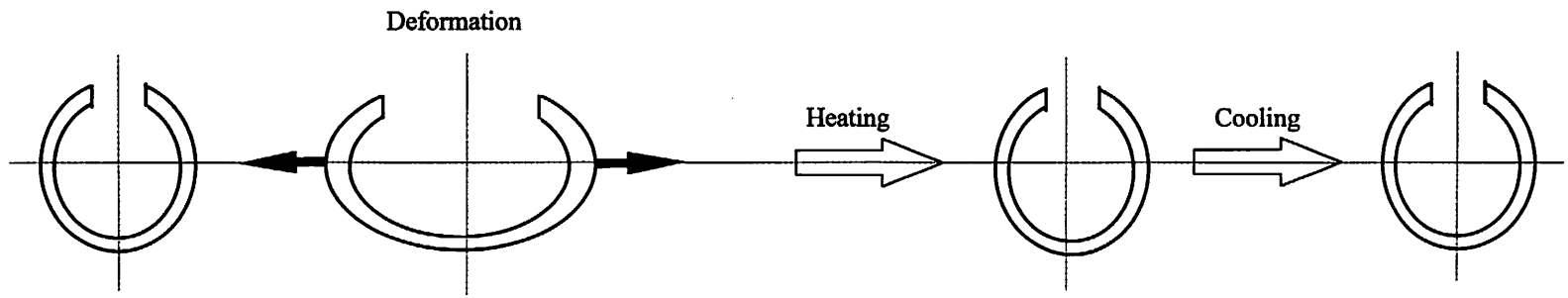

Fig. 1.1 Schematic illustration of the one-way shape memory effect.

Chapter 2

Ti-Pd Alloys

2.1 Equilibrium Phase Diagram of Ti-Pd Alloys System

There are many researches done in the equilibrium phase diagram of Ti-Pd alloy system[1-6]. An assessed phase diagram based on the synthesis of the results of previous investigations is shown in Fig. 2.1[7, 8]. The solid phases observed in the Ti-Pd alloys system are presented as follows:

1. (αTi) solid solution with CHP structure. This structure is the equilibrium form of α-titanium below 1155 K. The solubility of Pd in (αTi) is less than 1%.

2. (βTi) solid solution with BCC structure. This structure is the equilibrium form of β-titanium above 1155 K. The maximum solubility of Pd in (βTi) is approximately 45 at.%.

3. Ti_4Pd stoichiometric compound with A15 structure. The phase was defined as Ti_4Pd based on its stoichiometry. However, based on its ordered structure the phase must be defined as Ti_3Pd. In Fig. 2.1 Ti_4Pd is included, based on the previous mentioned references[7, 8] and a dashed line indicated the uncertainty about its stability as a binary phase.

4. Ti_2Pd stoichiometric compound with Si_2Mo-type structure and stable below 1233 K.

5. The high temperature form of TiPd compound denoted βTiPd with CsCl-type structure and the homogeneity range between 47 and 53 at.%Pd. βTiPd transforms into αTiPd at temperatures ranging between 700 and 900 K.

6. The low temperature form of TiPd compound αTiPd with AuCd-type structure.

7. The Ti_2Pd_3 stoichiometric phase which have an Au_2V-type orthorhombic structure.

8. Ti_3Pd_5 stoichiometric compound with the Si_2Mo-type structure. The equilibrium of Ti_3Pd_5 compound with neighbouring phases is not know and therefore not indicated in Fig. 2.1.

9. $TiPd_2$ phase with the Si_2Mo-type structure and a homogeneity range of 65 to 67 at.% Pd. A polymorphic transformation is possible to takes place within the $TiPd_2$ phase at about 1550 K and it is indicated by dotted line in Fig. 2.1.

10. $TiPd_3$ stoichiometric compound with $TiNi_3$-type structure.

11. (Pd) solid solution with FCC structure. The maximum solubility of Ti in this phase is about 22 at.%.

12. The existence of another stoichiometric compound $TiPd_4(\gamma)$ with Cu_3Au-type structure was postulated by some authors[2]. However, other reports indicate that alloys containing less than 85 at.% Pd exhibited long- range order while those containing less than 95 at.% Pd exhibited short-range order[9, 10]. Moreover, magnetic and hardness measurements supported the hypothesis of the absence of two-phase alloys. In Fig. 2.1 the dot-dash line represents the composition beyond the ordering was observed in (Pd) region.

The special points of Ti-Pd phase diagram are presented in Table 2.1.

In order to clarify the correlation between Ti_4Pd phase stoichiometry and its structure Jankowscki[11] prepared Ti-Pd alloys containing 20 – 30 at.%Pd by vapor phase deposition. From phase transformations and lattice parameters observations it was suggested that Ti_3Pd exist within a compositional domain ranging from 23 to 28 at.%Pd. The phase has the Cr_3Si structure and forms peritectoidally at a temperature between 723 and 823 K

Shugo and Honma[12] studied the phase boundary of TiPd phase using DSC and X-ray measurements. They found that TiPd phase exists at non-stoichiometric compositions only at Ti-rich side. The TiPd phase boundary at Pd-rich side is 50at.%Pd independent of temperature below 1180 K, whereas at Ti-rich side it is 49at.%Pd at 973 K and gradually decreases its Pd content down to 47.8at.%Pd at 1073 K. The same result was found by Nishida *et al.*[13]. These results as well as

that obtained by Jankowscki[11] are superimposed on the assessed phase diagram with dashed blue lines, as shown in Fig. 2.1.

Several attempts were made to calculate Ti-Pd alloys phase diagram from thermodynamic data. Kaufman and Bernstein[14] have done the first attempt, based on their estimations of the enthalpies and Gibbs energies of formation of many Ti-Pd intermetallic compounds. For example, they found the enthalpy of the formation of TiPd compound to be $\Delta_f H$ = -32 kJ/g atom at 298 K. A nearly identical enthalpy of formation, $\Delta_f H$ = -29 kJ/g atom, was calculated by Murray[15]. The phase diagram calculated with these values, although succeed in reproducing the liquidus and solidus of the solution phases, contains many features that are very implausible from the standpoint of thermodynamic modeling. On the other hand, Choudary[16] using mass-spectrometric investigations and Topor and Kleppa[17] using mixing calorimetry measurements, determined the energy of formation of TiPd compound at 298 K to be –80 and –51.6 kJ/g atom, respectively. These observations show that both thermodynamic data and some aspects of phase diagram calculations must be reevaluated before a reasonable calculation can be performed.

From the above review it becomes clear that Ti-Pd alloys system phase diagram is not yet well determined and there are many aspects that are waiting to be clarified by further research.

2.2 Crystallography of Martensitic Transformation and Shape Memory Effect in Ti-Pd Alloys

The MT in the Ti-Pd alloys was first reported by Donkersloot and Van Vucht[18]. Using high temperature X-ray diffraction they proved that the alloys near the equiatomic composition transform during cooling from an ordered B2-type parent phase (βTiPd) into B19-type martensitic phase (αTiPd). Since the transformation temperatures are around 800 K and the martensitic transformation proceeds thermoelasticaly, these alloys are considered as being promising materials for HTSMA's. Following this first report many other studies have been done in the martensitic transformation of the Ti-Pd alloys. Using DSC measurements Shugo and Honma[12] observed only one endothermic

and exothermic peak during heating and cooling, respectively. On the contrary, Nishida *et al.*[13] have been observed an unusual successive transformation behavior in near-equiatomic Ti-rich Ti-Pd alloys. These authors interpreted this behavior as being related with the formation of a new intermediate phase between B19 martensite and B2 parent phase but they could not identified the supposed new phases by electron diffraction experiments and image observations. Therefore, in near-equiatomic Ti-Pd alloys the occurrence of martensitic transformation in one or successive steps is still under discussion.

The crystallographic characteristics of βTiPd parent phase (or high temperature phase) and αTiPd martensitic phase are presented in Table 2. 2. The βTiPd phase has a BCC structure of CsCl-type. The crystal structure of parent phase is shown in Fig. 2.2(a). The αTiPd martensitic phase has a B19 orthorhombic structure, which was also reported in AuCd, TiPt, MgCd, TiAu[18, 19] and TiNi-Cu[20] martensites.

However, until now detailed studies of the microscopic mechanism of B2 to B19 transition was made only for Au-Cd and Ti-Ni-Cu alloys by utilizing various techniques[21 - 26], such as electrical resistivity, electron microscopy, X-ray and neutron diffraction, neutron diffuse scattering (phonon-dispersion relation), elastic constants measurements by resonance method etc. Ren and Otsuka[24] proposed a basal-plane picture to explain the microscopic mechanism of the matrensitic transformation that seems to be valid in most cases. The microscopic transformation mechanism is invariably based on the lattice instability due to the softening of the $\{1\bar{1}0\}\langle\bar{1}\,\bar{1}0\rangle_{B2}$ shear modulus $c' = (c_{11} - c_{12})/2$ of the BCC high temperature phase. Thus, the martensitic transformations are generally regarded to be triggered by a softening of elastic constant c' and TA_2 phonons, which correspond to $\{1\bar{1}0\}\langle\bar{1}\,\bar{1}0\rangle_{B2}$ shearing and shuffling of the $\{1\bar{1}0\}_{B2}$ close packed planes in the cubic parent phase. As a result, the close packed planes become the basal planes of the stacking order structure of martensite. Based on this mechanism the lattice changes during B2 to B19 transformation (schematic drawn in Fig. 2.2 (b) and (c)) can be described as follows. The B19 structure is produce by straining of the B2 structure along $[\bar{1}10]_{B2}$, $[001]_{B2}$ and $[110]_{B2}$ directions

plus a $(1\bar{1}0)[\bar{1}\bar{1}0]_{B2}$ shuffling. This shuffle can be also described as a traverse $\{1\bar{1}0\}<\bar{1}\bar{1}0>_{B2}$ wave (or shear wave) with a $[1\bar{1}0]_{B2}$ wave vector of $2d_{(1\text{-}10)B2}$ wavelength[22, 27].

In the Ti-Pd alloys martensite the stacking mode of the atomic close-packed planes was reported to be of 2H-type (Ramsdel notations) or $(1\bar{1})$-type (Zdanov symbols)[29]. The structural change from B2 parent phase into 2H martensite with long period stacking order structure is shown in Fig. 2.2(d) – (g). By forming of the long period stacking order structures it seems that the entropy term in the Gibbs free energy becomes negligible at low temperatures and the decrease of internal energy become more important[30, 31].

The lattice parameters in Table 2.2 were determined for TiPd phase with stoichiometric composition. In a study about phase boundary of TiPd phase, Shugo and Honma[12] determined the effect of annealing temperature on lattice parameters of the αTiPd phase over the whole non-stoichiometric composition of TiPd phase. The results are presented in Fig. 2.3(a), where 1073 K and 1173 K represent the annealing temperatures. Based on room temperature X-ray diffraction and density measurements the same authors concluded that the defect structure of αTiPd martensitic phase is of the substitutional type for entire compositional range of TiPd phase, as could be understood from Fig. 2.3(b).

The crystallography of twins in Ti-Pd alloy martensite was detailed studied by Nishida and coworkers[32 – 35] by means of TEM and high-resolution transmission electron microscopy (HRTEM) observations. They found in the B19 (2H) martensite of Ti-50at.%Pd alloy three twining modes, as follows: {111} Type I, <121> Type II and {101} compound twins. The crystallographic data of twins are listed in Table 2.3. The twining elements were calculated by Bilby-Crocker theory[36]. Five twinning elements, the K_1 plane, the K_2 plane, the η_1 direction, the η_2 direction, and a twinning shear s characterize deformation twinning[36]. The twinning elements are defined as follows[38 – 40]:

K_1 = the twinning plane, or the first undistorted plane;

K_2 = the second undistorted plane;

η_1 = the twinning shear direction;

η_2 = the direction defined by the intersection of the plane of shear with K_2;

s = twinning shear.

Considering the distortion of the original lattice by shearing process, deformation twinning may be classified into two groups: Type I and Type II twinning. Type I twinning is characterized by rational K_1 and η_2, and irrational K_2 and η_1. The two twin crystals are related by the mirror symmetry with respect to the K_1 plane. Type II twinning is characterized by rational K_2 and η_1, and irrational K_1 and η_2. In this case, the two twin crystals are related by 180^0 rotation around η_1. All the indices of the four elements are rational in the compound twinning.

In the Ti-50at.%Pd alloys the {111} Type I and <121> Type II twinning are conjugate to each other and coexist in the same martensite variant. The {111} Type I twinning was dominantly observed and therefore it was considered to be a lattice invariant shear (LIS). The <121> Type II twin plate appear in two forms. The first one was directly connected to the Type I plate, but inclined at crystallographically definite angle in comparison with this. The second one branched off from the Type I plate. Since no martensite variant consisting wholly of the <121> Type II twins was observed in the structure, these twins were considered to be deformation twins due to the elastic interaction during transformation. The {101} compound twins were sporadic observed in the martensite variant consisting of {111} Type I twins and therefore, these twins were also considered to be introduced as the result of elastic interactions during the transformation.

The twin boundary on atomic scale in near-equiatomic Ti-rich Ti-Pd alloys was studied by using HRTEM[34, 35]. For these observations the edge-on state is required[41]. For Type I twins the edge-on state is achieved when the incident electron beam is parallel with the K_1 plane. The obtained diffraction pattern consists of two sets of reflections that are in the mirror symmetry of each other with respect to the K_1 plane. For Type II twins the edge-on state imply that incident electron beam to be parallel with η_1 direction. The obtained diffraction pattern shows only one set of reflections.

After solution treatment at 1273 K, in the quenched Ti-49.5 and 50at.%Pd alloys the boundary of {111} Type I twin is straight and has mirror symmetry with respect to the K_1 plane. The boundary of {101} compound twin is also straight and the two twin crystals have mirror symmetry with respect to the (101) K_1 plane, although a broad strain contrast was observed in places. The strain contrast may be induced as an elastic interaction during the transformation. The irrational boundary of <121> Type II twin is gradually and randomly curved with broad strain contrast and has neither ledge nor step structure, as reported for <011> Type II twin boundary in Ti-Ni martensite[42]. This fact suggests that a strain around Type II boundary in the B19 martensite of Ti-Pd alloy is elastically relaxed by gradual displacement of the atoms instead of ledge and step structures, the same as in the B19' martensite of Ti-Ni alloy[43]. On the other hand, ledge and step structures were frequently observed at the boundary in the slowly cooled Ti-49.5at.%Pd alloy after the solution treatment. However, there was no <121> Type II twin boundary consisting wholly of the ledge and step structures and therefore, it was concluded that the essential feature of the irrational boundary is gradually and randomly curved with broad strain contrast along the K_1 plane.

So far, SME in binary Ti-Pd alloys was reported only for the equiatomic composition. Lindquist and Wayman[44] studied the shape recovery in a Ti-50at.%Pd alloy deformed at room temperature. The experiments were carried out on bending and tensile test specimens. For all the tested specimens the one way SME was observed. Shugo[45] also reported SME in bending tested specimens at room temperature. The same result as obtained by Yi and Moore[6, 46] who prepared Ti-50at.%Pd alloy specimens from Ti and Pd elemental powders by using combustion synthesis methods. They pointed out that no difficulties were encountered during hot rolling of Ti-Pd alloys. E. Quandt *et al.*[28] reported the two-way SME in TiPd thin-films prepared by magnetron sputter deposition onto unheated substrates, followed by annealing and training processes, but they did not gave any concrete data about shape recovery in those thin-films.

Since Ti-Pd alloys are suggest to be used as HTSMA's it is very important to know the shape recovery of the high temperature deformed specimens. The stress-strain curves of a Ti-50at.%Pd alloy tensile test at various temperatures are presented in Fig. 2.4[47]. With dashed line it is indicated the recovered strains upon heating to parent phase, due to SME. When the tensile test is carried out at room temperature about 60 % of strain recovery is obtained, as seen in Fig. 2.4 (299 K). No substantial SME was obtained with increasing of the tensile temperature. The poor SME was explained based on a significant decreasing of the critical stress for slip deformation with increasing temperature. At high temperature, the slip deformation occurs simultaneously with the reorientation of martensite variants and/or detwinning and, thereby, shape memory properties deteriorate. Several key factors for improving high temperature shape memory characteristics of Ti-Pd binary alloys were proposed, one of them being increase the critical stress for slip by third-element alloying addition.

2.3 Ti-Pd-Based Ternary Alloys

Otsuka *et al.*[47] pointed out that high transformation martensitic temperatures do not automatically guarantee good shape memory characteristics in Ti-Pd alloys since that at high temperature the slip deformation occurs simultaneously with the reorientation of martensite variants and/or detwinning and thereby, shape memory properties deteriorate. As a key factor for improving the shape memory characteristics of Ti-Pd binary alloys they proposed addition of a ternary element.

There are many researches focusing on the substitution of ternary element for Pd in equiatomic Ti-Pd alloy. According to those works, it was found that the changing of Pd concentration by increasing the content of the alloying element, lowers M_s temperature from about 800 K to liquid nitrogen temperature or below,. Enami *et al.*[29, 48–50] studied the effect of the substitution of Fe, Cr, V and Co for Pd on the transformation behavior of Ti-Pd alloys. For Ti-Pd-X (X = Fe, Cr, V) alloys it was reported the appearance of shape memory effect. In Ti-Pd-Fe and Ti-

Pd-Cr alloys, depending on Fe or Cr content, beside the twinned B19 (2H) martensite, another martensite with 9R structure and an intermediate (incommensurate) phase appear. Schwartz and Tanner[51] observed two displacive transformations in Ti-Pd-Cr alloys using Cr as substitute for Pd and a higher substitution percentage than those used by Enami *et al.*. At a low Cr content, B2 → B19 (a close packed phase) transformation was reported, while at Cr content higher than about 8 at.%, B2 → IC (incommensurate phase with a non-close-packed structure) transformation was observed. Enami *et al.*[52] also reported the influences of substitution of V for Ti on MT of Ti-Pd alloys.

Extensive works have been done on the effect of Ni addition on the Ti-Pd alloys. The M_s temperature can be varied from the room temperature to about 800 K by controlling the alloy composition. Thus, Ti-Pd-Ni alloys are promising candidates for high temperature SMA. However, in these alloys, the same as in Ti-Pd ones, the high transformation temperatures do not guarantee good shape memory characteristics[53-55]. For the improving of the high temperature shape memory characteristics in Ti-Pd-Ni alloys one or a combination of the following three methods were used[56]:

i) thermomechanical treatment;

ii) precipitation hardening;

iii) addition of quaternary element.

i) The thermomechanical treatments consisting of cold plastic deformation followed by annealing are generally used to obtain favorable microstructures, and consequently desired properties by "combined reactions"[57]. Combined reactions can be composed from up to three different solid state reactions: phase transformation, recrystallization (healing out defects) and precipitation (local change in chemical composition). The effect of thermomechanical treatment on MT and SME of Ti-Pd-Ni alloys was reported by Lo and Wu[58] and Golberg *et al.*[59–61], respectively. The last authors found that the annealing at 673 K for 3.6 ks after cold working was very effective for the alloys with Ni content less then 30 at.%, as shown in Fig. 2.5. The recovery

rate by SME has maximum value up to 5.5 % total strain, for thermomechanical treated specimens, but only up to 2 % total for solution-treated specimens. Figure 2.6 shows the stress-strain curves of the solution-treated and thermomechanical treated specimens tensile tested at constant total strain (5 %). The dashed arrows indicate the strains recovered on heating above A_s after unloading (the shape memory strain). The appearance of superelastic behavior is observed in thermomechanically treated specimen tested at 535 K.

It is worthy to note that thermomechanical treatments have been also successfully applied to improve mechanical properties and shape memory characteristics of Ti-Ni binary alloys[62, 63]. However, to the best of our knowledge, until now there is no report on the effect of thermomechanical treatments on martensitic transformation and shape memory properties of the Ti-Pd binary alloys.

ii) The precipitation hardening method was applied to improve the shape memory characteristics of Ti-Pd-Ni alloys with Ti content slightly different from stoichiometric composition (Ti:(Pd, Ni) $\neq$ 50:50). Shimizu *et al.*[64] reported that the shape memory characteristics were improved substantially by aging $Ti_{50.6}Pd_{30}Ni_{19.4}$ alloy at 773 K for 3.6 ks. The recovery rate at high temperature was about 10% higher than that of $Ti_{50}Pd_{30}Ni_{20}$ alloy. The improvement of shape memory characteristics was explained by hardening effect due to the homogeneously distributed fine precipitates produced by aging at 773 K. Two-way shape memory effect during the thermal cycling between room temperature and 523 K was reported in $Ti_{48}Pd_{31}Ni_{21}$ alloy aged under constrained conditions at 673 K[65]. This behavior was related to the phase decomposition: fine precipitates appearing during aging process may produce an internal stress field to control the growth of martensite phase.

iii) The addition of quaternary element method was used in conjunction with precipitation hardening one. Thus, Suzuki *et al.*[66] investigated the effect of small addition of boron on the mechanical properties and high-temperature shape memory characteristics of $Ti_{50}Pd_{30}Ni_{20}$ alloy. The microstructure analysis showed that TiB_2 precipitates with an average size larger than 1 μm

were produced in the alloy structure by the homogenization treatment at 1273 K for 18 ks. The precipitates were too big for precipitation hardening and, although the high temperature ductility of the alloy had been improved, there was no noticeable influence on high-temperature shape memory characteristics.

2.4 Effect of Martensite Aging and Thermal Cycling on Transformation Behavior of Ti-Pd Alloys

Another interesting phenomenon that affects the high-temperature shape memory behavior of Ti-Pd is martensite aging effect alloys and therefore, should be taken into account in developing these materials[67, 68]. The term "martensitic aging effect" involves two time-dependent phenomena that occurred during aging in martensitic phase. One it is called martensite stabilization and refers to the phenomenon that martensite appears to be more stable with respect to the parent phase during aging. The effect of martensite stabilization is increasing of the reverse transformation temperatures. The other it is called rubber-like behavior (RLB) and refers to the phenomenon that martensite exhibits a recoverable or pseudo-elastic deformation behavior after aging together with an increase in critical stress. Over the past decades, in order to explain the origin of martensite aging effect several models were proposed, as follows: pseudotwin-type models, long-range ordering models, short-range ordering models and domain (twin) boundary pinning models[67]. Recently, new attempts on modeling martensite aging effect have been done by Giampaoli *et al.*[69], Ren and Otsuka[70] and Marukawa *et al.*[71]. The general model proposed by Ren and Otsuka, based on symmetry-conforming short-range order principle (SC-SRO), appears to be able to explain all of the available experimental observations on the aging effect[72, 73]. According to this principle, the two necessary conditions for martensite aging phenomenon are the existence of point defects and the possibility of diffusion in the martensite. Metallic alloys, generally satisfy the first condition, but the second one depends on the reduced martensitic transformation temperature M_s/T_m, where M_s

and T_m are the martensitic transformation temperatures and melting point of an alloy, respectively. In order to show a strong martensite aging effect, an alloy must have M_s/T_m ratio about 0.23 – 0.5.

In the Ti-50at.%Pd alloy the M_s/T_m ratio is about 0.49 and therefore, according to the SC-SRO model, the alloy may show strong martensite aging effect. Cai and Otsuka[74, 75] examined the martensite aging effect in Ti-Pd equiatomic alloy and reported that aging effect of this alloy exhibits a unique feature, which is not found in other SMA's. This is, after aging at 833 K (in the martensitic state) for various time, the reverse martensitic transformation temperatures A_s and A_f increase in two stage, without saturation, with aging time. The pronounced increase of A_s and A_f temperatures in the first stage (aging time shorter than 57.6 ks) was explained by symmetry-conforming short-range order (SC-SRO) mechanism. In the second stage (aging time longer than 57.6 ks) the martensite recovery-recrystallization process was found to be responsible for slightly increase of A_s and A_f temperatures.

Thermal cycling can also greatly affect martensitic transformation temperatures and therefore, the SME's. Miyazaki *et al.*[76] reported the decrease of transformation temperatures in the thermally cycled Ti-Ni alloys. Lots of dislocations were induced in the specimen structure during the thermal cycling and the changing of transformation temperatures was attributed to the stress field around dislocations. Lots of dislocations were also induced in the Ti-50at.%Pd alloy after thermal cycling[77, 78]. However, in spite of the increase of volume fraction of {101} compound twinning and the dislocation density, no obvious change in transformation temperatures was observed upon thermal cycling. This is possible due to the high transformation temperatures of the Ti-Pd alloys (about 800 K) when either (1) the stress field around dislocations is relaxed[77] or (2) the dislocation may disappear easily after their formation[78]. However, it is clear that further investigations are necessary for understanding this behavior.

It is worthy to note that until now there is no report about martensitic aging effect and thermal cycling effect on transformation behavior of near-equiatomic Ti-Pd alloys.

2.5 Recovery and Recrystallization Process in Equiatomic Ti-Pd Alloy

An interesting phenomenon in the αTiPd martensite of Ti-Pd alloy with equiatomic composition was reported by Xu *et al.*[79]. They found that the αTiPd martensite recrystallizes by aging at a proper temperature without introducing prior deformation. After solution treatment at 1173 K a quenched Ti-50at.%Pd alloy was annealed in martensitic state at 823 K for various periods. The reverse transformation start temperature A_s = 845.3 K of the solution-treated specimens was determined by DSC. From the electron microscopy observations it was concluded that since no stress was applied, the recrystallization process have been carried out by atomic diffusion at high temperatures, rather than the movement of twin boundaries by shear. Therefore, the recrystallization proceeds by nucleation and growth processes. Twinned crystals within certain martensite plates behave as nuclei for recrystallization, and they grow into neighboring plates with a non-crystallographic interface. The recrystallized grains have the same B19 martensite structure of TiPd intermetalic compound. However, the recrystalized martensite is strain-free, without the LIS characteristic of the martensitic transformation. Since it affects the high temperature shape memory characteristics, by removing the LIS, this phenomenon should be considered for further developing of Ti-Pd HTSMA's.

The same authors also demonstrated the recrystallization process in the martensitic state for a cold-rolled Ti-50at.%Pd alloy by using TEM observation and hardness measurements of annealed specimens[80]. Both, the mechanism of the recrystallization process and the crystallographic and morphologic characteristics of recrystallized martensite are the same as described above. However, in this case two types of twins were sporadically observed within the recrystallized regions: {111} Type I and {101} compound. The former twinning mode is the same as the LIS upon martensitic transformation. Perhaps, these twins were introduced after the annealing process by the deformation twinning upon quenching.

2.6 Applications of Ti-Pd Alloys

Ti-Pd alloys are used in several areas of applications where the structural and functional characteristics of these metals justify their selection. The main structural characteristics for which Ti-Pd alloys are used in practical applications are corrosion resistance and biocompatibility.

The corrosion resistance of titanium in sulphuric acid is greatly improved by alloying with palladium that produces a shift in the open-circuit potential to the passive range[81]. The Ti-Pd alloys with less than 1 % palladium are used in chemical processing and storage applications, where the media is mildly reducing or fluctuates between oxidizing and reducing[82]. A typical application of Ti-Pd alloys in a corrosive environment is the electron transparent window used in the treatment of SO_2 and NO_x gases emitted by fossil fuel combustion in the electric power plants[83, 84].

Titanium, like the palladium, has good corrosion resistance in a simulated physiological solution and it is biocompatible[85]. The corrosion resistance can be further improved by alloying with palladium, which makes hydrogen evolution easier at cathodic sites so that the anodic and cathodic reactions balance in the passive region[86]. The Ti-Pd alloys with Pd content between 10 and 30 at.% Pd were reported to be used for dental applications[87, 88].

E. Quandt *et al.*[28] reported the two-way SME in the Ti-Pd thin-films prepared by magnetron sputtering technique onto unheated substrates, followed by annealing and training processes. These materials are particularly important for the advanced development of new or improved micro-actuators.

Morizono *et al.*[89, 90] showed that the Ti-Pd HTSMA's can be used as stress relaxation layers for joining Si_3N_4 to carbon steel. No crack was observed in the Si_3N_4 after joining process, and the joint showed improved mechanical strength and fatigue life.

Amorphous and nonequilibrium crystalline Ti-Pd alloys produced by mechanical alloying and vapor quenching methods were also reported by few authors[91-93].

2.7 Objectives

From the above literature survey it becomes clear that still there are several unsolved problems concerning near-equiatomic Ti-Pd alloys:

1) The equilibrium phase diagram in near-equiatomic region, which is very important for Ti-Pd shape memory alloys applications, it is still under discussion and more experimental and theoretical work is necessary in order to clarify it.
2) There are divergent reports about martensitic transformation behavior in near-equiatomic Ti-rich Ti-Pd alloys: do martensitic transformation proceed in one or successive steps?

For a better understanding of the Ti-Pd high temperature shape memory alloys the followings objectives are discussed in the present thesis:

1) Clarifying the martensitic transformation behavior in near-equiatomic Ti-rich Ti-Pd alloys: martensitic transformation takes place or not in successive steps.
2) The answer of the previous question is positive: in near-equiatomic Ti-rich Ti-Pd alloys martensitic transformation takes place in successive steps. Therefore, another task of this thesis is to clarify the mechanism of successive transformation.
3) Since the mechanism of successive transformation is connected with the nucleation and growth of Ti_2Pd precipitates, which are controlled by diffusion process, both aging temperature and time will greatly affect the transformation behavior. Therefore, we will investigate the effect of aging on successive martensitic transformation in near-equiatomic Ti-Pd alloys. From here, the homogeneity range of TiPd intermetallic compound will be determined.
4) The number of Ti_2Pd precipitates depends on the nucleation site (martensitic phase or parent phase). The morphological and crystallographic aspects of Ti_2Pd precipitates nucleated in martensitic and parent matrices in aged Ti-rich Ti-Pd alloys will be discussed, including precipitate variants selection and their influence on martensite morphology.

Based on these investigations the potential of the Ti-Pd high temperature shape memory alloys for different practical applications can be significantly increased.

References

1. H. W. Rosenberg and D. B. Hunter: *Trans. AIME,* **233** (1965) 681.
2. E. Raub and E. Roeschel: *Z. Metallkd.,* **59** (1968) 112.
3. V. N. Eremenko and T. D. Shtepa: *Porosh. Metall.,* **111** (1972) 75 (in Russian); tr. *Sov. Powder Metall.,* (1972) 228.
4. P. Lamparter, T. Krabichler and S. Steeb: *Z. Metallkd.,* **64** (1973) 720.
5. J. C. Williams, H. I. Aaronson and B. S. Hickman: *Metall. Trans.,* **4** (1973) 1181.
6. H. C. Yi, J. J. Moore and A. Petric: *Metall. Trans. A,* **23A** (1992) 59.
7. *Phase Diagrams of Binary Titanium Alloys,* ed. Joanne L. Murray, ASM Int., Metals Park, OH (1987) 239.
8. *Binary Alloys Phase Diagrams, 2nd ed.,* ed. T. B. Massalski *et al.,* ASM Int., Metals Park, OH (1990) 181.
9. J. Evans and I. R. Harris: *J. Less-Common Met.,* **64** (1979) 39.
10. J. Evans, I. R. Harris and P. F. Martin: *J. Less-Common Met.,* **75** (1980) 49.
11. A. F. Jankowski: *J. Alloys Compounds,* **182** (1992) 32.
12. Y. Shugo and T. Honma: J. Institute of Mineral - Dressing and Smelting, Tohoku Univ., **43** (1987) 128.
13. M. Nishida, Y. Morizono, H. Kijima, A. Ikeya, H. Iwashita and K. Hiraga: *Materials for Smart Systems II, Symposium Proceedings Volume 459,* ed. by E. P. George, R. Gotthard, K. Otsuka, Susan T. McKinstry and Marilyn Wun-Fogle, Materials Research Society (1997) 375.
14. L. Kaufman and H. Bermstein: *Computer Calculation of Phase Diagrams,* Academic Press, New York (1970).
15. J. L. Murray: *Bull. Alloy Phase Diagrams,* **3** (1982) 329.
16. U. V. Choudary, K. A. Gingerich and L. R. Cornwell: *Metall. Trans.,* **8A** (1977) 1487.
17. Letitia Topor and O. J. Kleppa: *Z. Metallkde.,* **77** (1986) 633.
18. H. C. Donkersloot and J. H. N. Van Vucht: *J. Less-Common Metals,* **20** (1970) 83.
19. A. E. Dwight, R. A. Conner, Jr. and J. W. Downey: *Acta Cryst.,* **18** (1965) 835.
20. T. H. Nam, T. Saburi and K. Shimuzu: *Mater. Trans. JIM,* **31** (1990) 959.
21. T. Ohba, Y. Emura, S. Miyazaki and K. Otsuka: *Mater. Trans. JIM,* **31** (1990) 12.
22. G. R. Barsch, T. Ohba and D. M. Hatch: *Mater. Sci. Eng. A,* **273-275** (1999) 161.
23. T. Ohba: *Materia Japan,* **41** (2002) 101.
24. X. Ren and K. Otsuka: *Scr. Mater.,* **38** (1998) 1669.
25. X. Ren, K. Taniwaki, K. Otsuka, T. Suzuki, K. Tanaka, Y. I. Chumlyakov and T. Ueki: *Philos. Mag. A,* **79** (1999) 31.
26. P. L. Potapov, A. V. Shelyakov and D. Schryvers: *Scr. Mater.,* **44** (2001) 1.
27. M. B. Cortie and F. C. Levey: *Intermetallics,* **10** (2002) 23.
28. E. Quandt, C. Halene, H. Holleck, K. Feith, M. Kohl, P. Schloßmacher, A. Skokan and K. D. Skronbanek: *Sensor and Actuators A,* **53** (1996) 434.
29. K. Enami, H. Seki and S. Nenno: *ISIJ Tetsu-to-Hagane,* **72** (1986) 563.
30. Z. Nishiyama: *Martensitic Transformation,* Academic Press, New York, San Francisco, London (1978).
31. K. Otsuka and C. M. Wayman: *Shape Memory Materials,* ed. K. Otsuka and C. M. Wayman, Cambridge University Press (1998) 1.
32. M. Nishida, T. Hara, Y. Morizono, A. Ikeya, H. Kijima and A. Chiba: *Acta Mater.,* **45** (1997) 4847.
33. M. Nishida, T. Hara, A. Chiba and K. Hiraga: *Displacive Phase Transformations and Their Applications in Materials Engineering,* ed. K. Inoue, K. Mukherjee, K. Otsuka, and H. Chen, The Minerals, Metals & Materials Sociery (1998) 257.
34. S. Ii, M. Nishida and K. Hiraga: *Proc. Int. Conf. Solid-Solid Phase Transformation '99 (JIMIC-3),* ed. M. Koiwa, K. Otsuka and T. Miyazaki, The Japan Institute of Metals (1999) 1060.
35. M. Nishida and S. Ii: *Shape Memory Materials, Proc. Int. Symp. on Shape Memory Materials, Kanazawa, Japan, 1999,* ed. T. Saburi, Trans Tech Publications, 2000, 103.
36. B. A. Bilby and A. G. Crocker: *Proc. Royal Soc.,* London, **Ser. A 288** (1965) 240.
37. J. W. Christian: *The Theory of Phase Transformation in Metals and Alloys,* 2nd ed. Pergamon Press, Oxford (1975) 49.
38. K. Otsuka: *Proc. Int. Conf. on Martensitic Transformation,* The Japan Institute of Metals (1986) 35.
39. K. Otsuka: *Materials Science Forum Vols. 56 – 58,* Trans Tech Publications, Switzerland (1990) 393.
40. J. W. Christian and S. Mahajan: *Progr. Mater. Sci.,* **39** (1995) 1.
41. K. Yamaguchi, M. Nishida, I. Itai, K. Kitamura and A. Chiba: *Mater. Trans. JIM,* **37** (1996) 210.
42. K. M. Knowles: *Phil. Mag.,* **A45** (1982) 357.
43. M. Nishida, K. Yamauchi, I. Itai, H. Ohgi and A. Chiba: *Acta Metall. Mater.,* **43** (1995) 1229.
44. P. G. Lindquist and C. M. Wayman: *Proceedings of the International Conference on Engineering Aspects of Shape Memory Alloys,* Butterworth-Heineman, London (1990) 58.
45. Y. Shugo: *Materials Science Forum Vols. 56 – 58,* Trans Tech Publications, Switzerland (1990) 631.
46. H. C. Yi and J. J. Moore: *Materials Science Forum Vols. 56 – 58,* Trans Tech Publications, Switzerland (1990) 735.
47. K. Otsuka, K. Oda, Y. Ueno, Min Piao, T. Ueki and H. Horikawa: *Scr. Metall. Mater.,* **29** (1993) 1355.

48. K. Enami, T. Yoshida and S. Nenno: *Proc. Int. Conference on Martensitic Transformation,* The Japan Institute of Metals (1986) 103.
49. K. Enami, Y. Kitano and K. Horii: Proc. MRS International Meeting on Advanced Materials, **9** (1989) 117.
50. K. Enami, K. Horii and J. Takahashi: *ISIJ International,* **29** (1989) 430.
51. A. J. Schwartz and L. E. Tanner: *Scr. Metall. Mater.,* **32** (1995) 675.
52. K. Enami, K. Morota, M. Hisa and K. Inoue: *Shape Memory Materials, Proc. Int. Symp. on Shape Memory Materials, Kanazawa, Japan, 1999,* ed. T. Saburi, Trans Tech Publications, 2000, 287.
53. K. Otsuka: *Materia Japan,* **37** (1998) 125.
54. Ya Xu, S. Shimizu, Y. Suzuki, K. Otsuka, T. Ueki and K. Mitose: *Acta Mater.,* **45** (1997) 1503.
55. Ya Xu, K. Otsuka, T. Ueki and K. Mitose: *Mat. Res. Soc. Symp. Proc.,* Material Research Society **459** (1997) 413.
56. K. Otsuka and X. Ren: *Intermetallics,* **7** (1999) 511.
57. E. Hornbogen: *Metall. Trans.,* **10A** (1979) 947.
58. Y. C. Lo and S. K. Wu: *Advanced Materials '93, V / B: Shape Memory Materials and Hydrides,* ed. K. Otsuka et al., Trans. Mat. Res. Soc. Japan **18B** (1994) 1029.
59. D. Golberg, Ya Xu, Y. Murakami, S. Morito, K. Otsuka, T. Ueki and H. Horikawa: *Scr. Metall. Mater.,* **30** (1994) 1349.
60. D. Golberg, Ya Xu, Y. Murakami, S. Morito, K. Otsuka, T. Ueki and H. Horikawa: *Intermetallics,* **3** (1995) 35.
61. D. Golberg, Ya Xu, Y. Murakami, K. Otsuka, T. Ueki and H. Horikawa: *Mater. Lett.,* **22** (1995) 241.
62. D. Treppmann, E. Hornbogen and D. Wurzel: *J. Physique IV,b Colloque C8, suppl. J. Physique III,* **5** (1995) C8-569.
63. T. Saburi: *Shape Memory Materials,* ed. K. Otsuka and C. M. Wayman, Cambridge University Press, 1998, 49.
64. S. Shimizu, Ya Xu, E. Okunishi, S. Tanaka, K. Otsuka and K. Mitose: *Mater. Lett.,* **34** (1998) 23.
65. Y. Shirakawa, Y. Morizono and M. Nishida: *Shape Memory Materials, Proc. Int. Symp. on Shape Memory Materials, Kanazawa, Japan, 1999,* ed. T. Saburi, Trans Tech Publications, 2000, 171.
66. Y. Suzuki, Ya Xu, S. Morito, K. Otsuka and K. Mitose: *Mater. Lett.,* **36** (1998) 85.
67. X. Ren and K. Otsuka: *Phase Transitions,* **69** (1999) 329.
68. T. Ito, T. Haraguchi, M. Kogachi, T. Ohba, X. Ren and K. Otsuka: *Proc. Int. Conference on Solid-Solid Phase transformations '99 (JIMIC-3),* ed. M. Koiwa, K. Otsuka and T. Miyazaki, The Japan Institute of Metals (1999) 879.
69. A. Giampaoli, J. L. Pelegrina and K. Ahlers: *Acta Mater.,* **46** (1998) 3333.
70. X. Ren and K. Otsuka: *Nature,* **389** (1997) 579.
71. K. Marukawa, S. Moteki and K. Tsuchiya: Shape Memory Materials, Proc. Int. Symp. on Shape Memory Materials, Kanazawa, Japan, 1999, ed. T. Saburi, Trans Tech Publications, 2000, 461.
72. X. Ren and K. Otsuka: *Proc. Int. Conference on Solid-Solid Phase transformations '99 (JIMIC-3),* ed. M. Koiwa, K. Otsuka and T. Miyazaki, The Japan Institute of Metals (1999) 839.
73. X. Ren and K. Otsuka: Shape Memory Materials, Proc. Int. Symp. on Shape Memory Materials, Kanazawa, Japan, 1999, ed. T. Saburi, Trans Tech Publications, 2000, 413.
74. W. Cai and K. Otsuka: *Scr. Mater.,* **41** (1999) 1311.
75. W. Cai, K. Otsuka and M. Asai: *Mat. Trans. JIM,* **40** (1999) 895.
76. S. Miyazaki, Y. Igo and K. Otsuka: *Acta Metall. Mater.,* **34** (1986) 2045.
77. S. Ii, N. Matsuzaki, Y. Morizono and M. Nishida: *Shape Memory Materials, Proc. Int. Symp. on Shape Memory Materials, Kanazawa, Japan, 1999,* ed. T. Saburi, Trans Tech Publications, 2000, 167.
78. W. Cai and K. Otsuka: *Proc. Int. Conference on Solid-Solid Phase transformations '99 (JIMIC-3),* ed. M. Koiwa, K. Otsuka and T. Miyazaki, The Japan Institute of Metals (1999) 1036.
79. Ya Xu, K. Otsuka, E. Furubayashi and K. Mitose: *Mater. Lett.,* **34** (1998) 14.
80. Ya Xu, K. Otsuka, E. Furubayashi, T. Uechi and K. Mitose: *Mater. Lett.,* **30** (1997) 189.
81. N. Tomashov, R. Altovsky: *J. Electrochem. Soc.,* **108** (1961) 113.
82. *Metals Handbook, Ninth edition,* Vol. 3, American Society for Metals, Metals Park, OH, 1986, 372.
83. S. D. Barson, P. Skeldon, G. E. Thompson, J. Piekoszewski, A. G. Chmielewscki, Z. Werner, R. Grötzschel and E. Wieser: *Corrosion Science,* **42** (2000) 1213.
84. Z. Werner, J. Piekoszewski, A. Barcz, R. Grötzschel, F. Proket, J. Stanislavski and W. Szymczyc: *Nuclear Instrum. Methods Phys. Res. B,* **175-177** (2001) 767.
85. L. Gavril, E. Ghali, M. Fishet and E. J. Knystautas: *Canadian Metallurgical Quaterly,* **38** (1999) 113.
86. P. Munn and G. K. Wolf: *Nuclear Instrum. Methods Phys. Res. B,* **7/8** (1985) 205.
87. Y. Takada, O. Okuno, H. Nakajima and T. Okabe: *J. Dent. Res.,* **76** (1997) Abstract 3111.
88. M. Yoda, T. Konno, Y. Takada, K. Iijima, J. Griggs, O. Okuno, K. Kimura and T. Okabe: *Biomaterials,* **22** (2001) 1675.
89. Y. Morizono, M. Nishida and A. Chiba: *Advanced Materials III/B: Composites, Grain Boundaries and Nanophase Materials,* **16B**, ed. M. Sakai, M. Kobayashi, T. Suga, R. Watanabe, Y. Ishida and K. Niihara, Trans. Mat. Res. Soc. Japan (1994) 1151.
90. Y. Morizono, M. Nishida and A. Chiba: *Solid → Solid Phase Transformations,* ed. W. C. Johnson, J. M. Howe, D. E. Laughlin, W. A. Soffa and P. A. Warrendale, TMS Publications (1994) 841.
91. J. R. Thompson and C. Politis: *Europhys. Lett.,* **3 (2)** (1987) 199.

92. S. Zhang, K. Sumiyama and Y. Nakamura: *Mater. Trans. JIM,* **30** (1989) 733.
93. H. Tsunoda, M. Yamada, K. Tanaka, K. Sumiyama and K. Suzuki: *Mater. Trans. JIM,* **34** (1993) 397.

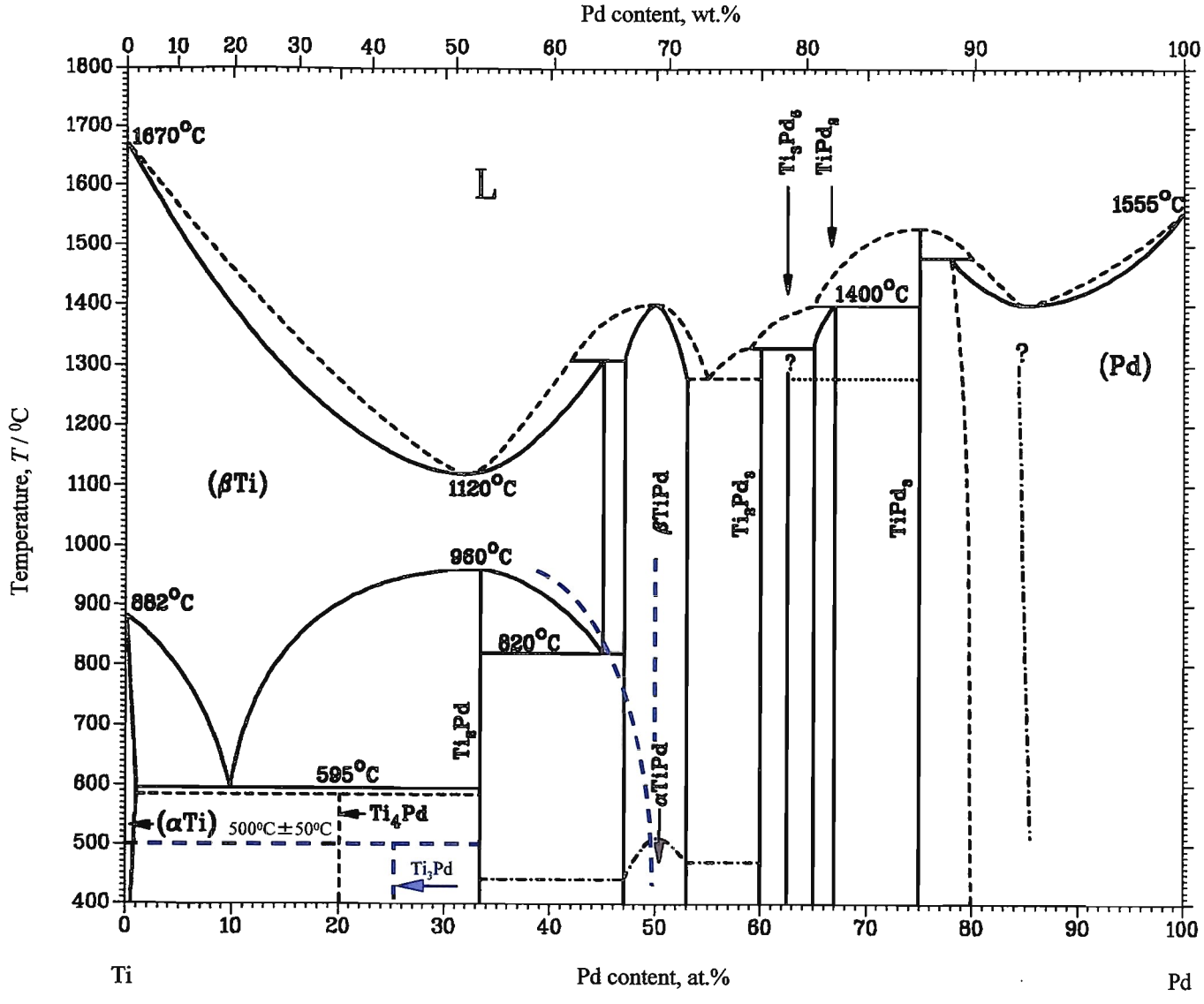

Fig. 2.1 Equilibrium phase diagram of Ti-Pd alloys system[7, 12, 13].

Table 2.1 Special points of Ti-Pd phase diagram[7, 11].

Reaction	Temperature, [K]	Compositions of the respective phases, [at.% Pd]			Reaction type
(βTi) ↔ (αTi)	1155		0		Allotropic transformation
L ↔ (βTi)	1943		0		Melting point
L ↔ (Pd)	1828		100		Melting point
L ↔ (βTi)	1393		32		Congruent
L ↔ βTiPd	1673		50		Congruent
L ↔ $TiPd_3$	1803		75		Congruent
L ↔ (Pd)	1673		~ 85		Congruent
(βTi) ↔ Ti_2Pd	1233		33.3		Congruent
L ↔ αTiPd + Ti_2Pd_3	1553	~ 58	~ 53	60	Eutectic
L + αTiPd ↔ (βTi)	1583	~ 42	~ 47	~ 45	Peritectic
L + $TiPd_2$ ↔ Ti_2Pd_3	1603	~ 59	65	60	Peritectic
L + $TiPd_3$ ↔ $TiPd_2$	1673	~ 65	75	67	Peritectic
$TiPd_3$ + L ↔ (Pd)	1753	75	80	~ 78	Peritectic
(βTi) ↔ (αTi) + Ti_2Pd	868	9.8	< 1	33.3	Eutectoid
(βTi) ↔ Ti_2Pd + αTiPd	1093	~ 45	33.3	~ 47	Eutectoid
(αTi) + Ti_2Pd ↔ Ti_4Pd	~ 823 to 858	1	33.3	20	Peritectoid
Update reaction					
(αTi) + Ti_2Pd ↔ Ti_3Pd	773 ± 50	< 1	33.3	25	Peritectoid

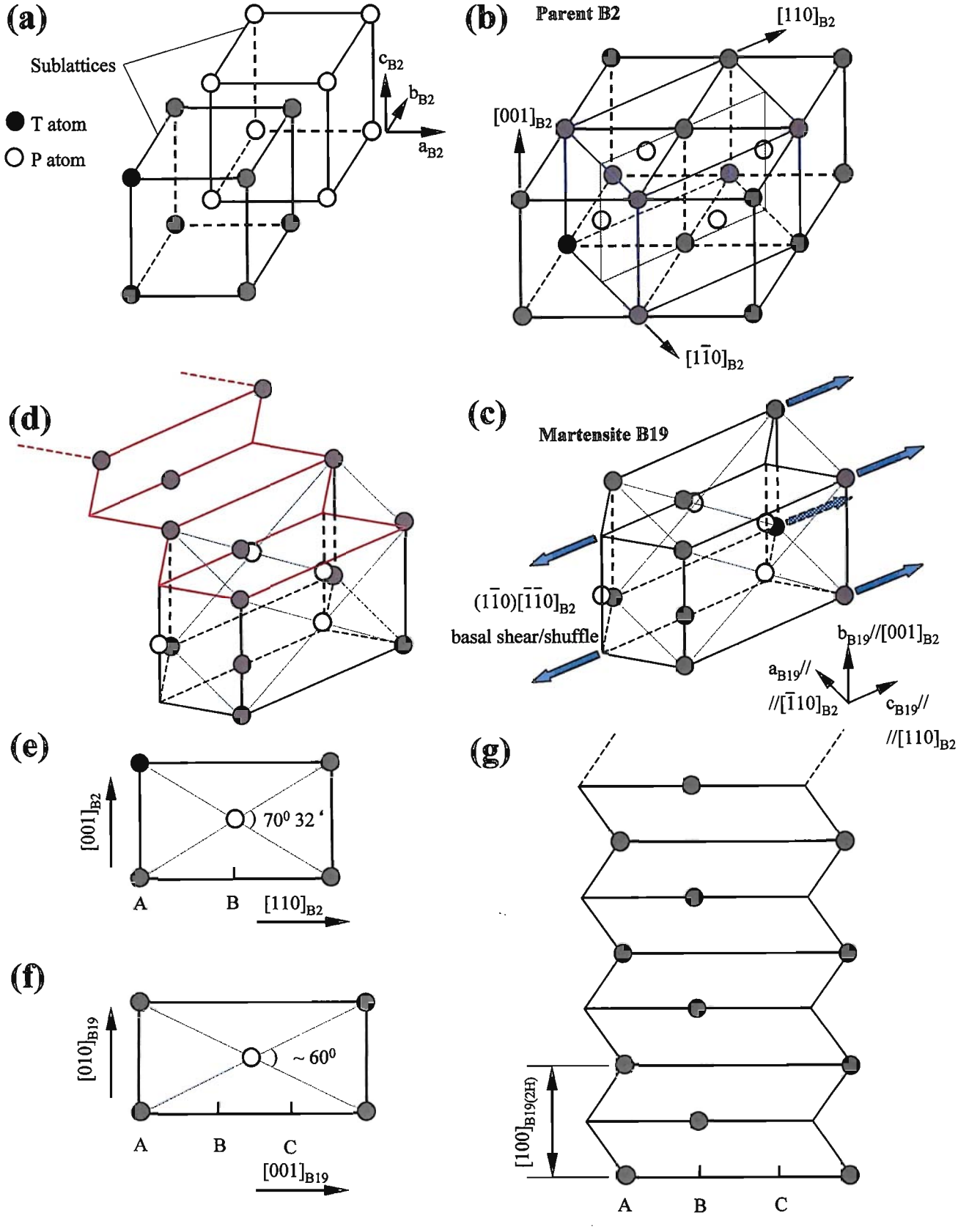

Fig. 2.2 Schematic representation of the formation of B19 martensite from B2 parent phase. (a) The B2 (CsCl) structure. (b) The parent phase B2 cells with a FCT cell inserted and the basal plane indicated with thin dash-lines. (c) B19 orthorhombic martensite formed by shear/shuffle of the basal plane $(1\bar{1}0)_{B2}$ along $[\bar{1}\bar{1}0]_{B2}$ direction. (d) - (g) The structural change from B2 parent phase into B19(2H) martensite with long period stacking structure.

Table 2.2 Crystallographic characteristics of βTiPd and αTiPd phases.

Phase	Strukturbericht designation	Crystal structure	Space group	Prototype	Temp., [K]	Lattice parameters, [nm]			Method	Reference
						a	b	c		
βTiPd	B2	BCC	$Pm\bar{3}m$	CsCl	973	0.3180			High temperature X-ray diffraction	Donkersloot and Van Vucht[18]
					293	0.3196			X-ray diffraction on thin-film	E. Quandt et al.[28]
αTiPd	B19	Orthorhombic	*Pmma*	MgCd, AuCd	293	0.456 ± 0.001	0.281 ± 0.001	0.489 ± 0.001		Dwight et al.[19]
						0.455	0.282	0.487	X-ray diffraction	Raub and Röschel[2]
						0.455	0.278	0.486		Donkersloot and Van Vucht[18]
						0.458	0.279	0.484		Eremenko and Sthepa[3]
						0.4594	0.2789	0.4893	X-ray diffraction on thin-film	E. Quandt et al.[28]

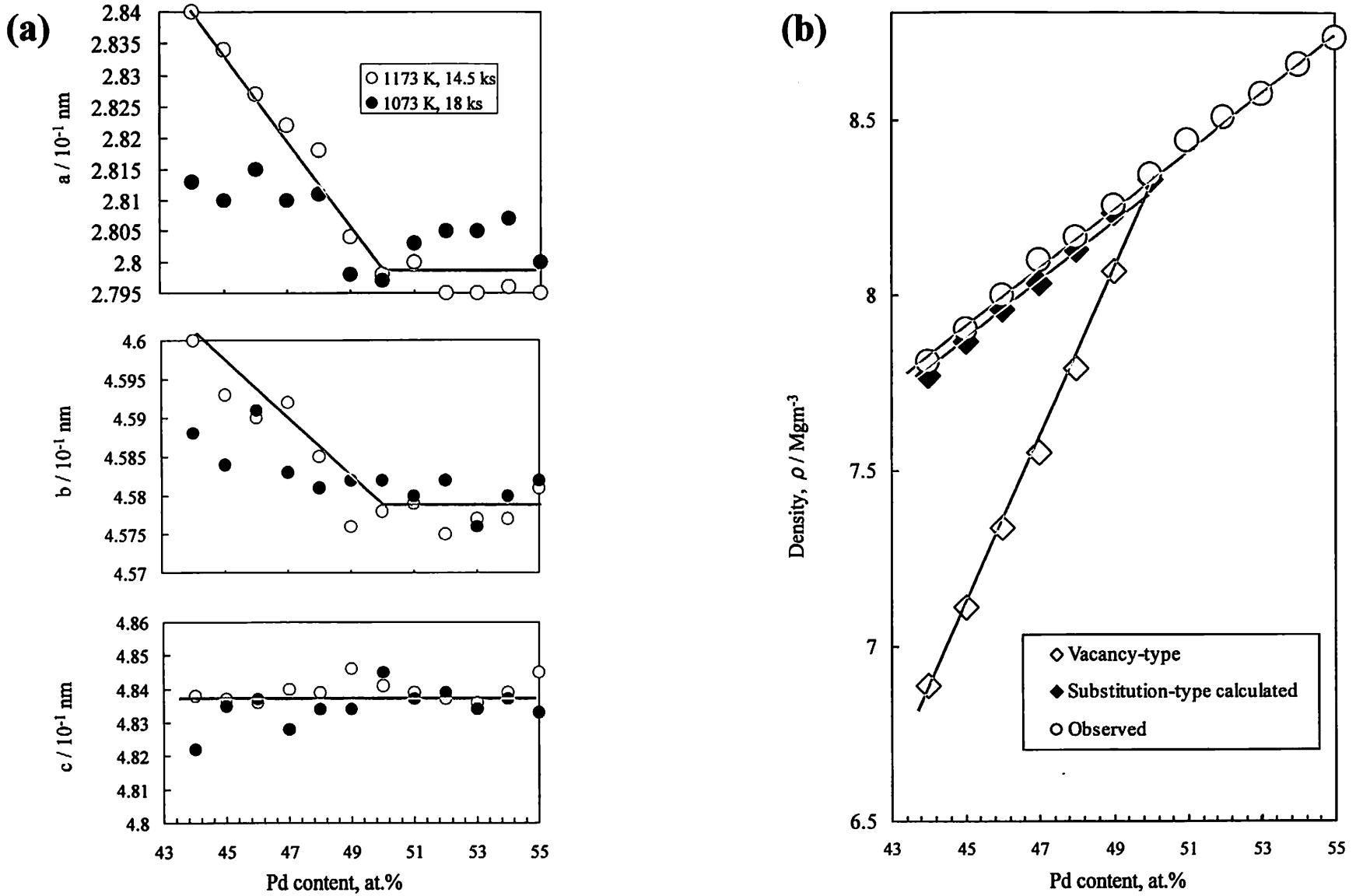

Fig. 2.3 (a) Effect of annealing temperature on the lattice parameters of the TiPd phase measured at 293 K. (b) Density dependence on Pd content in near-equiatomic Ti-Pd alloys. The measured densities are compared with calculated ones for substitution-type and vacancy-type defect structures.

Table 2.3 Twinning elements in B19 martensite of the Ti-Pd alloys[32-34].

Twinning mode	K_1	η_1	K_2	η_2	s
{111} Type I	(111)	$\overline{[0.671\ 1\ 0.329]}$	(1 $\overline{0.678}$ 0.356)	[121]	0.361
<121> Type II	(1 $\overline{0.678}$ 0.356)	[121]	(111)	$\overline{[0.671\ 1\ 0.329]}$	0.361
{101} Compound	(101)	[101]	$(10\bar{1})$	[101]	0.140

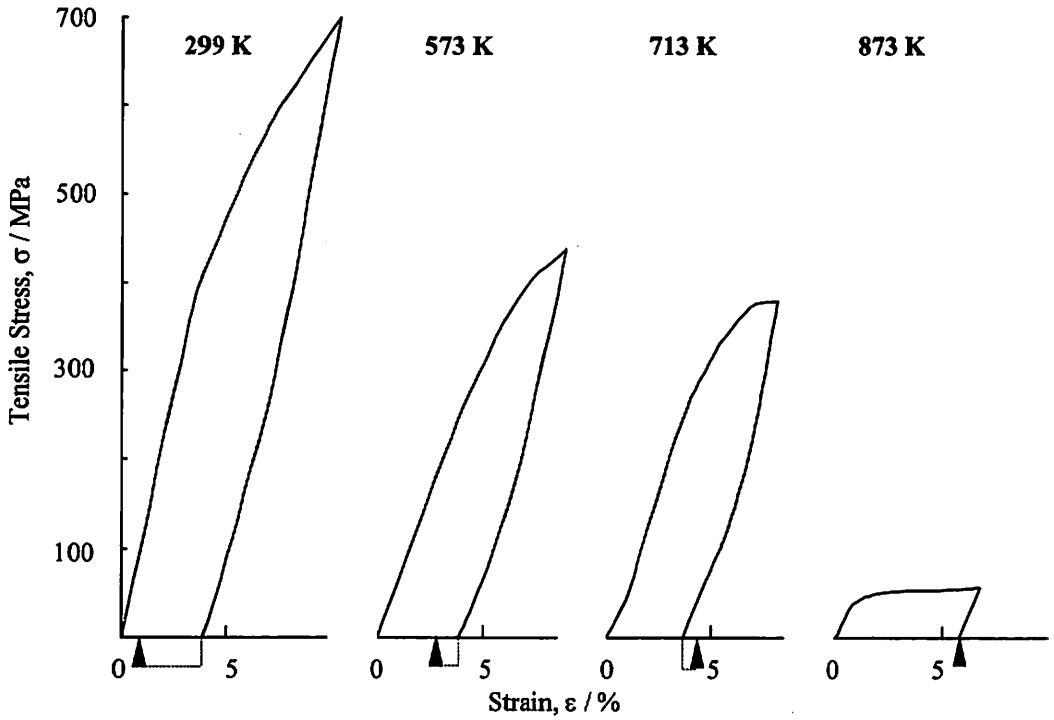

Fig. 2.4 Stress-strain curves of a Ti-50at.%Pd alloy, tensile tested at the indicated temperatures. Dotted lines with arrows indicate the strain recovered upon heating to 923 K.

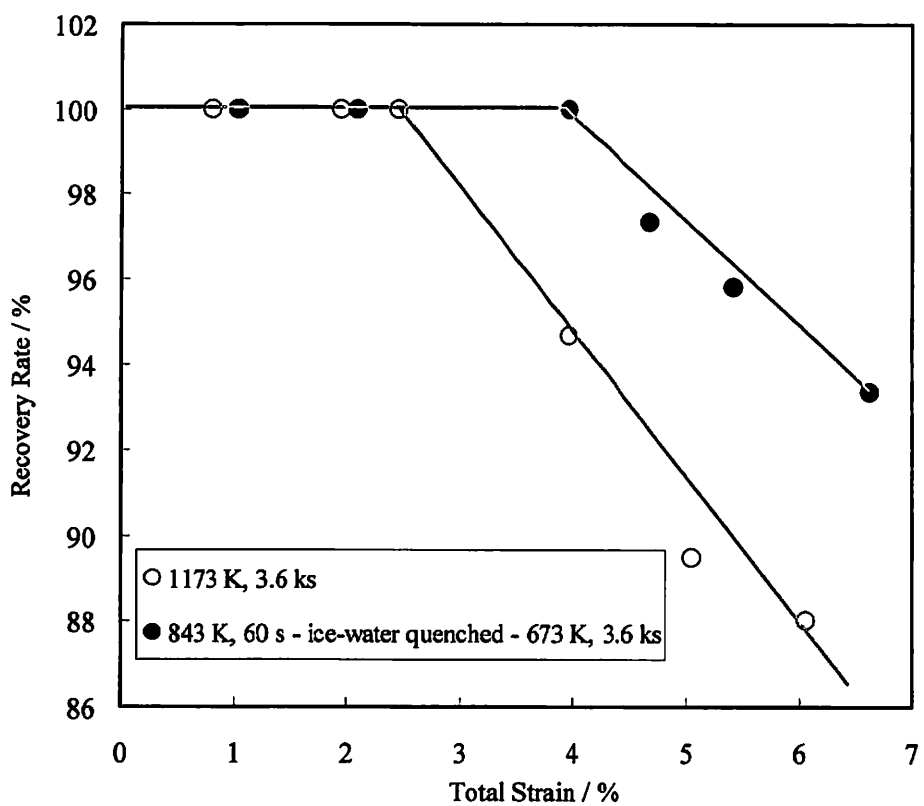

Fig. 2.5 Recovery rate, plotted against total strain for the solution treated (1173 K, 3.6 ks) and thermomechanically treated (cold rolled and heat treated at 873 k for 60 s - ice water quenched - annealed at 673 K for 3.6 ks) alloy. Tensile tests were carried out at 618 K.

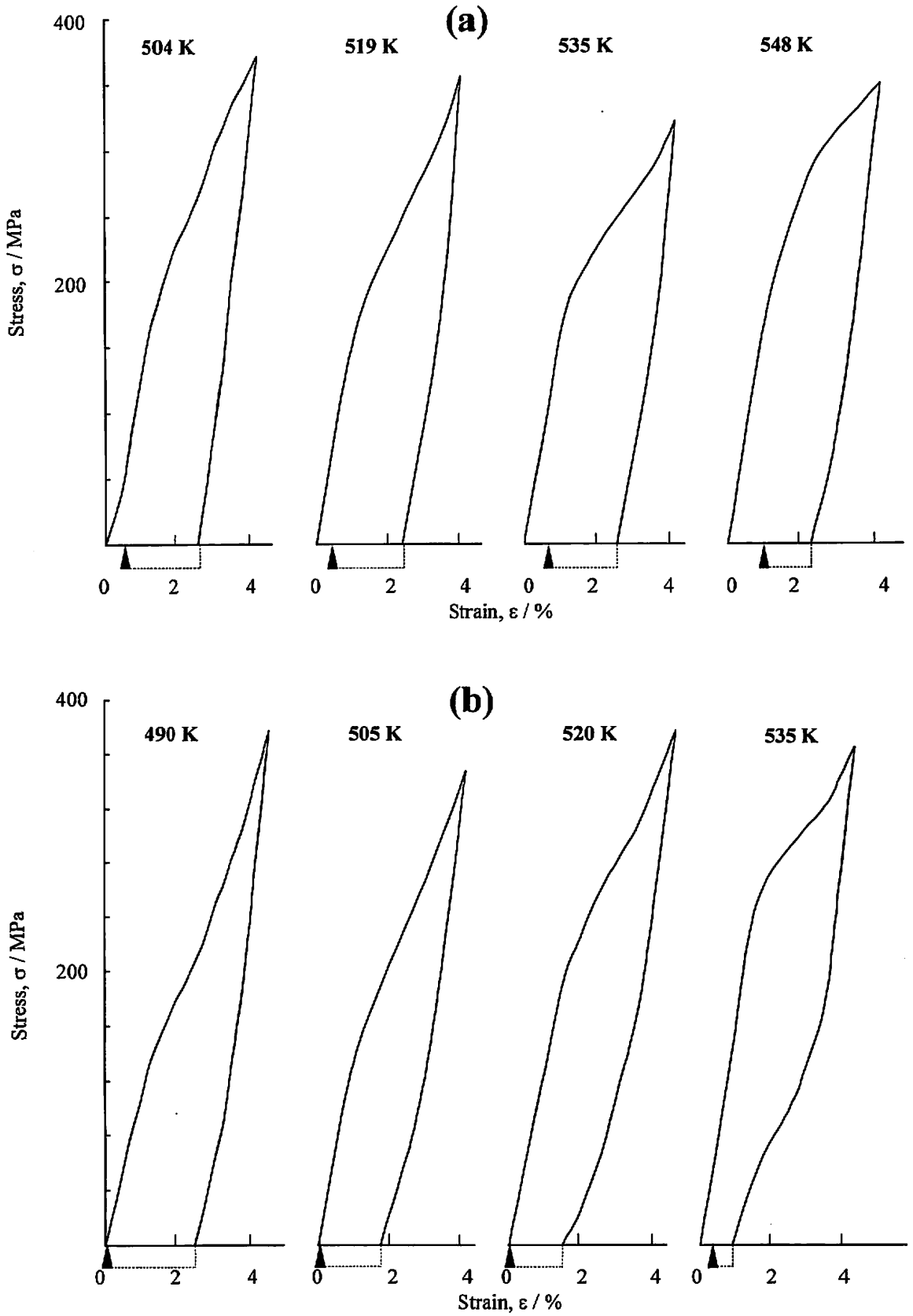

Fig. 2.6 Stress-strain curves of (a) fully annealed and (b) thermomechanically treated (annealed at 673 K for 3.6 ks after cold rolling 24.5 %) Ti-30at.%Pd-20at.%Ni alloy. Test temperatures are shown in the figure. The arrows indicate the strain recovery after heating to 673 K.

Chapter 3

Materials, Specimens Preparation and Analysis Methods

3.1 Materials

The Ti-Pd alloy ingots have been prepared by melting from pure Ti and pure Pd. Titanium with a minimum purity of 99.8 mass % and palladium with a minimum purity of 99.95 mass % provided by Nilaco Corporation were employed in alloys preparation. Titanium and palladium were placed together in a water-cooled cooper crucible inside of an arc furnace. The conventional arc melting technique with consumable tungsten electrode was employed to prepare the Ti-Pd alloys. The melting was carried out under a $2x10^5$ Pa argon atmosphere. The ingots-buttons with 20 g in weight were melted consecutively for six times in order to assure a good homogenization. The ingots were further homogenized in vacuum (about 10^{-3} Pa) at 1273 K for 36 ks. Weighing the initial materials before and ingots after melting and homogenization showed that negligible weight changes occurred. Thin metallic sheets have been cut from the buttons by using Buehler-Isomet or Maruto low speed saws. The sheets with 0.15 – 0.8 mm in thickness were used for preparing DSC and TEM specimens. Other metallic sheets with 1.5 – 2 mm in thickness were hot-rolled for preparing tensile test specimens.

3.2 Differential Scanning Calorimetry

The phase transformation in the Ti-Pd high temperature shape memory alloys were investigated using differential scanning calorimetry (DSC). This technique is widely applied for

studying martensitic transformation in shape memory alloys[1]. There are several definitions of Differential Scanning Calorymetry, which are basically identical[2-4]. DSC is a calorimetrically "pure" method. It is based on heating or cooling a sample (S) and a reference (R) at a preset rate and in a specified atmosphere, while keeping their temperatures the same, and measuring the compensating heat flux that keeps the temperature of the sample within the limits of a preset program. The experimental DSC curves show the heat flux Φ (in mJ/s or mW) or the specific heat capacity C_p (J/gK) against the temperature (in isothermal experiments against the time). The compensating heat flux at a particular temperature during a phase transformation is directly proportional to the change in the internal energy (enthalpy) of the specimen. In other words, the quantity of heat flow at a particular temperature directly corresponds to the quantity of the transformed matter at that temperature.

In Fig. 3.1 that shows the DSC heating and cooling curves of a Ti-47at.%Pd alloy, the characteristic transformation temperatures measured by DSC during martensitic transformation are defined as follows:

M_s: martensite start temperature upon cooling;

M*: martensite peak temperature upon cooling;

M_f: martensite finish temperature upon cooling;

A_s: reverse transformation start temperature upon heating;

A*: reverse transformation peak temperature upon heating;

A_f: reverse transformation finish temperature upon heating.

The method used for determination of the transformation temperatures is indicated in Fig 3.1. The transformation temperatures were determined by crossing point of two straight lines, which are tangential to the baseline of the DSC curve and transformation peak slope, respectively. The temperatures determined by this method do not correspond exactly with the definition of the martensitic transformation temperatures. For instance, following the definition, the M_s is the temperature when the first plate of martensite is formed, and M_f is the temperature when the last

part of parent phase transforms into martensite. However, this method is convenient for practical applications and is therefore widely used.

Basically two types of Differential Scanning Calorimeters must be distinguished: the heat flux DSC and the power compensation DSC[4]. In our experiments we used a DSC-50 Shimadzu heat flux DSC with a disk-type measuring system. A schematic drawing of this measuring system is presented in Fig. 3.2. The characteristic feature of this type of DSC is that the main heat flow from the furnace to the samples passes symmetrically through a disk (made from metal, quartz glass or ceramics) of good thermal conductivity. The samples placed on the sample containers (crucible, pan or cell) are positioned on the disk symmetrical to the center. The temperature sensors are fixed on disk surface or integrated into the disk. The arrangement of the containers containing the sample and the reference substance must always be the same (containers centered on the disk) in order to keep the uncertainties of measurement as small as possible. When the furnace is heated, heat flows through the disk to the samples. In a theoretical case, when the samples are of the same kind (arrangement ideal symmetrical), the heat flow rates through the sample and reference will be identical. The differential temperature signal ΔT is then zero. If this equilibrium state is disturbed by a sample transition, a differential signal is generated which is proportional to the difference between the heat flow rates to the sample and to the reference. The signal is processed by a computer and then sent to a recorder.

The samples for DSC measurements were cut from metallic sheets by using a low speed saw into a nearly cubic or rectangular shape, mechanical ground and then ultrasonic cleaned in acetone. The weight of the samples varied from 10 mg to 30 mg. After encapsulated in evacuated quartz tubes the samples were subjected to different heat treatment and finally lightly mechanical ground in order to remove the surface scale. For carrying out DSC measurements the sample and the reference material were placed in alumina containers (cell, pan). A standard α-Alumina (α-Al_2O_3) powder, supplied by Shimadzu Corporation was used as reference material. The measurements were made under nitrogen atmosphere in a DSC-50 Shimadzu differential scanning calorimeter. The

heating and cooling rates were usually taken to be 10 K/min, a rate that is generally employed for the investigations of the SMA's phase transformations. The kinetics of the transformations was obtained by varying the heating and cooling rate at 3, 5, 15, and 25 K/min. The temperature range of the DSC measurements was from 293 K to 973 K. The experimental data were automatic processed by a TA-50 Shimadzu thermal analyzer and the transformation temperatures, and transformation heats were calculated by a specialized software package in a NEC personal computer.

3.3 Transmission Electron Microscopy

The transmission electron microscopy (TEM) was used to investigate the phase morphology, the crystal structure and the orientation relationships between different phases. A JEOL JEM-2000FX electron microscope operating at 200 kV and equipped with a double tilt specimen holder EM-STH 10 was used.

Disk-shaped specimens with a diameter of 3 mm were obtained from the metallic sheets with 20-50 μm in thickness, by ultrasonic cutting or by punching. After heat treatments in evacuated quartz tubes, the specimens were lightly mechanically polished with 1200-grit emery paper in order to remove the surface scale. The specimens were electropolished using twin-jet technique in an electrolyte consisting of 20 pct H_2SO_4 and 80 pct CH_3OH, by volume. A scheme of twin-jet apparatus is shown in Fig. 3.3[5-6]. The working temperature was around 253 K. Occasionally, the disks were ion milled under argon atmosphere in a JEOL JIT-100 Ion Beam Thinner machine.

3.4 Tensile Testing

In the present work the Ti-Pd alloy specimens were tensile deformed in martensitic state in order to obtain a single martensite variant under stress. The deformation in martensite proceeds by

growing of one variant at the expense of other, i. e. twinning and detwinning, as shown in Fig. 3.4. This deformation mechanism is at the origin of SME[7-11].

For the preparing of the tensile specimen, metallic sheets with about 1.5-2 mm in thickness were plastically deformed by hot rolling into 0.25-0.35 mm thick sheets with 0.05-0.1 mm thick reduction per step. Because of the ductility limit of the Ti-Pd alloys, a higher thick reduction per step was not available. One "step" means one rolling operation effectuated between intermediate anneals at 923 K. The tensile specimens with 5 mm in width were spark-cut, from as-rolled sheets, by using a SANKYO Engineering machine. Before heat treatment the specimens were mechanically polished in order to remove the oxide layer. The tensile specimens, encapsulated in evacuated quart tubes, were solution treated at 1273 K for 3.6 ks and then quenched into ice water. Following this heat treatment the recovery and recrystallization process was complete and the structure was in the martensitic state at the room temperature as observed by electron microscopy.

The tensile deformation was conducted with a Shimadzu AGS-500B material tester machine. The strain ε was preset at 4, and 8 % from the gauge length. The testing parameters used in present experiments were: full scale 250 kg, tests speed 0.5 mm/min and charts speed 20 mm/min. A typical stress-strain curve of a quenched Ti-48at.%Pd alloy deformed at room temperature is shown in Fig. 3.5.

References

1. W. Yu: *Thermal Analysis in Metallurgy,* ed. R. D. Shull and A. Joshi, The Minerals, Metals & Materials Society (1992) 187.
2. G. Lombardi: *For Better Thermal Analysis, 2nd edition,* International Confederation for Thermal Analysis (ICTA), Rome (1980) 20.
3. V. A. Bershtein and V. M. Egorov: *Differential Scanning Calorimetry of Polymers: physics, chemistry, analysis, technology,* tr. from Russian T. J. Kemp, Ellis Horwood (1994).
4. G. Höhne, W. Hemminger and H. J. Flammersheim: *Differential Scanning Calorimetry, An Introduction for Practitioners,* Springer (1996).
5. T. Sano, R. Nishihara, H. Yotsumoto, Y. Miura and M. Nemeto: *Bulletin of the Faculty of Engineering, Kyushu University, Japan,* **56** (1983) 491.
6. D. B. Williams C. B. Carter: *Transmission Electron Microscopy,* Plenum Press, New York and London (1996).
7. K. Otsuka and K. Shimizu: *Int. Metals Rev.,* **31** (1986) 93.
8. K. Otsuka: *Functional Metallic Materials,* ed. M. Doyama and R. Yamamoto, University of Tokyo Press, in Japanese (1985) 56.
9. S. Ichinose, Y. Funatsu and K. Otsuka: *Acta Metall.,* **33** (1985) 1613.
10. T. Saburi, C. M. Wayman, K. Takata and S. Nenno: *Acta Metall.,* **28** (1980) 15.
11. K. Otsuka and C. M. Wayman: *Shape Memory Materials,* ed. K. Otsuka and C. M. Wayman, Cambridge University Press (1998) 27.

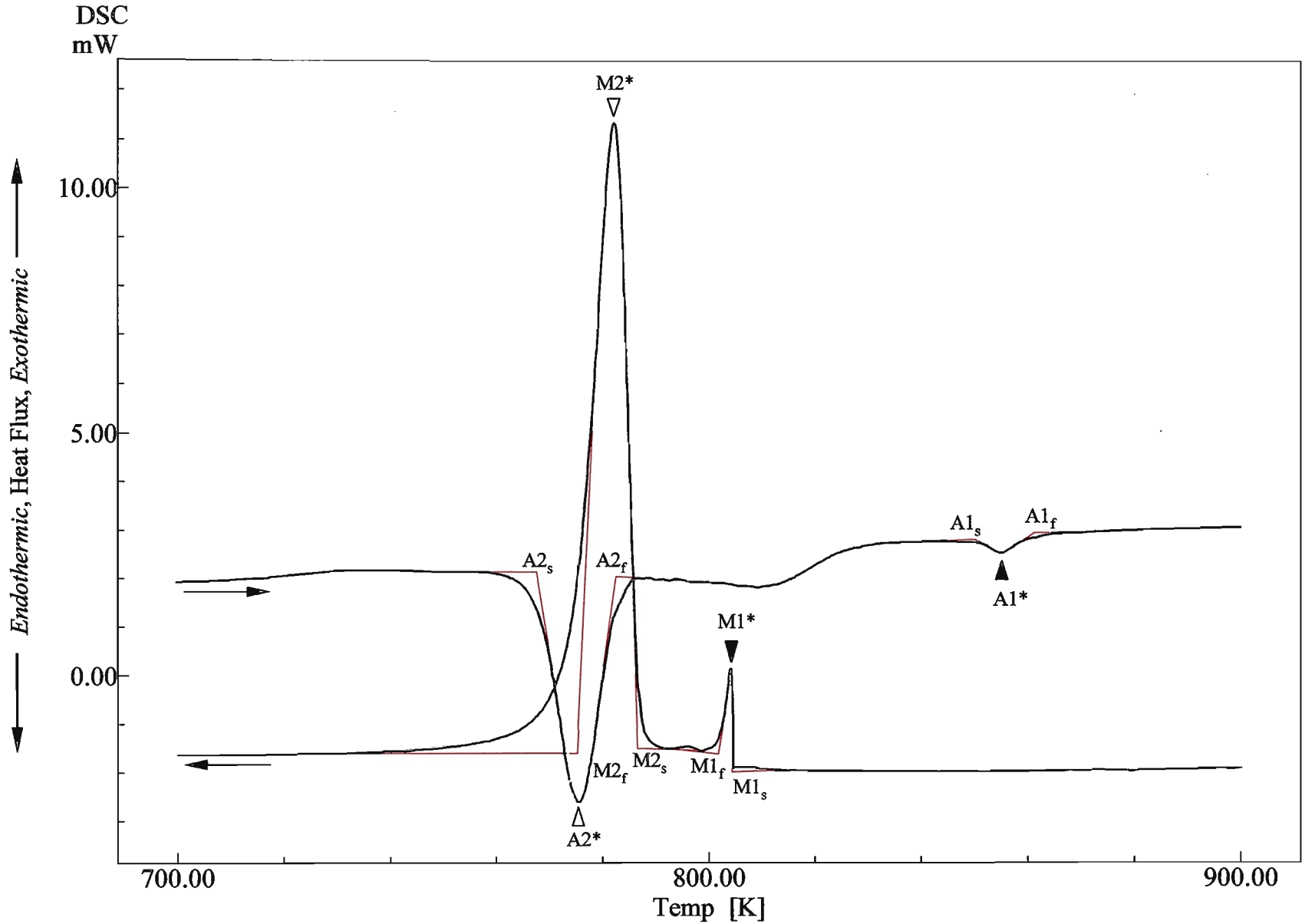

Fig. 3.1 Schematic description of the method for transformation temperature determination on the DSC heating and cooling curves, exemplified for a quench Ti-47at.%Pd alloy solution treated at 1273 K for 3.6 ks.

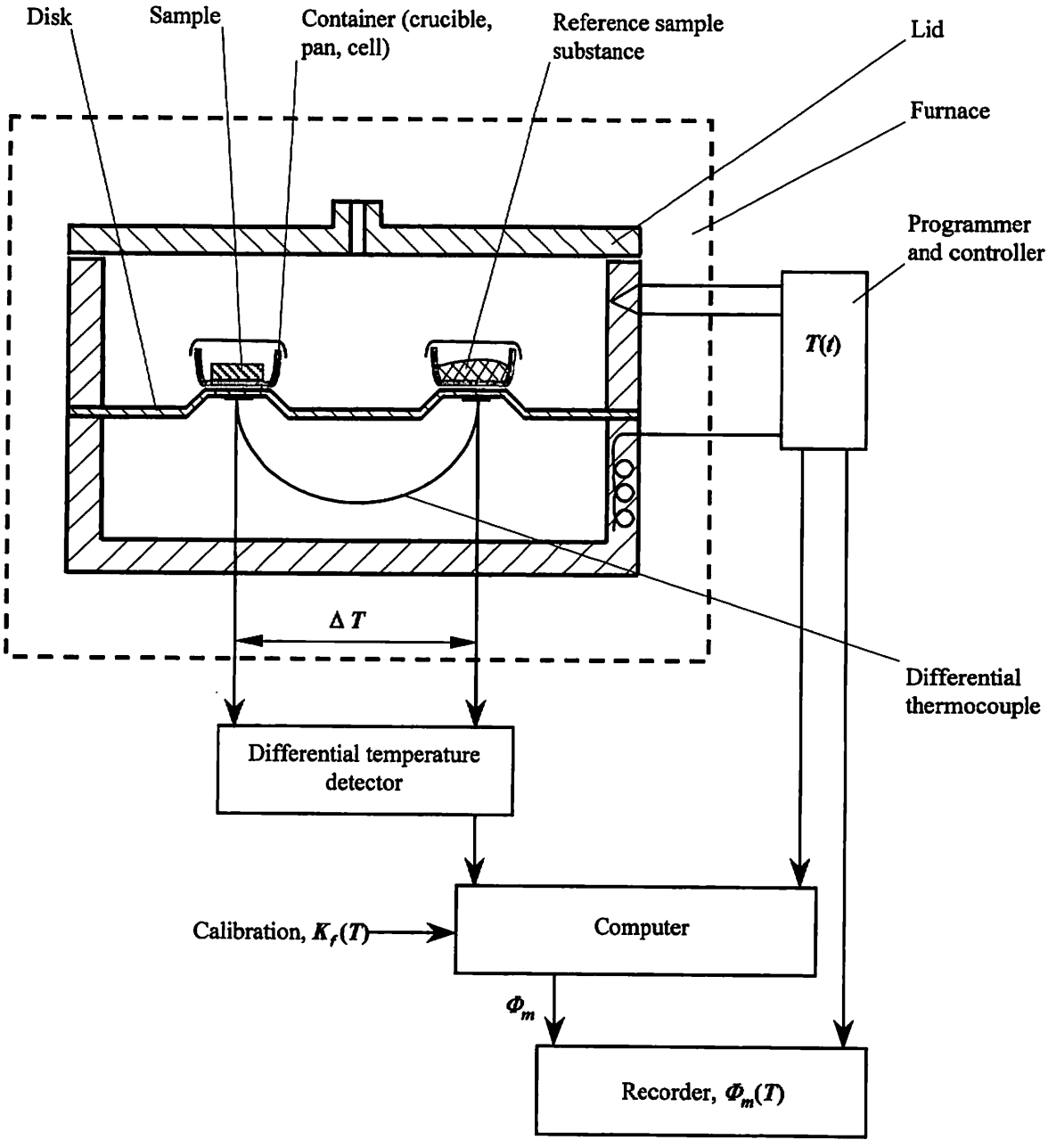

Fig. 3.2 Schematic drawing of a heat flux DSC with disk-type measuring system. T - temperature, t - time, Φ_m - measured heat flow rate, K_f - calibration factor[4].

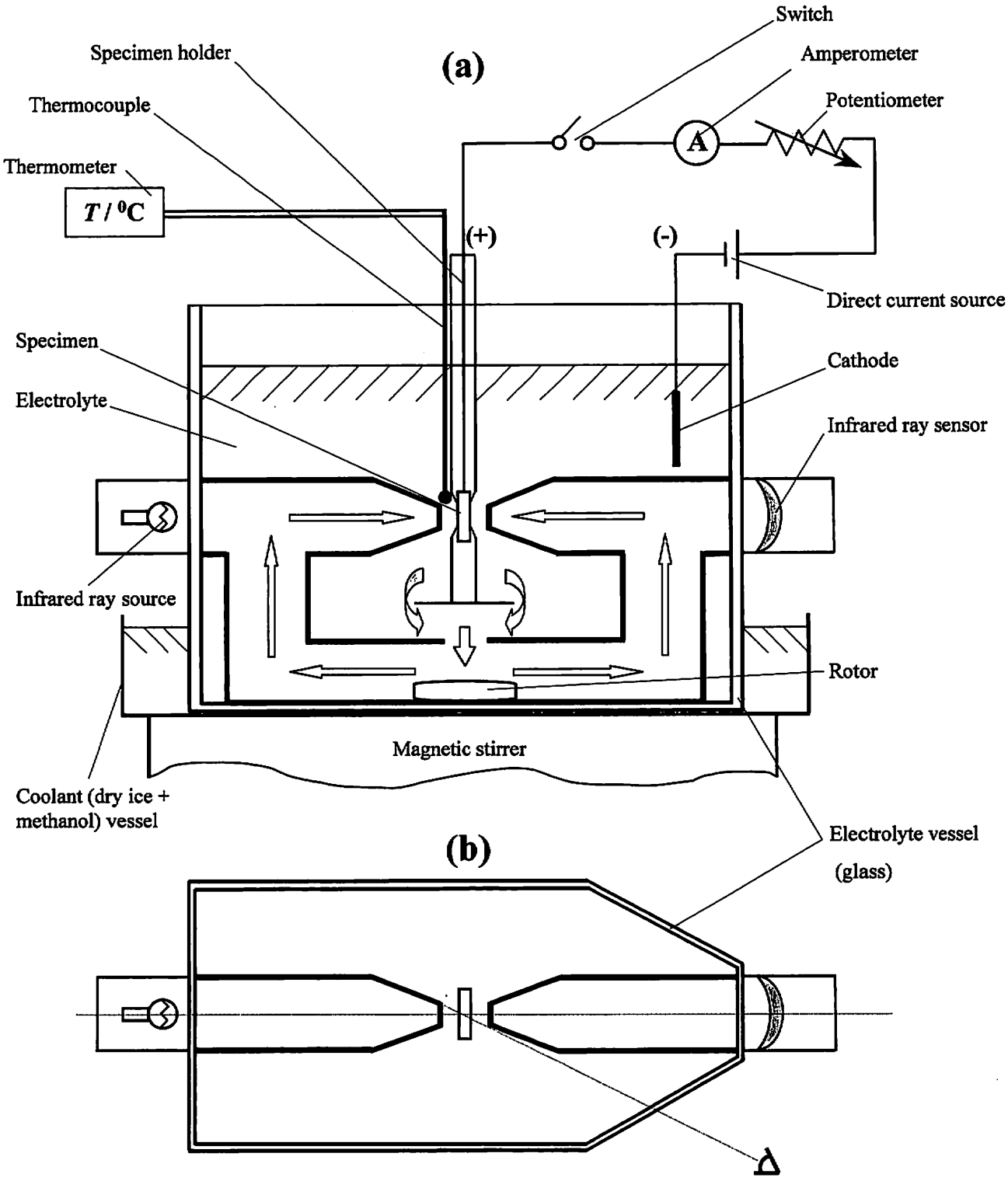

Fig. 3.3 Schematic drawing of twin-jet electropolishing apparatus. (a) Lateral view. (b) Top view showing how the specimen surface is monitored during polishing[5].

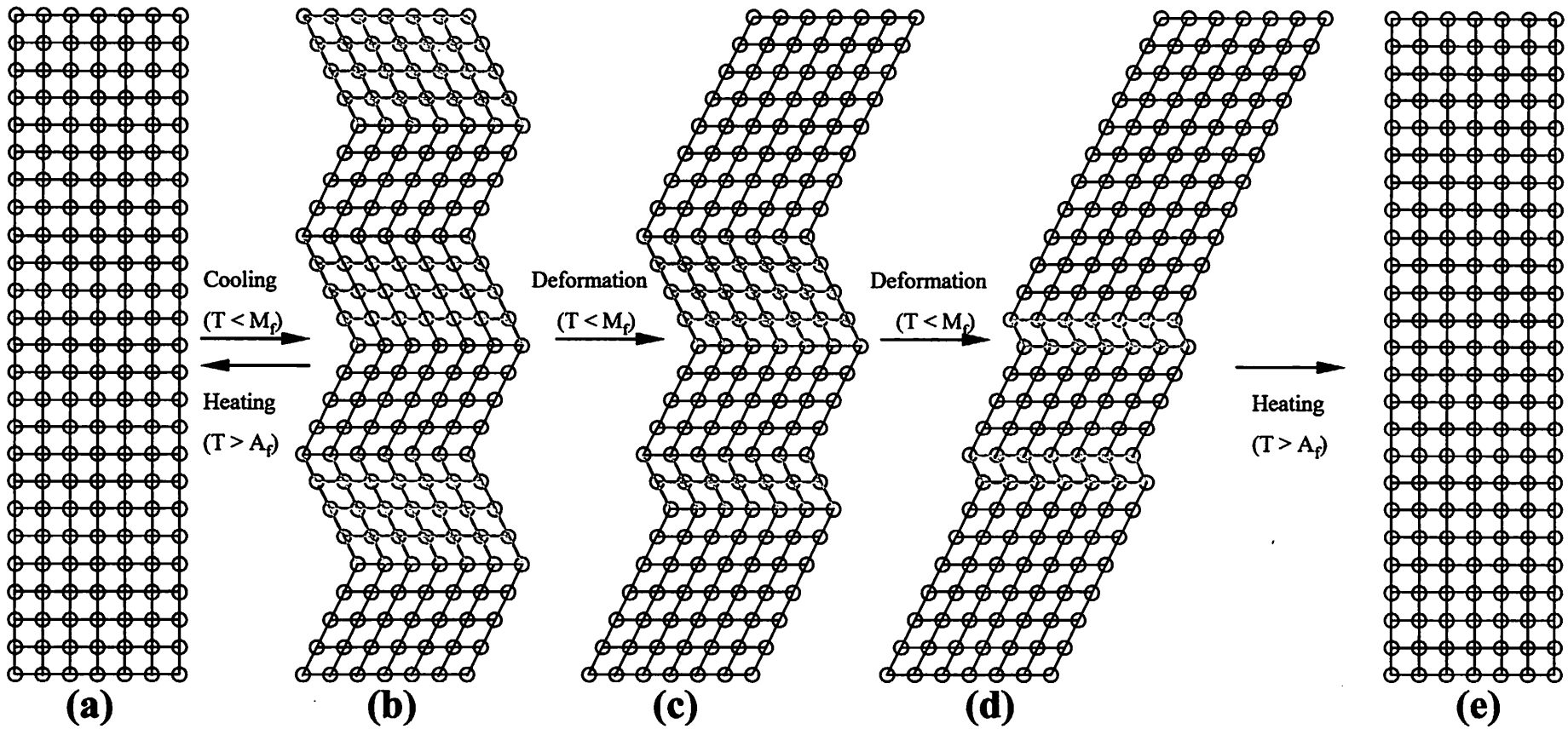

Fig. 3.4 Schematic illustration of the mechanism of shape memory effect: (a) parent phase; (b) self-accommodated martensite; (c - d) deformation in martensite proceeds by the movement of intervariant boundary (i. e. twinning or detwinning); (e) upon heating to a temperature above A_f, each variant reverts to the parent phase in the original orientation by virtue of the crystallographic reversibility of the martensitic transformation[11].

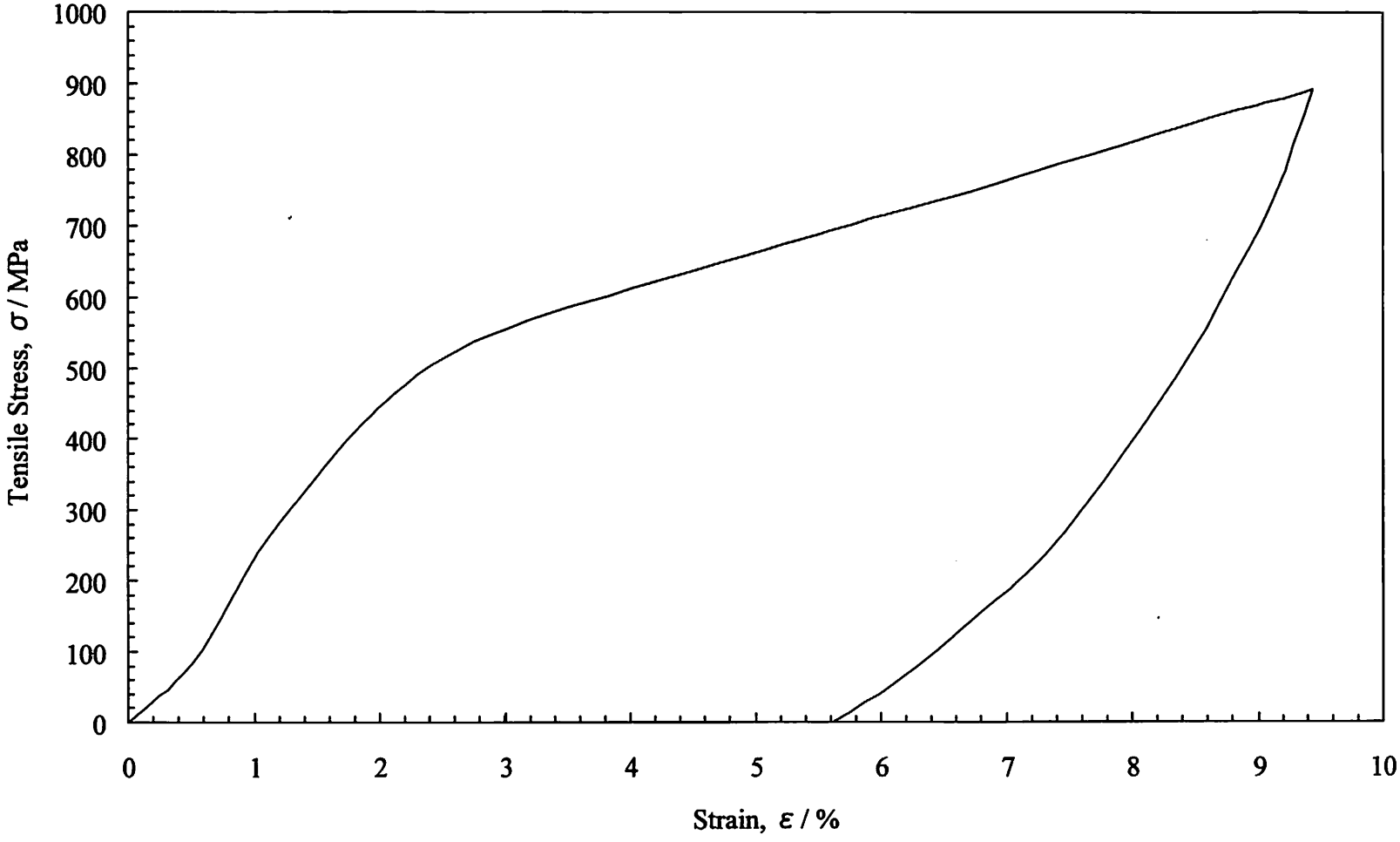

Fig. 3.5 Typical stress-strain curve of a quenched Ti-48at.%Pd alloy deformed at room temperature.

Chapter 4

Martensitic Transformation Behavior of Near-Equiatomic Ti-Pd Shape Memory Alloys

4.1 Introduction

In the world of shape memory materials the Ti-Pd alloys are known as potential materials for high temperature applications. This is because the intermetallic TiPd phase undergoes a thermoelastic martensitic transformation from B2 to B19 type structure around 800K upon cooling. In the near-equiatomic Ti-Pd alloys the martensitic transformation temperatures are strongly dependent on the Pd concentration. Donkersloot and Van Vucht[1] reported that in Ti-rich side the transformation temperatures increase with Pd content reaching the maximum values for the Ti-50at.%Pd composition. For Pd-rich side the transformation temperatures were almost constant with the concentration. Shugo and Honma[2, 3] had obtained the same result using DSC measurements. They pointed out two characteristics of the martensitic transformation behavior in Ti-rich Ti-Pd alloys. First, the martensitic transformation occurred only in one step. Second, the transformation hysteresis (A_s - M_s) is greatly affected by composition and become negative in these alloys that is not usual in a typical martensitic transformation. The A_s and M_s notations represent reverse and direct martensitic transformation starting temperatures, respectively.

Different from the above mentioned results Nishida *et al.*[4] found that in the near-equiatomic Ti-rich alloys martensitic transformation occurs in two successive steps B2 → X → B19 with the formation of unknown intermediate phase X.

From the above survey it results that the transformation behavior in the near-equiatomic Ti-Pd alloys is not elucidated until now. Therefore, in the present chapter, the martensitic transformation behavior in the near-equiatomic Ti-Pd alloys is studied and discussed based on the DSC measurements.

4.2. Experimental Procedure

The arc melting technique with consumable tungsten electrode was used to prepare eight Ti-Pd alloys with the following compositions: 45, 46, 47, 48, 49, 50, 52.5 and 55 at.%Pd. For each alloy pure titanium (99.8 mass %) and pure palladium (99.95 mass %) components were melted consecutively for six times in an argon atmosphere. The weight loss during the melting was negligibly small. The as-melted buttons were homogenized at 1273 K for 36 ks. Thin sheets have been cut from the buttons by using a low speed saw. Parallelepiped-shaped specimens were carefully cut from sheets, mechanically polished, encapsulated in evacuated quartz tubes and then heat-treated. Depending on the heat treatment two series of specimens had been prepared. The specimens of the first series have been solution treated at 1273 K for 3.6 ks followed by quench into ice water without crushing the capsules. The specimens of the second series have been kept at 1273 K for 3.6 ks and then furnace cooled to the room temperature. The cooling rate of 40 K/h was controlled from 1273 K to about 700 K, then the specimens were left in the furnace after turning off the electricity. After the heat treatment the specimens were lightly mechanically polished in order to remove the surface scale. The transformation temperatures were determined by DSC measurements. The heating and cooling rate was 10K/min.

4.3 Results and Discussion of DSC Measurements

DSC curves of the quenched near-equiatomic Ti-Pd alloys after solution treatment at 1273 K for 3.6 ks are shown in Fig. 4.1. Transformation behavior was found to be nearly identical in

quenched equiatomic and quenched Pd-rich Ti-Pd alloys employed in the present investigation and therefore, we show only the DSC curves of the Ti-50at.%Pd in Fig. 4.1. Two types of curves were obtained by varying the composition. In the Ti-50at.%Pd alloy only a single sharp peak is observed upon heating and cooling and there is no inversion between reverse and forward transformations. On the other hand, two endothermic and two exothermic reactions are clearly observed in Ti-rich Ti-Pd alloys upon heating and subsequent cooling. We defined the first and second peaks on heating as A2* and A1*, respectively. In the same way the first and second peaks on cooling are denoted as M1* and M2*, respectively. The inversion of A2* and M2* is clearly seen. However, it must be also noted that A1* lies very close to the reverse transformation peak temperature of the Ti-50at.%Pd alloy. The direct and reverse martensitic transformation temperatures as well as the peaks temperatures determined from DSC curves for the quenched near-equiatomic Ti-rich Ti-Pd alloys solution treated at 1273 K for 3.6 ks are presented in Table 4.1.

In order to establish the correspondence between the reactions observed on heating and cooling in the quenched Ti-47at.%Pd alloy the incomplete thermal cycling experiments have been performed as shown in Fig. 4.2. In Fig. 4.2(a) the specimen is heated from room temperature to just beyond the A2* peak and then cooled. A one-to-one correspondence between the A2* and the M2* transformations can be confirmed by the appearance of the exothermic peak on cooling. In the same way, a one-to-one correspondence between the A1* and the M1* transformations can be confirmed in Fig. 4.2(c), where the specimen is heated just beyond the A1* peak. In this case M1* lies at almost identical temperature with that of the single peak observed on cooling in the equiatomic alloy. There is no inversion between A2* and M2* in Figs. 4.2(a) to (c). The A2* and M2* peak temperatures increase and M1* decreases with increasing the maximum heating temperature, which will be discussed in the next chapter, then the inversion between A2* and M2* occurs, as shown in Fig. 4.2(e). However, A1* is independent of the maximum heating temperature as clearly seen in Figs. 4.2(c) to (e).

Based on these measurements it is apparent that successive transformation takes place in Ti-rich Ti-Pd alloys. Comparing the individual peak area of the A2* and A1* or M2* and M1* reactions, it is likely that the lower temperature reaction is attribute to the transformation in almost entire volume of the specimen. On the other hand, the reaction at higher temperature may be due to the transformation in a small volume of the specimen.

The DSC curves of the furnace cooled near-equiatomic Ti-Pd alloys are shown in Fig. 4.3. In the Ti-50at.%Pd and Pd-rich alloys the transformation behavior is identical to that of the quenched alloys. On the other hand, in Ti-rich alloys only a rather broad single peak denoted as A* is observed on heating instead of two peaks in the quenched alloy. A* lies nearly at the same temperature as the A1* of the quenched Ti-rich alloys.

Compositional dependence of transformation peak temperatures during heating process in the quenched and the furnace cooled alloys is plotted in Fig. 4.4 and the obtained DSC results so far are summarized as follows. There is no difference of transformation behavior and temperature in the quenched and the furnace cooled Ti-50at.%Pd and Pd-rich alloys as pointed out above. In the furnace cooled specimens, only one peak was observed on heating curve. The temperature of this peak for all the compositions lies very close to the endothermic peak temperature of Ti-50at.%Pd alloy. On the other hand, two peaks appear on the heating curves of quenched Ti-rich alloys. The temperature of A2* rises gradually with increasing Pd content and reaches the maximum at 50at.%Pd. The temperature of A1* is almost constant with Pd content and is identical to the transformation peak temperatures A* of the furnace cooled specimens. The change of transformation behavior with Pd content and thermal history suggests that the phase boundary of TiPd compound in Ti-rich side vary significantly with temperature and concentration. This aspect will be discussed in Chapter 6.

4.4 Conclusions

Martensitic transformation behavior in near-equiatomic Ti-Pd alloys was studied by means of DSC measurements. As a result, the following conclusions were obtained.

1) In Ti-rich alloys martensitic transformation takes place in successive steps as indicated by the two pairs of endothermic-exothermic peaks on DSC curves of those alloys. The transformation temperatures of the first step indicated by well defined, sharp pairs of peaks on DSC curves, increase with Pd content reaching the maximum at equiatomic composition. The transformation temperatures of the second step indicated by higher temperature pair of peaks on DSC curves do not change with Pd content and are almost the same with transformation temperatures of Ti-50 at.% Pd alloy.

2) In Pd-rich alloys martensitic transformation occurs in only one step as could be understand from DSC measurements. The transformation temperatures do not vary with the composition and are nearly equal with transformation temperatures of the equiatomic Ti-Pd alloy.

References

1) H. C. Donkersloot and J. H. N. Van Vucht: *J. Less-Common Met.*, **20** (1970) 83.
2) Y. Shugo and T. Honma: *J. Institute of Mineral - Dressing and Smelting, Tohoku Univ.*, **43** (1987) 128.
3) Y. Shugo: *Mater. Sci. Forum*, **56-58** (1990) 631.
4) M. Nishida, Y. Morizono, H. Kijima, A. Ikeya, H. Iwashita and K. Hiraga: *Materials for Smart Systems II, Symposium Proceedings Volume 459*, ed. by E. P. George, R. Gotthard, K. Otsuka, Susan T. McKinstry and Marilyn Wun-Fogle, Materials Research Society (1997) 375.

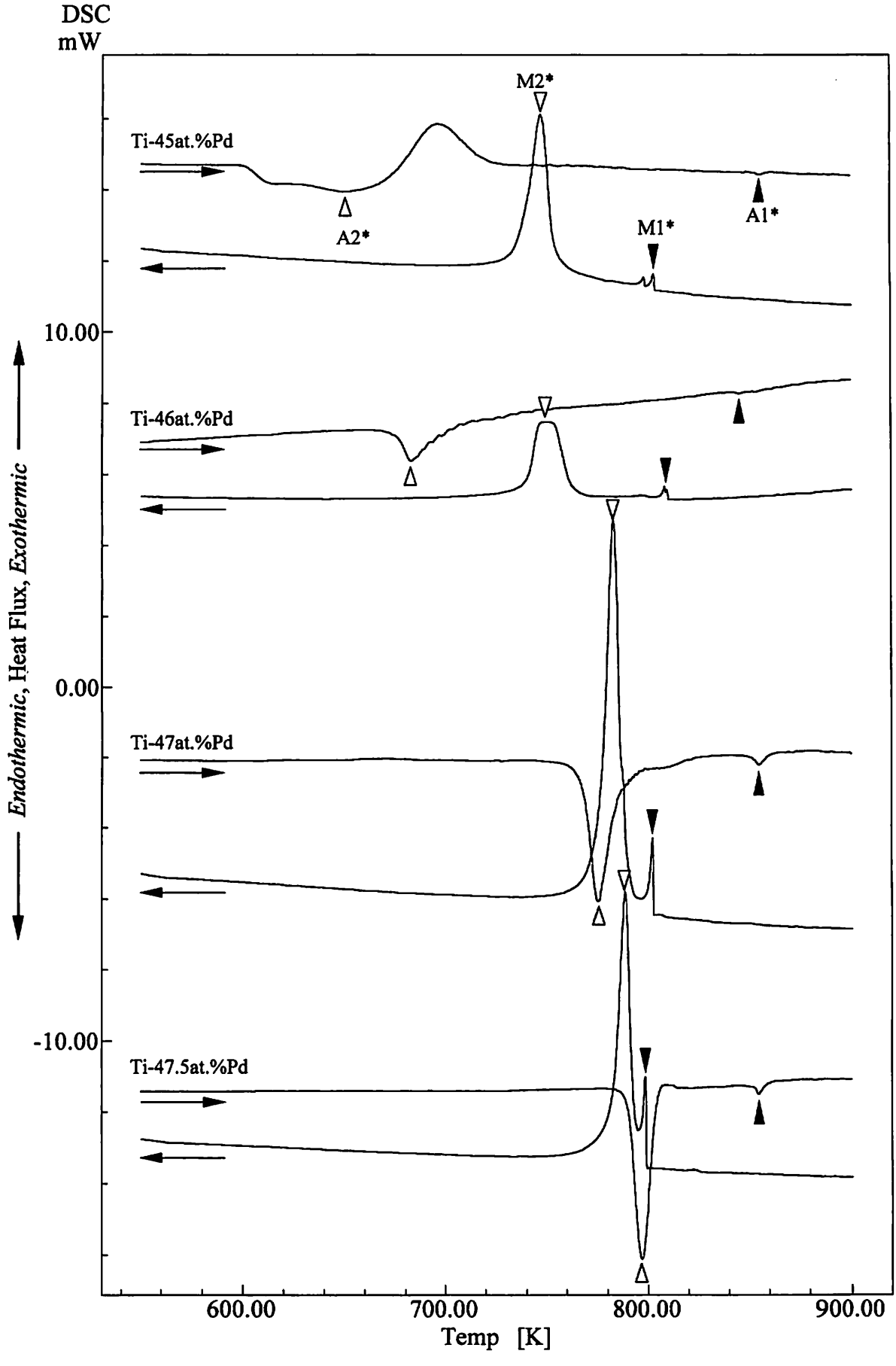

Fig. 4.1 Typical DSC curves of quenched near-equiatomic Ti-Pd alloys solution treated at 1273 K.

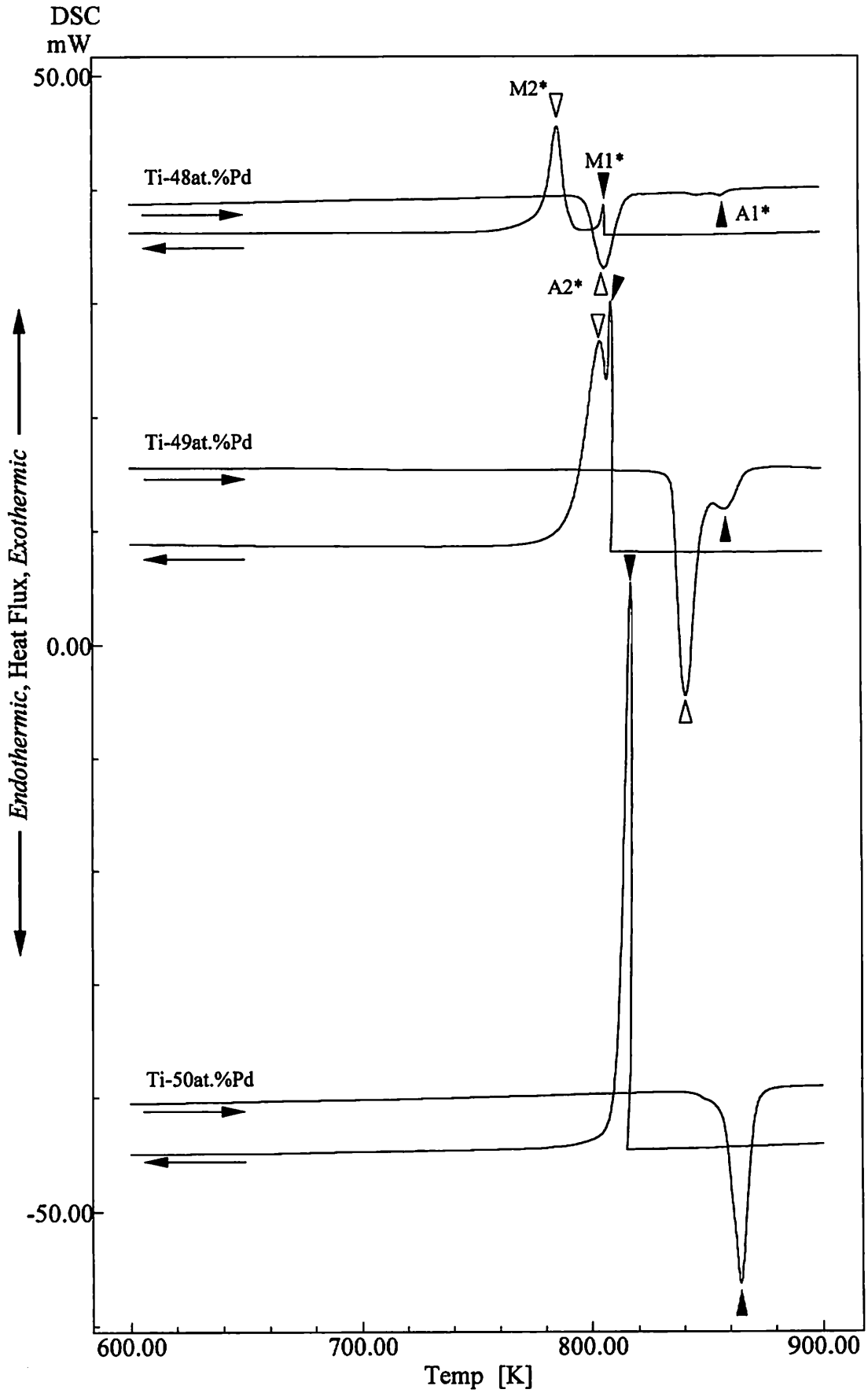

Fig. 4.1 (cont.) Typical DSC curves of quenched near-equiatomic Ti-Pd alloys solution treated at 1273 K.

Table 4.1 Direct and reverse martensitic transformation temperatures of the quenched near-equiatomic Ti-rich Ti-Pd alloys solution treated at 1273 K for 3.6 ks.

Pd content	$A2_s$	**A2***	$A2_f$	$A1_s$	**A1***	$A1_f$	$M1_s$	**M1***	$M1_f$	$M2_s$	**M2***	$M2_f$
[at. %]						[K]						
45	602.28	**649.9**	692.19	851.11	**855.59**	860.6	803.26	**802.74**	794.24	753.77	**747.48**	735.71
46	675.5	**682.82**	703.41	842.11	**850.37**	852.29	810.18	**808.1**	805.93	762.57	**750.04**	740.01
47	767.15	**774.87**	785.83	850.69	**855**	860.32	802.68	**801.96**	799.77	788.01	**782.91**	775.89
47.5	789.53	**796.79**	803.57	851.78	**854.71**	859.55	798.8	**798.25**	796.53	792.74	**788.44**	782.35
48	797.97	**806.05**	814.29	841.63	**857.18**	861.42	806.79	**806.2**	803.9	791.23	**785.99**	779.2
49	835.26	**841.09**	847.55	854.64	**858.81**	867.56	809.1	**808.9**	806.93	806.93	**804.19**	791.62
50	-	-	-	856.81	**864.59**	870.17	816.69	**816.69**	811.46	-	-	-

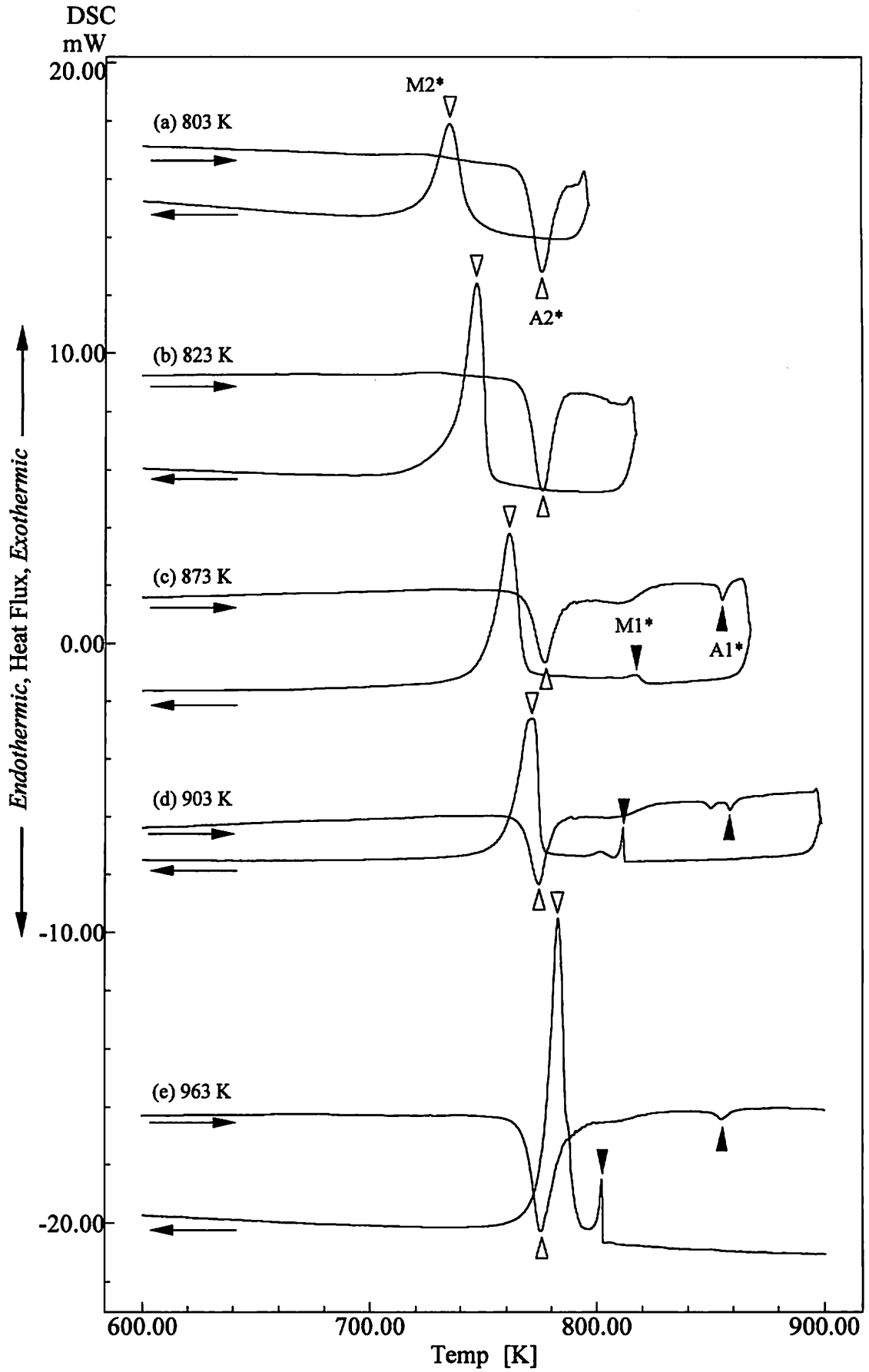

Fig. 4.2 DSC curves of incomplete transformation cycles for quenched Ti-47at.%Pd alloy. For each cycle the maximum heating temperature in DSC is indicated on the left side of the figure.

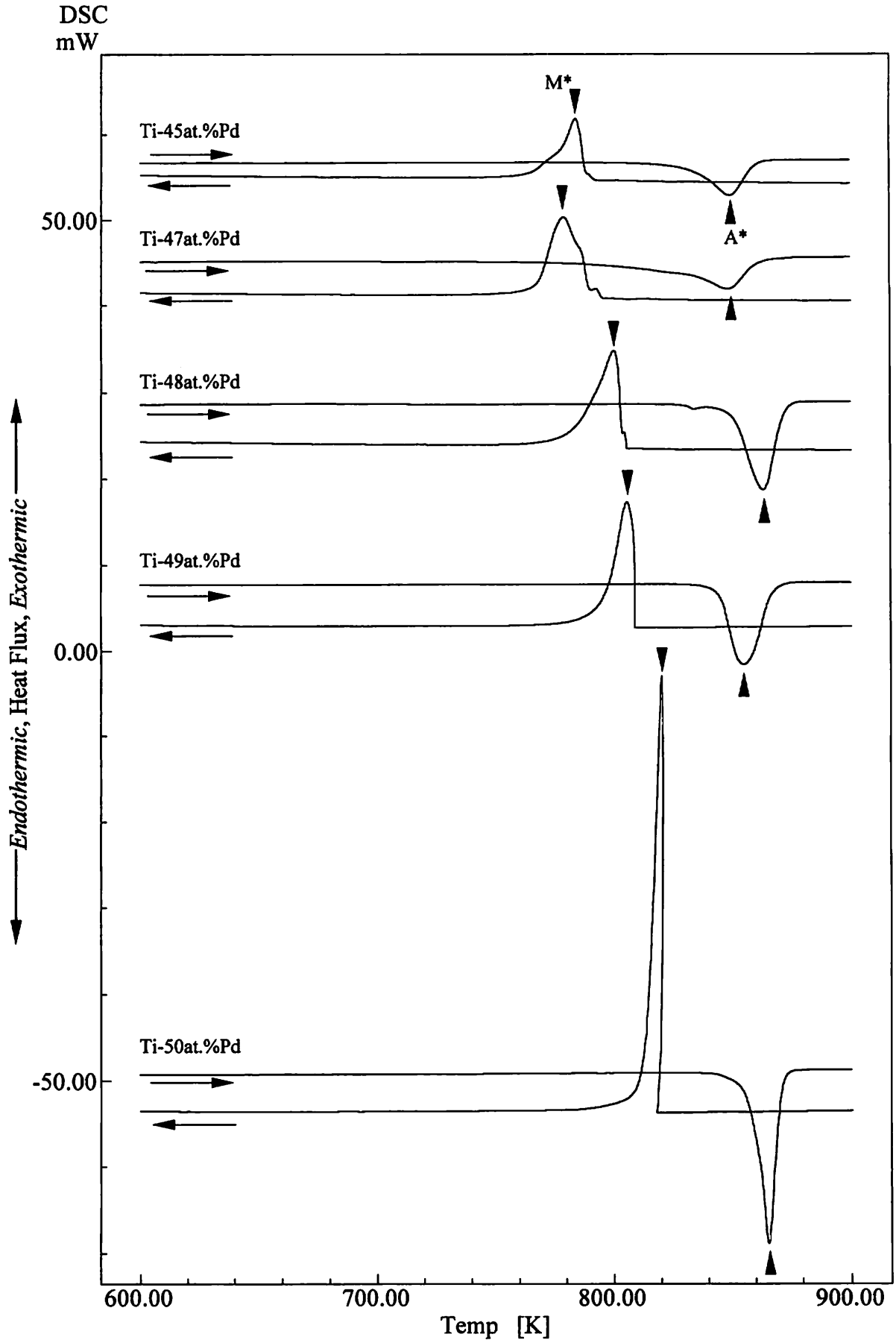

Fig. 4.3 Typical DSC curves of the furnace cooled near-equiatomic Ti-Pd alloys.

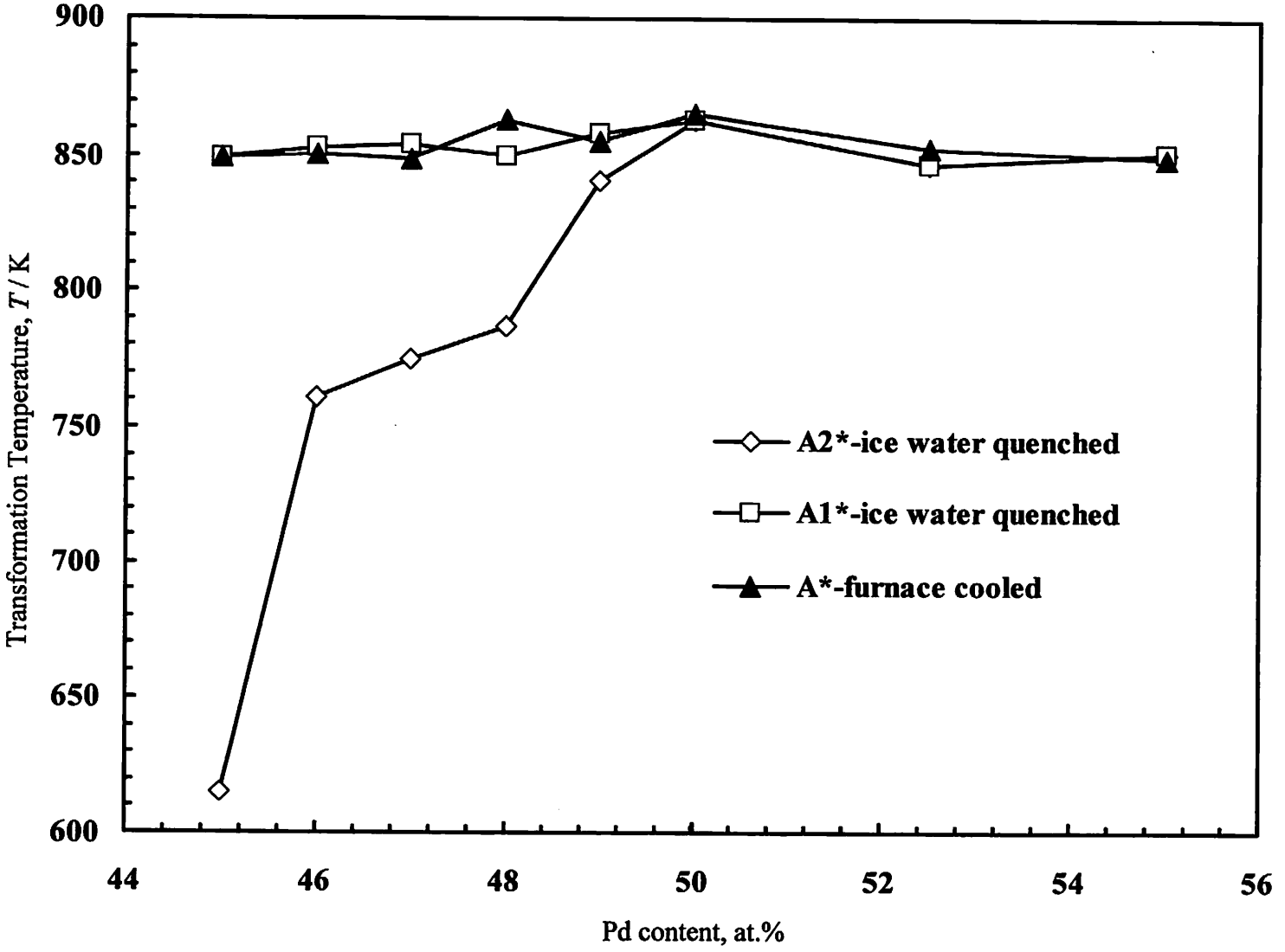

Fig. 4.4 Compositional dependence of transformation peak temperatures during heating process in guenched and furnace cooled Ti-rich Ti-Pd alloys.

Chapter 5

Mechanism of Successive Transformation in Near-Equiatomic Ti-Pd Alloys

5.1 Introduction

Ti-Pd shape memory alloys are well-known as potential materials for high temperature applications, since the intermetallic phase of TiPd undergoes a thermoelastic martensitic transformation around 800 K. Donkersloot and Van Vucht[1] firstly found the B2 to B19 type martensitic transformation in these alloys using high-temperature X-ray diffraction. They have determined the transformation temperatures, i.e., A_s, A_f, M_s and M_f from the intensity change of $(101)_{B19}$, $(010)_{B19}$ and $(010)_{B2}$ reflections upon heating and cooling. They have reported that M_s is higher than A_s in Ti-45 and 55 at.% Pd alloys which are close to the phase boundary of TiPd single phase at Ti-rich and Pd-rich sides, respectively. The inversion of M_s and A_s is unusual in the martensitic transformation. This inversion was confirmed by the DSC measurements effectuated by Shugo and Honma[2-3], who also pointed out that in the near-equiatomic Ti-Pd alloys martensitic transformation proceeds only in one step. On the other hand, Nishida *et al.*[4] had been observed an unusual successive transformation behavior in near-equiatomic Ti-rich Ti-Pd alloys (45 to 49 at.% Pd). The authors interpreted this behavior as being related with the formation of a new intermediate phase between B19 martensite and B2 parent phases but they could not identified the supposed new phases by electron diffraction experiments and image observations.

In the previous chapter the occurrence of successive martensitic transformation in the near-equiatomic Ti-rich Ti-Pd alloys was proved by means of DSC measurements. The purpose of the

present chapter is to clarify the origin and the mechanism of successive transformation based on the results of systematic investigations carried out with the aid of TEM observations.

5.2 Experimental Procedure

Ti-47 and 50 at.%Pd alloys were prepared by arc melting in an argon atmosphere. The starting materials were pure Ti (99.8 mass %) and pure Pd (99.95 mass %). Ingots of 20g in weight were melted repeatedly six times for homogenization. The obtained buttons were annealed in vacuum at 1273 K for 36 ks, and then furnace cooled to room temperature. The weight loss of each button after these treatments was less than 0.2%, and thus the chemical analysis has not been performed. Sheets of about 0.2 mm in thickness were cut from the buttons. Disk-shaped TEM specimens of 3 mm in diameter were punched out from metallic sheets. A half of TEM specimens were solution-treated at 1273 K for 3.6 ks and then quenched into ice water. The rest were furnace cooled to room temperature after the solution treatment at 1273 K for 3.6 ks. The cooling rate of 40 K/h was controlled from 1273 K to about 700 K, then the specimens were left in the furnace after turning off the electricity. As mentioned in previous chapter, the DSC measurements were employed to determine the transformation temperatures by using a heating and cooling rate of 10 K/min. Some of the quenched and the furnace cooled TEM specimens were subjected to the same thermal history of DSC measurement. That is, they were heated up to prescribed temperatures with the rate of 10 K/min in a muffle furnace equipped with digital program controller, and then quenched into ice water. This treatment is calls DSC-like treatment hereinafter. The TEM specimens were lightly mechanically polished to remove the surface scale. They were finally electropolished in an electrolyte consisting of 20% H_2SO_4 and 80% CH_3OH (by volume) by using twin-jet method. The electrolyte temperature was around 253 K. TEM observations were carried out in a JEM-2000FX electron microscope operated at 200 kV.

The crystal structure of the B19 martensite is of MgCd type with an orthorhombic unit cell. The following lattice parameters were used for the present analysis: a = 0.489 nm, b = 0.281 nm and c = 0.456 nm[5].

5.3 Orientation Relationship between Ti_2Pd Precipitates and TiPd Matrix

An understanding of the crystallography of any transformation is important since the properties of the interfaces between different crystals, and finally the properties of the material, depend on the relative dispositions of the crystals[6]. Also the crystallography determines the orientation dependence of the interface energy, which in turn determines the development of the structure morphology. Experimental observations show that during phase transformations the orientation relationships are not arbitrary, but take place in a way that allows best fit at the interface between the two crystals[7-8]. Thus, the interface energy will be reduced and hence the activation energy for nucleation. Embryos that during phase transformation are orientated in this manner would relatively easy grow into successful nuclei, giving rise to specific orientation relationships mentioned above. This principle also applies for Ti-Pd alloys, and specific orientation relationships appear between Ti_2Pd precipitates and TiPd matrix as will be discussed below and in Chapter 7.

Figure 5.1(a) presents the microstructure of the quenched Ti-47at.%Pd alloy. The micrograph shows typical B19 martensite morphology consisting of alternating platelets with {111} Type I twin relation, as could be understand from selected area electron diffraction pattern (SAEDP) presented in Fig. 5.1(b). This twinning mode in Ti-Pd alloys was also reported by other authors and it was considered to be a LIS[9, 10]. Since no secondary phase is observed in the alloy, it is apparent that the alloy is quenched from a single region of B2 parent phase and no decomposition occurs during quenching. A similar twinned martensite is observed in the quenched and the furnace cooled Ti-50 at.% Pd alloys, as shown in Fig. 5.2. It can be concluded that there is no

microstructure change in the Ti-50at%Pd alloy irrespective of heat treatment. In other words, no phase decomposition occurs in the alloy with stoichiometric composition.

Bright field image of the furnace cooled Ti-47 at.% Pd alloy is shown in Fig. 5.3(a). There are three precipitate variants marked with I, II and III in the B19 martensite matrix. The electron diffraction patterns taken from the variants I, II and III are shown in Fig. 5.3(c), (e) and (g), respectively. The pattern in (g) is a micro area pattern obtained only from the variant III. All the diffraction spots from precipitate can be indexed by assuming Ti_2Pd phase of $C11_b$-type structure with a = 0.3090 and c = 1.0054 nm[11]. Schematic key-diagrams of the electron diffraction patterns in Fig. 5.3(c), (e) and (g) are presented in Fig. 5.3(d), (f) and (h). The orientation relationships between the precipitates and the martensite matrix are as follows:

Variant I: $(001)_{C11b} // (101)_{B19}$, $[010]_{C11b} // [010]_{B19}$

Variant II: $(001)_{C11b} // (10\bar{1})_{B19}$, $[100]_{C11b} // [010]_{B19}$

Variant III: $(001)_{C11b} // (010)_{B19}$, $[001]_{C11b} // [010]_{B19}$

We can notice that apparent habit planes of the variants I, II and III are $(101)_{B19}$, $(10\bar{1})_{B19}$ and $(010)_{B19}$, respectively. These notations of the variants are used invariantly hereinafter with respect to the apparent habit planes in the martensite matrix. According to the orientation relationship between the B2 parent and the B19 martensitic phases, these planes are derived from $\{001\}_{B2}$. The shape of precipitate is estimated to be disk-like and/or elliptic plate.

Similar crystallographic and morphological characteristics of precipitates of the $C11_b$ phase in B2 and/or B19 matrices have been reported in Ti-Ni-Cu shape memory alloys[12,13].

In order to make a clear distinction among the diffraction spots coming from TiPd matrix and Ti_2Pd precipitates in Fig. 5.3(c) and (e) SAEDP's taken separately from TiPd matrix and Ti_2Pd precipitate are shown in Fig. 5.4(b) and (d). Figure 5.4(a) is the BF image of a Ti-47at.%Pd alloy aged at 1073 K for 36 ks and then DSC-like treated at 923 K. A large Ti_2Pd precipitate (more than 100 nm in length) could be observed in the TiPd matrix. The schematic key-diagrams

corresponding to electron diffraction patterns in Fig. 5.4(b) and (d) are presented in Fig. 5.4(c) and (e), respectively.

5.4 Microstructure Modification during Successive Transformation

In order to clarify the microstructure change during DSC measurement, the same thermal history was given to the quenched and the furnace cooled Ti-47 and 50at.%Pd alloys.

From Fig. 5.5 becomes clear that there is no microstructure change in both quenched and furnace cooled Ti-50at.%Pd alloys, as expected from the above results.

Figure 5.6 shows bright field images and corresponding electron diffraction patterns in the quenched Ti-47at.%Pd alloy after DSC. There are fine precipitates in the martensite matrix in the quenched alloy as seen in Fig. 5.6(a) and (c). The electron diffraction pattern in Fig. 5.6(b) is taken from area B in (a). The pattern can be indexed the same as those in Fig. 5.3(b) and/or (c). Therefore, the precipitates are Ti_2Pd phase. It seems that there is only one variant in Fig. 5.6(a), which is more obvious in Fig. 5.6(c). A bright field image in Fig. 5.6(c) is taken along $[10\bar{1}]_{B19}$ as recognized from the corresponding diffraction pattern in (d). The pattern consists of three sets of reflections in which two of them are in mirror symmetry with respect to the (111) plane, thus alternate platelets are (111) twins. The rest pattern, as indicated by arrows, represents $[001]_{C11b}$ zone axis, the same as that in Fig. 5.3(d). From these observations we deduced that the morphology of the precipitates formed in the quenched Ti-47at.%Pd alloy after DSC measurement is disk-like with an average size about 40 nm in diameter and 15 nm in thickness. In addition, the habit plane of precipitates in Fig. 5.3(a) and (c) is $\{101\}_{B19}$, which corresponds to the variants I or II. We could not observe the variant III with habit plane of $(010)_{B19}$ in the quenched Ti-47at.%Pd alloy after DSC measurement throughout the present experiment.

Figure 5.7 shows a bright field image of the furnace cooled Ti-47at.%Pd after DSC. There is no significant difference in comparison with the microstructure before DSC seen in Fig. 5.3.

Therefore, it can be assumed that the successive transformation is closely related to the formation of fine Ti_2Pd precipitate during DSC measurement.

In order to confirm the above hypothesis, the microstructure change during DSC measurement was observed in detail along the DSC curves upon heating as shown in Fig. 5.8. The quenched Ti-47at.%Pd alloys are heated from ambient temperature to 743, 848 and 873 K with a heating rate of 10 K/min and then quenched into ice water. At 743 K, fine precipitates of less than 2 nm with strain contrast nucleate in the martensite matrix as seen in Fig. 5.9(a). The habit plane of the precipitates could not be recognized in this state. The precipitates grow with increasing heating temperature as shown in Fig. 5.9(b) and (c). Again, the variant III could not be observed in the quenched specimens heated up in DSC to 848 and 873 K. It seems that if the precipitates are nucleated in martensitic phase only two Ti_2Pd precipitate variants form in TiPd matrix. The precipitate variant selection in Ti-rich Ti-Pd alloys will be treated in Chapter 7.

5.5 Transformation Mechanism

On the basis of TEM observations and DSC measurements presented in Chapter 4 the successive transformation mechanism in the quenched Ti-rich Ti-Pd alloys can be summarized with the schematic illustration shown in Fig. 5.10. Below A2* peak fine Ti_2Pd precipitates nucleate in the martensite matrix during heating. By increasing the heating temperature the Ti_2Pd precipitates grow as shown in Fig. 5.9. The first endothermic peak represents the reverse martensitic transformation of the matrix. Since the Pd concentration increases in the local region around the precipitates, in these areas martensitic phase must be preserved after the occurrence of the first peak. Therefore, the A1* peak can be attributed to the reverse martensitic transformation of the local region around the precipitates. It is likely that the local equilibrium between the Ti_2Pd precipitate and the matrix with nearly equiatomic composition is completed around the precipitate.

This is supported by the fact that the A1* peak position of all the quenched Ti-rich alloys used in the present study is almost the same as the single endothermic peak of the Ti-50at.%Pd alloy as indicated in Figs. 4.1, 4.2 and 4.4. Figure 5.11 shows the schematic illustration of the successive martensitic transformation mechanism in quenched Ti-rich Ti-Pd during cooling process.

Based on the TEM observations, discussed above, the shift of transformation peaks with increasing the heating temperature in the incomplete thermal cycle experiments in Fig. 4.2 is explained as follows. The increase of A2* and M2* is due to the increase of Pd concentration in the matrix with the precipitation of Ti_2Pd phase. Since the precipitate reaction occurs not only during heating but also during cooling the Pd concentration of the matrix is different between heating and cooling processes. It is also likely that the reaction during cooling becomes more active with increasing the heating temperature. Therefore, the Pd concentration in the matrix during cooling may be higher than that during the previous heating. Consequently, the inversion between A2* and M2* takes place in Fig. 4.2(e). The decrease of M1* in Fig. 4.2(c) to (e) may be related to the strain field around the coherent precipitates which usually stabilizes the parent phase in the marensitic transformation[14-19]. We notice the strain contrast around the Ti_2Pd precipitate in Figs. 5.6(a), (c) and 5.9(a) to (c).

5.6 Conclusions

The martensitic transformation behavior of the Ti-rich Ti-Pd shape memory alloys has been investigated by TEM observations. The obtained results are summarized as follows.

(1) The quenched Ti-rich Ti-Pd alloys solution treated at 1273 K for 3.6 ks show successive martensitic transformation during heating in DSC. Before heating in DSC in the structure of these alloys there is only one phase, namely TiPd martensite with B19-type structure. After heating in DSC, beside TiPd phase, small Ti_2Pd precipitates could be observed. On the other

contrary, in the furnace cooled alloys that show a single step transformation no structural changes were observed during heating in DSC. At room temperature, two phases coexist in equilibrium, TiPd and Ti_2Pd, in the structure of furnace cooled alloys. Therefore, the successive transformation behavior is closely related to the formation of fine Ti_2Pd precipitates.

(2) The mechanism of successive transformation could be explained as follows. The first peak on DSC heating curve represents the reverse martensitic transformation of the TiPd matrix and the second one is due to the reverse martensitic transformation in the local neighboring areas of the precipitates in which Pd concentration is higher than that in matrix.

(3) The precipitate is Ti_2Pd with $C11_b$-type structure. There are three variants of precipitates, i. e., I, II and III with the apparent habit planes of $(101)_{B19}$, $(10\bar{1})_{B19}$ and $(010)_{B19}$, respectively, in the furnace cooled Ti-47at%Pd alloy in which the precipitate nucleates in the B2 parent phase. On the other hand, only two variants I and II are observed when precipitates nucleate in the martensitic phase.

References

1) H. C. Donkersloot and J. H. N. Van Vucht: *J. Less-Common Met.*, **20** (1970) 83.
2) Y. Shugo and T. Honma: *J. Institute of Mineral - Dressing and Smelting, Tohoku Univ.*, **43** (1987) 128.
3) Y. Shugo: *Mater. Sci. Forum*, **56-58** (1990) 631.
4) M. Nishida, Y. Morizono, H. Kijima, A. Ikeya, H. Iwashita and K. Hiraga: *Materials for Smart Systems II, Symposium Proceedings Volume 459*, ed. by E. P. George, R. Gotthard, K. Otsuka, Susan T. McKinstry and Marilyn Wun-Fogle, (Materials Research Society, 1997) pp. 375.
5) A. E. Dwight, R. A. Conner, Jr. and J. W. Downey: *Acta Cryst.*, **18** (1965) 835.
6) H. K. D. H. Bahadeshia: *Prog. Mater. Sci.*, **29** (1985) 321.
7) W. C. Johnson, C. L. White, P. E. Marth, P. K. Ruf, S. M. Tuominen, K. D. Wade, K. C. Russell and H. I. Aaronson: *Metall. Trans. A*, **6A** (1975) 911.
8) W. Pitsch and P. L. Ryder: *Scr. Metall.*, **11** (1977) 431.
9) K. Enami, H. Seki and S. Nenno: *Tetsu-to-Hagane (Journal of The Iron and Steel Institute, Japan)*, **72** (1986) 563.
10) M. Nishida, T. Hara, Y. Morizono, A. Ikeya, H. Kijima and A. Chiba: *Acta Metall.*, **11** (1997) 4847.
11) M. W. Nevitt and J. W. Downey: *Trans. of the Metallurgical Society of AIME*, **224** (1962) 195-196.
12) L. Chang and D. S. Grummon: *Scr. Metall.*, **25** (1991) 2079-2084.
13) T. Fukuda, M. Kitayama, T. Kakeshita and T. Saburi: *Mater. Trans. JIM*, **10** (1996) 1540-1546.
14) E. Hornbogen and W. Meyer: *Acta Metall.*, **15** (1967) 584-591.
15) M. Nishida and T. Honma: *Scr. Metall.*, **18** (1984) 1299-1302.
16) S. Miyazaki and K. Otsuka: *Metall. Trans. A*, **17A** (1986) 53-63.
17) S. Kajiwara, T. Kikuchi, T. Matsunaga and S. Miyazaki: *Philos. Mag. Lett.*, **74** (1996) 137-144.
18) J. Zhang, W. Cai, X. Ren, K. Otsuka and M. Asai: *Mater. Trans. JIM*, **40** (1999) 1367-1375.
19) H. Rösner, P. Schloßmacher, A. V. Shelyakov and A. M. Glezer: *Acta Mater.*, **49** (2001) 1541-1548.

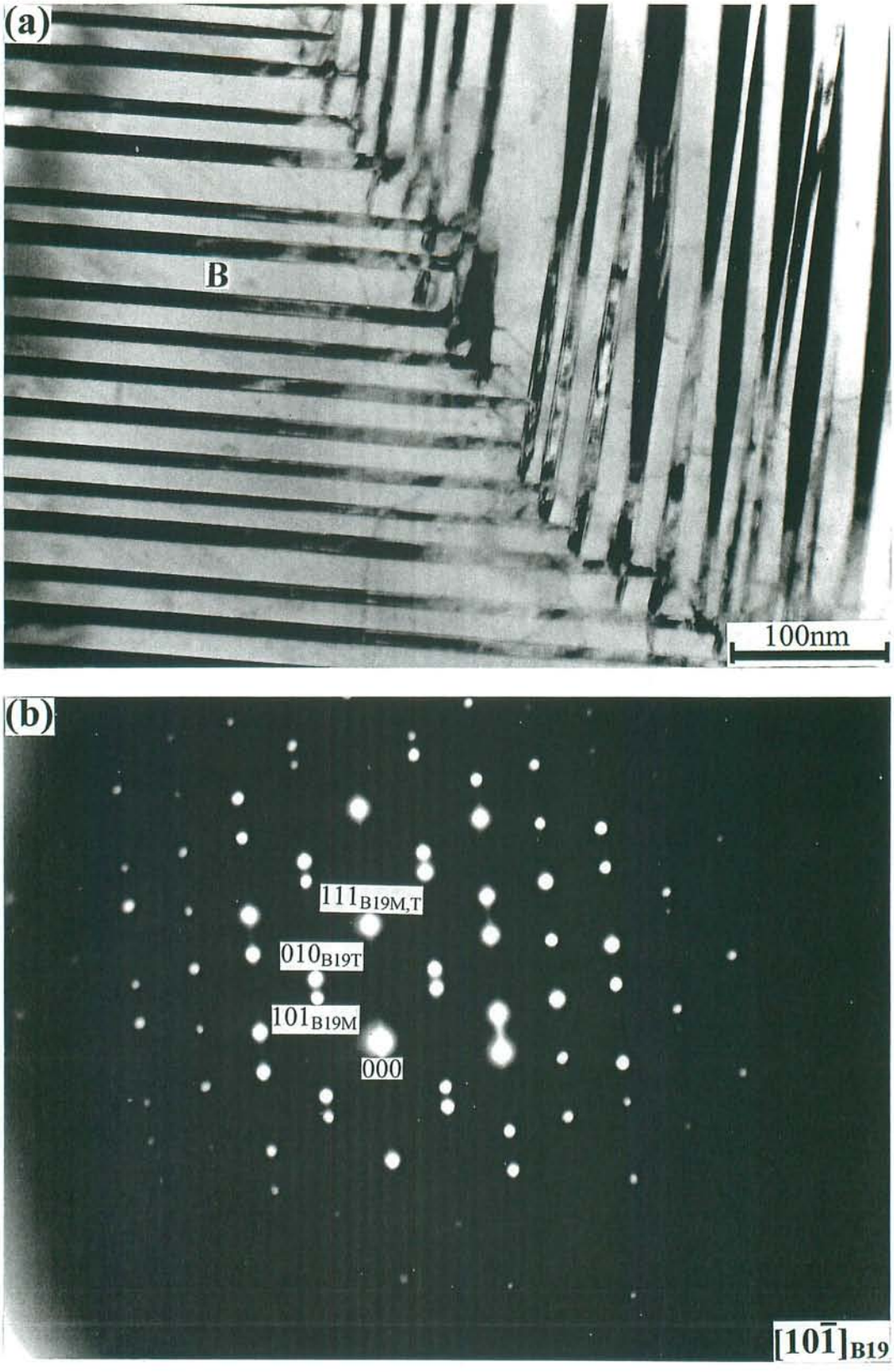

Fig. 5.1 (a) Bright field image of the B19 martensite in a quenched Ti-47at.%Pd alloy solution treated at 1273 K for 3.6 ks. (b) Selected area diffraction pattern taken from variant B in (a), showing the {111} Type I twin relation.

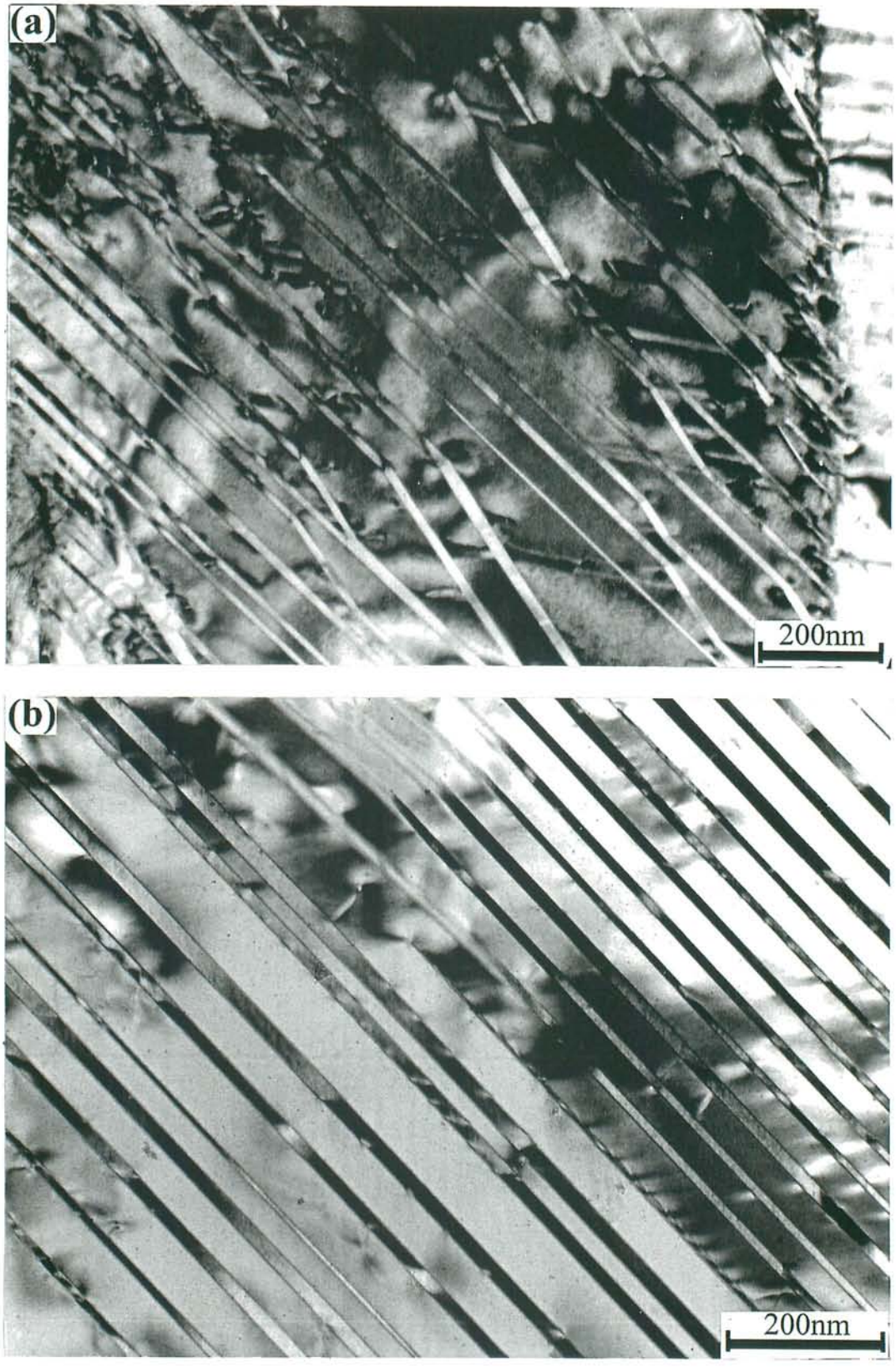

Fig. 5.2 Bright field images of (a) quenched and (b) furnace cooled Ti-50at.%Pd alloy solution treated at 1273 K for 3.6 ks.

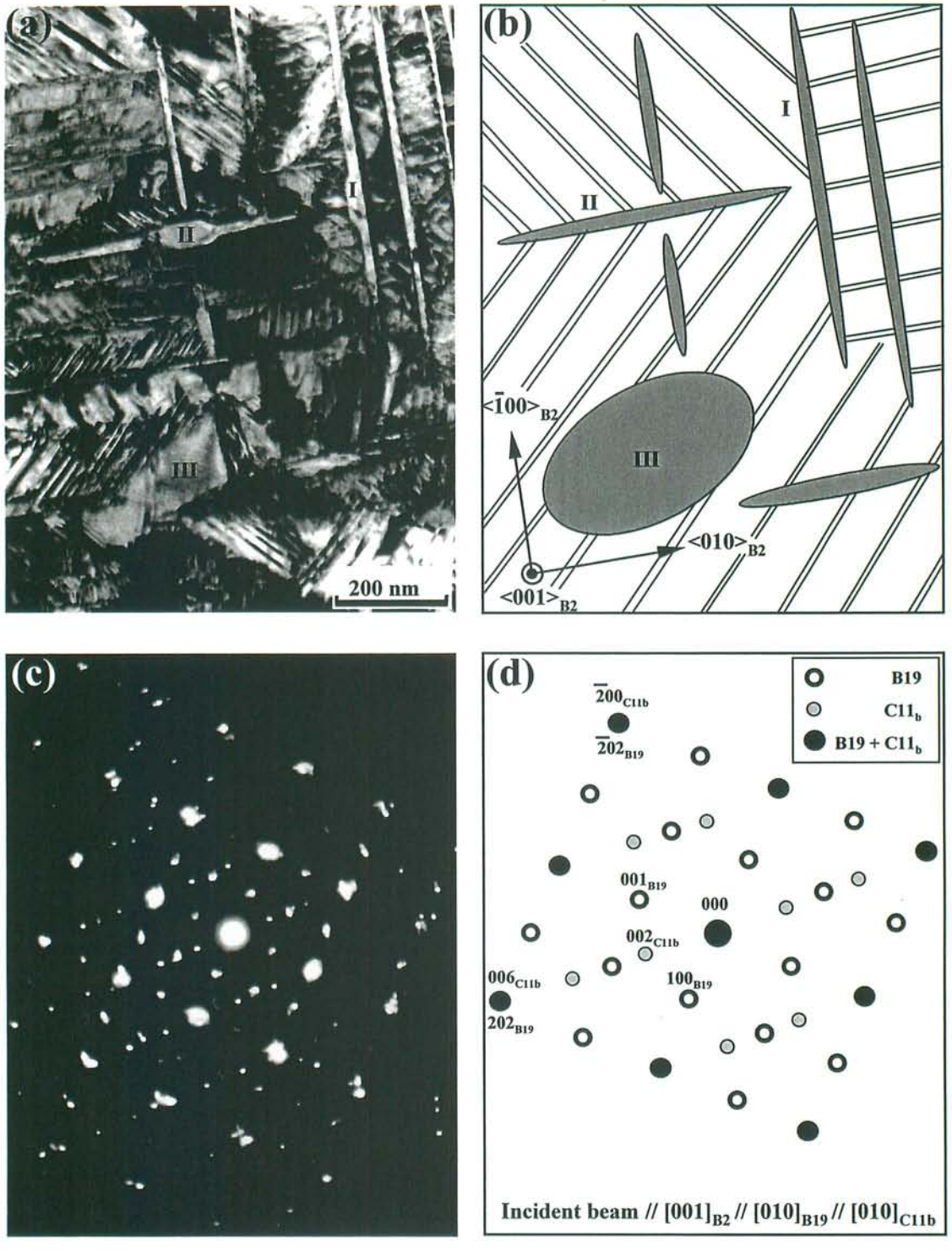

Fig. 5.3 (a) Bright field image of a furnace cooled Ti-47at.%Pd alloy. (b) Schematic drawing of (a). (c) Selected area electron diffraction pattern taken from Ti_2Pd precipitate variant I in (a). (d) Schematic key-diagram of electron diffraction pattern in (c).

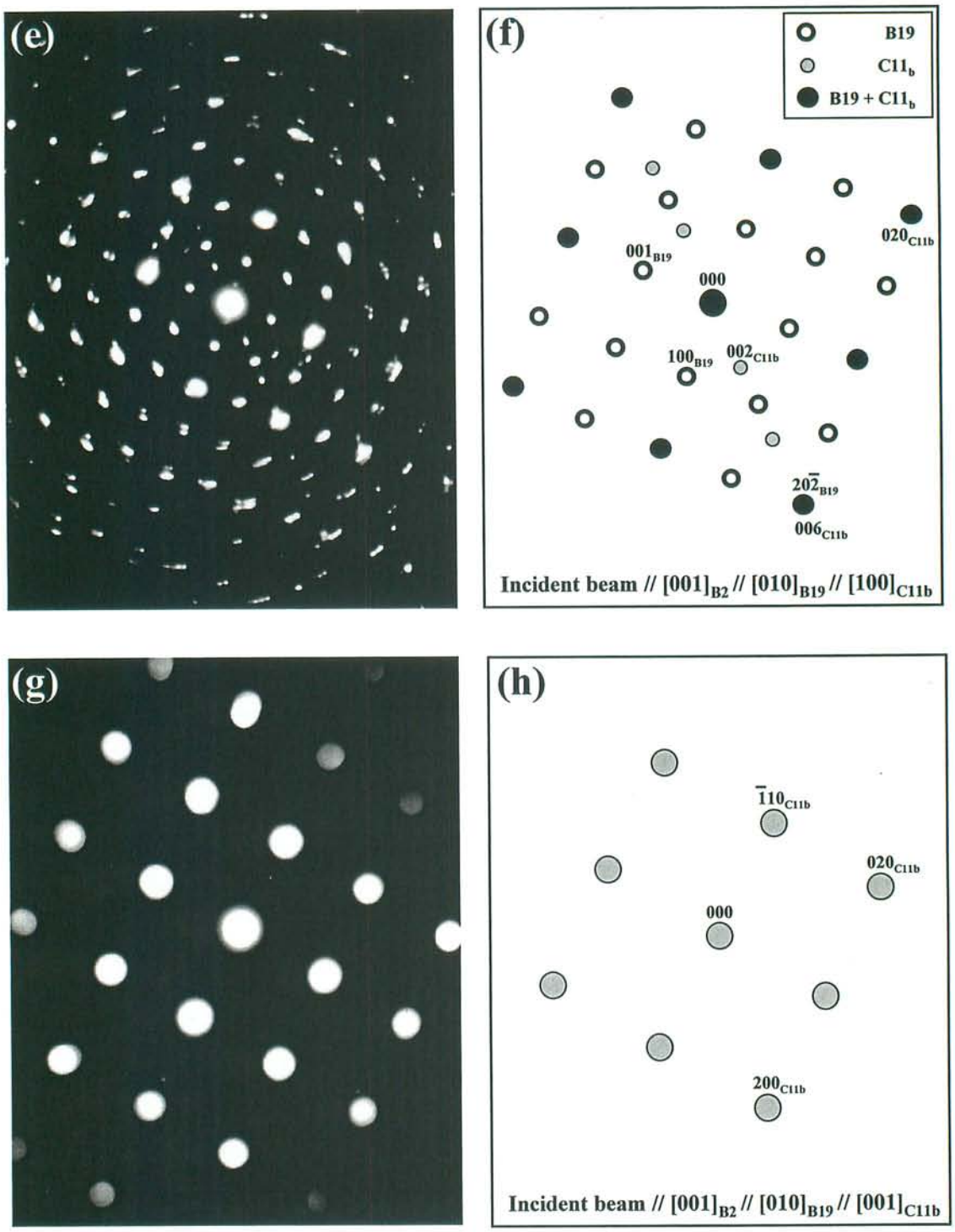

Fig. 5.3 (cont.) (e) Selected area electron diffraction pattern taken from precipitate variant II in (a). (g) Micro area electron diffraction pattern taken from precipitate variant III in (a). (f), (h) Schematic key-diagrams of diffraction patterns in (e) and (g), respectively.

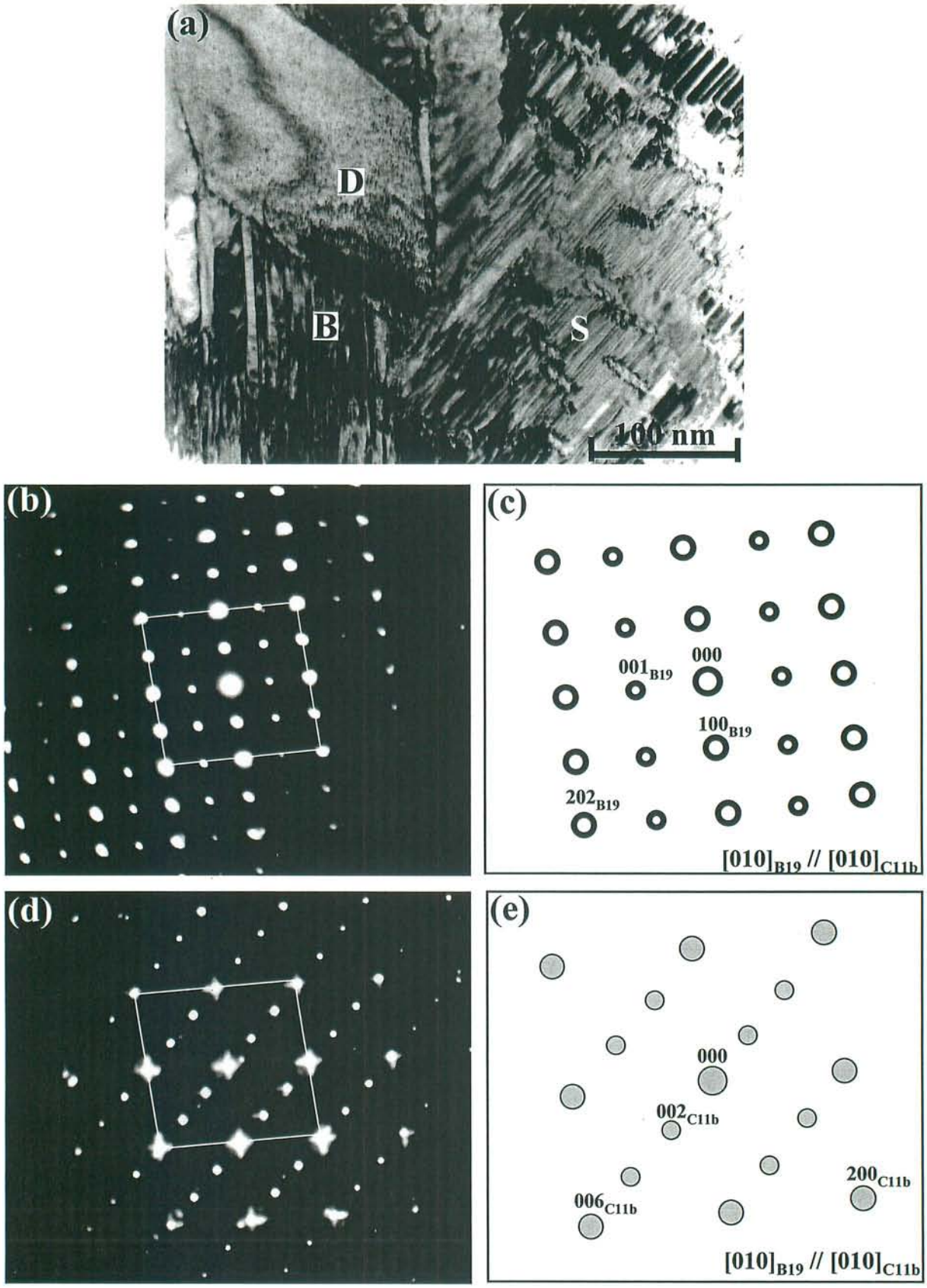

Fig. 5.4 (a) BF image of a Ti-47at.%Pd alloy aged at 1073 K for 36 ks and then DSC-like treated at 923 K showing three distinct zones: D - large Ti_2Pd precipitate, B - martensite matrix (TiPd phase) and S - small Ti_2Pd precipitates in TiPd matrix. (b), (d) SAEDP taken from TiPd matrix (area B in (a)) and from Ti_2Pd precipitate (area D in (a)), respectively. (c), (e) Schematic key-diagrams of the EDP's in (c) and (d), respectively.

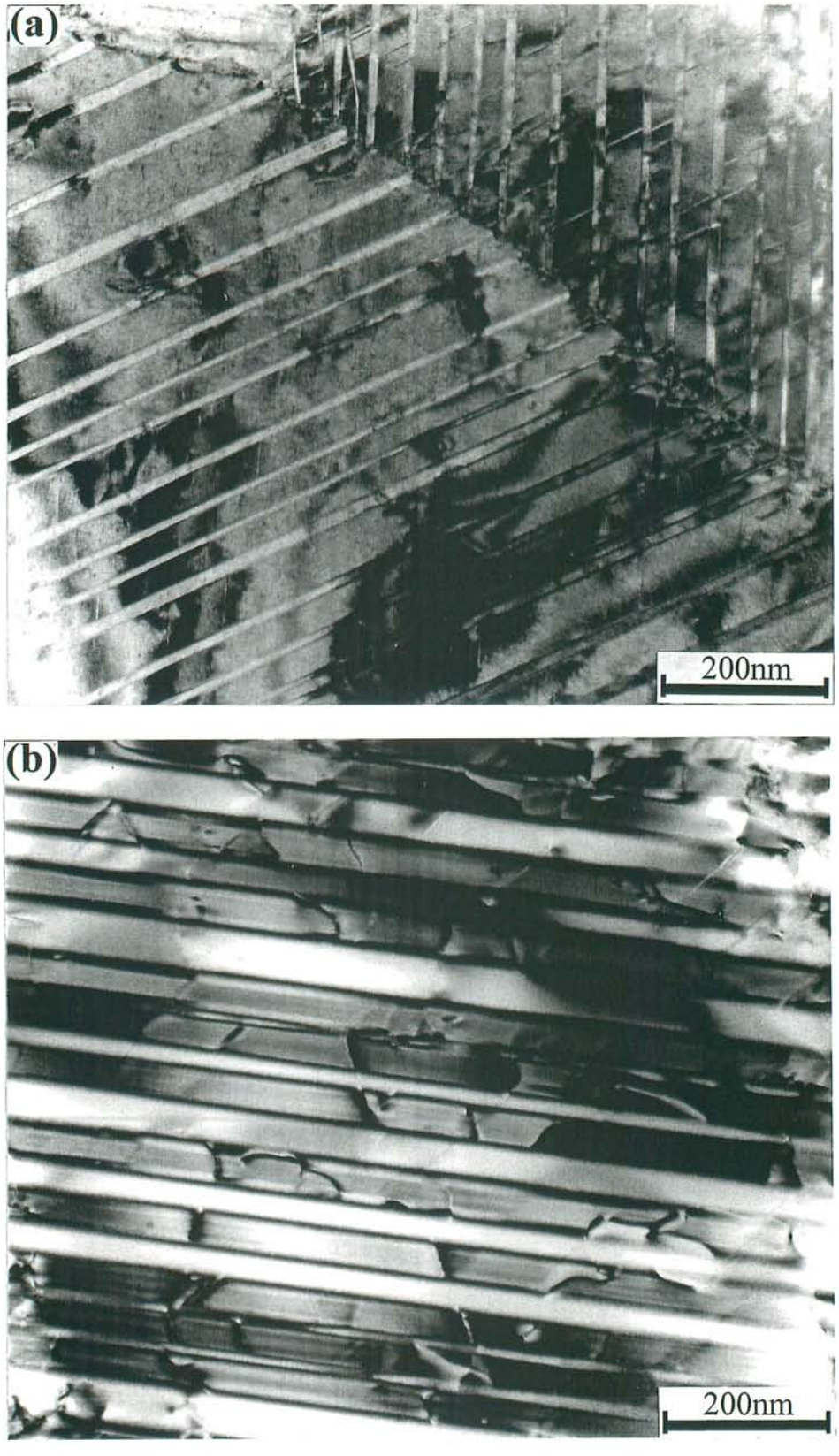

Fig. 5.5 Bright field images of (a) quenched and (b) furnace cooled Ti-50at.%Pd alloy after heated in DSC at 973 K and then quenched into ice water.

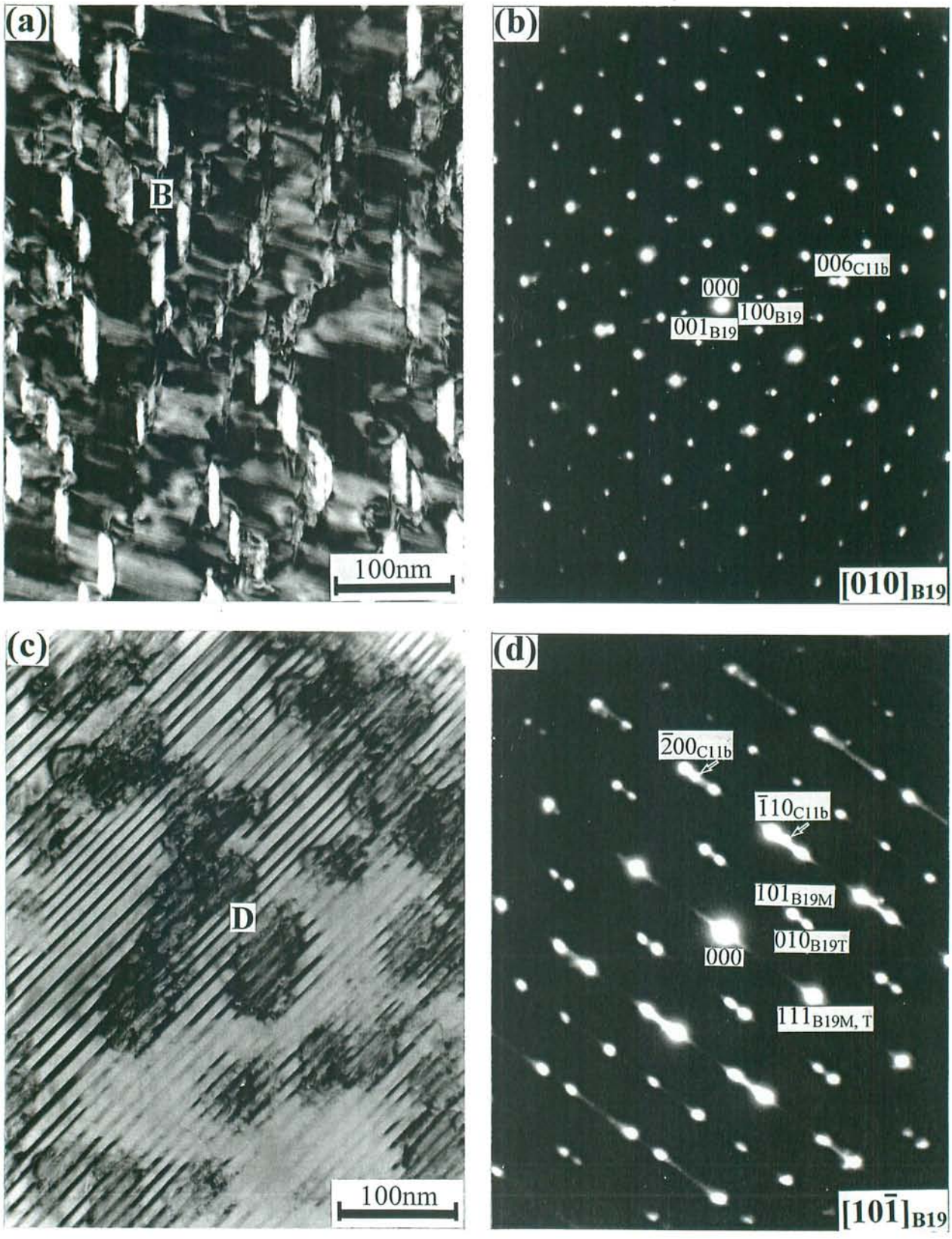

Fig. 5.6 (a), (c) Bright field images of water quenched Ti-47at%Pd alloy after heated in DSC at 973 K and then quenched into ice water. (b), (d) Selected area electron diffraction patterns taken from (a) and (c) showing $[010]_{B19}$ and $[10\bar{1}]_{B19}$ zone axes, respectively. Subscripts M and T are used to denote matrix and twin, respectively.

Fig. 5.7 Bright field image of furnace cooled Ti-47at.%Pd alloy after heated up in DSC at 973 K and then quenched into ice water.

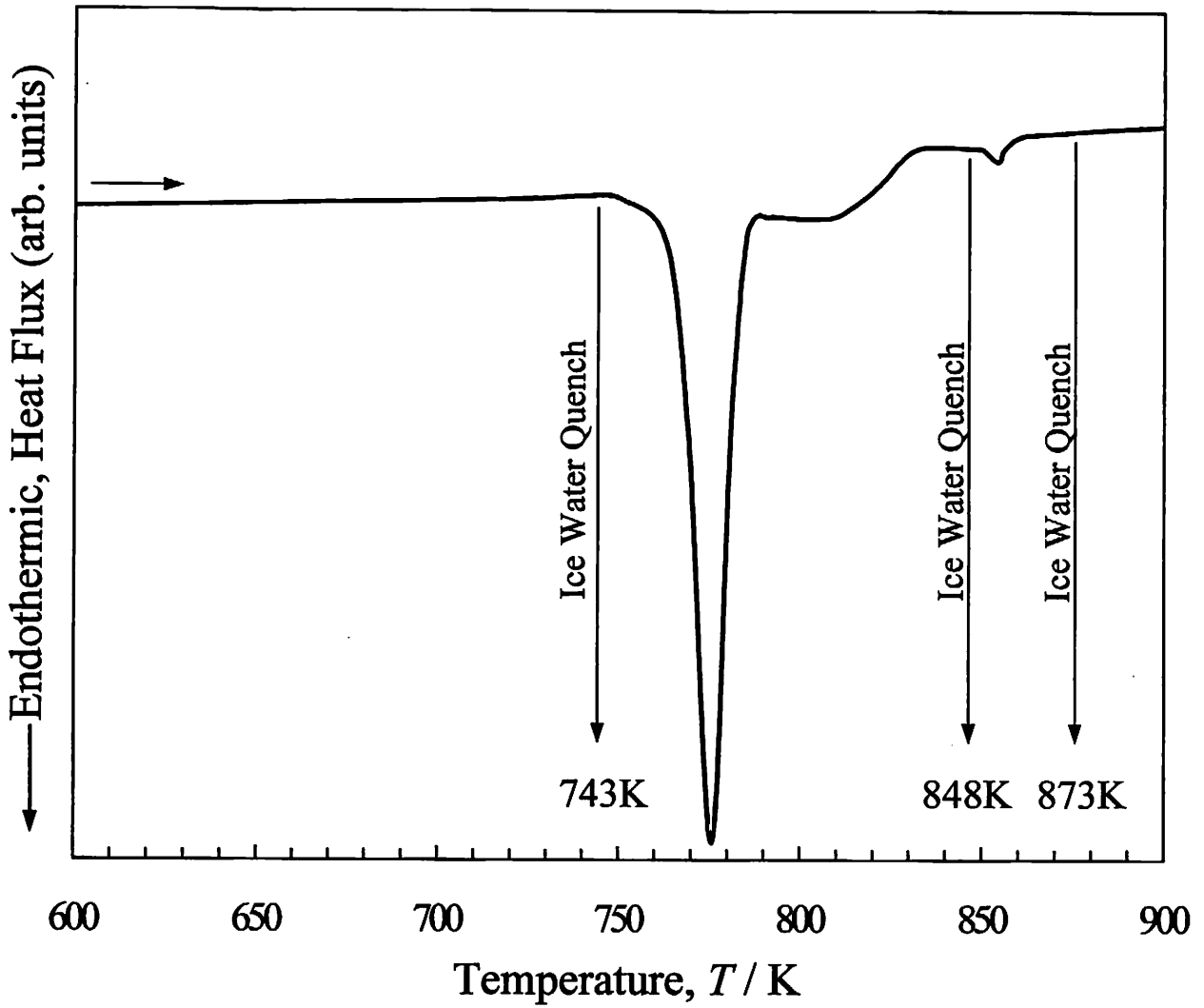

Fig. 5.8 Schematic diagram showing temperatures of TEM observations of the quenched Ti-47at.%Pd alloy. The specimens for TEM observations were heated up to 743, 848 and 873 K with the same heating rate of 10 K/min as in DSC and finally quenched into ice water.

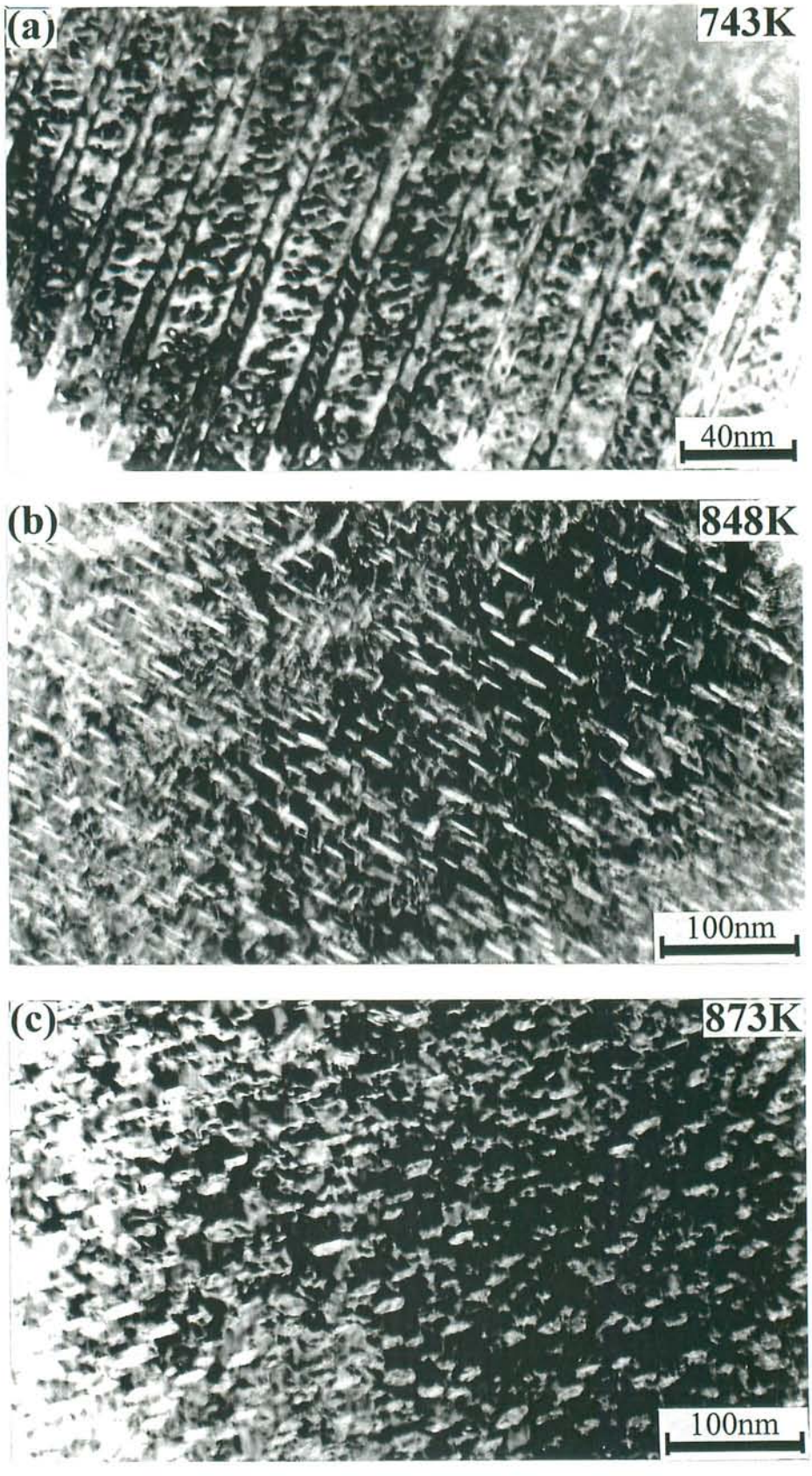

Fig. 5.9 Bright field images of the Ti-47at.%Pd alloy quenched from (a) 743 K, (b) 848 K and (c) 873 K after DSC-like heat treatment.

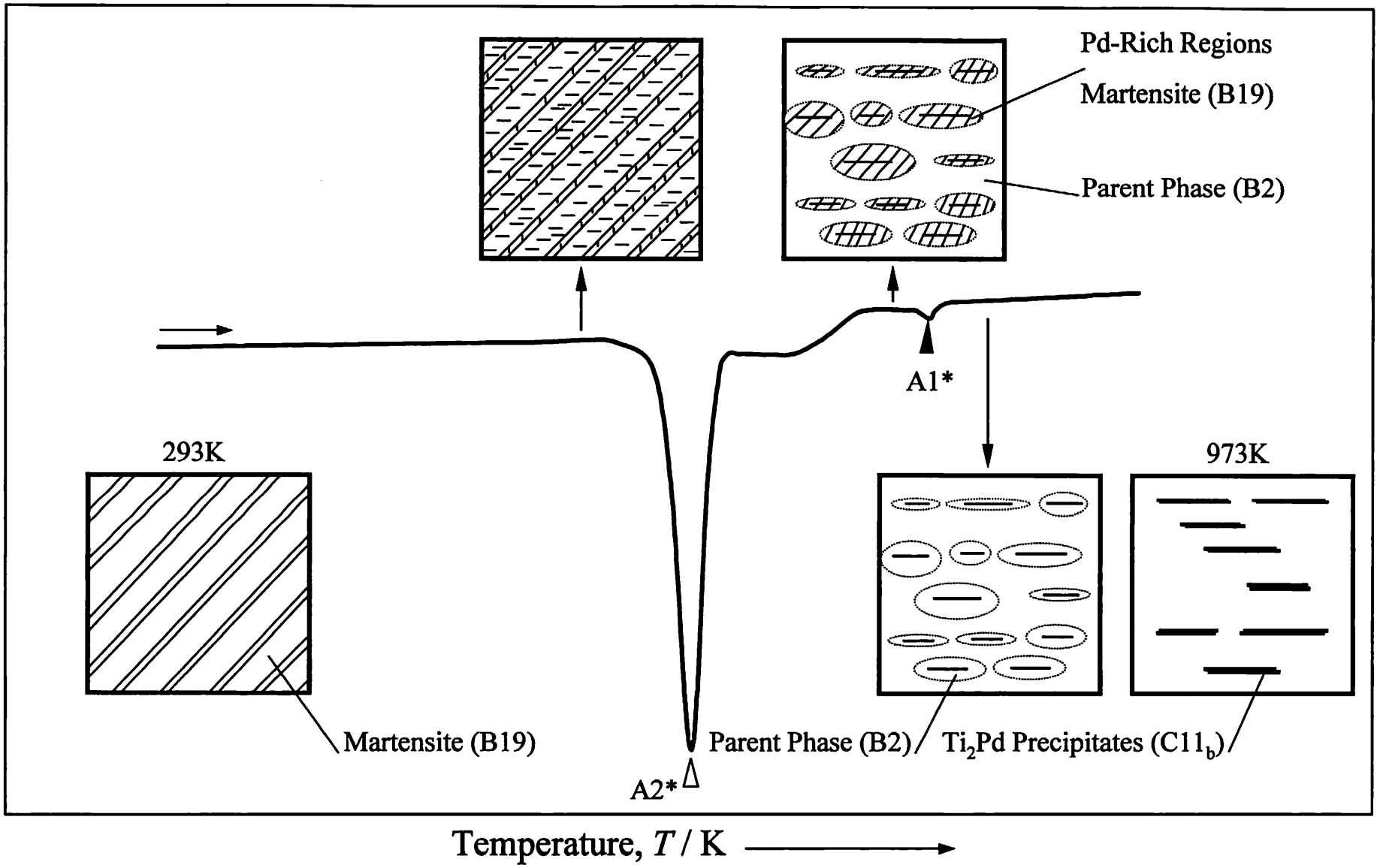

Fig. 5.10 Schematic illustration of the successive transformation mechanism in Ti-rich Ti-Pd alloys quenched from the single B2 parent phase during heating in DSC.

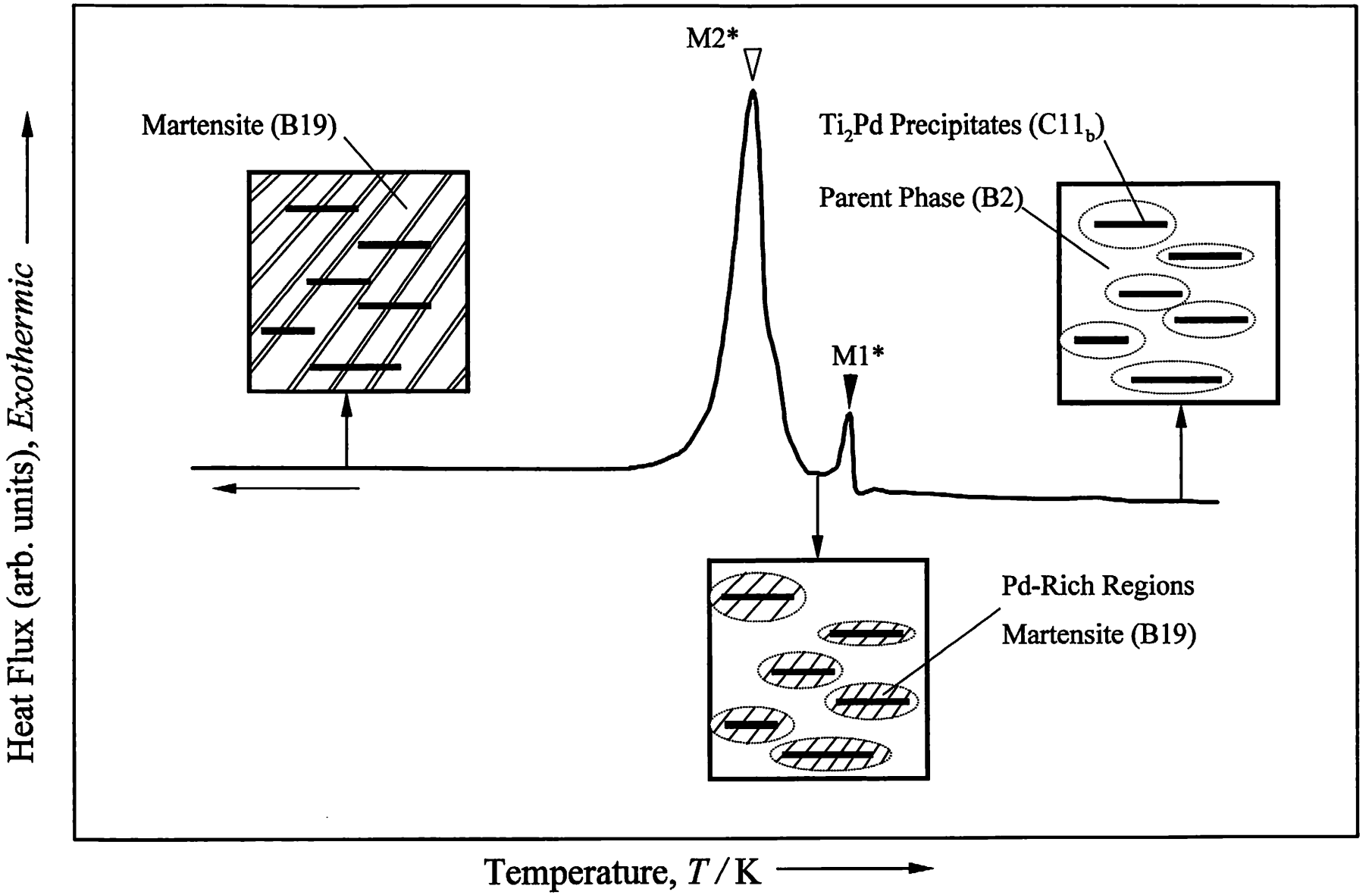

Fig. 5. 11 Schematic illustration of the successive martensitic transformation mechanism in quenched Ti-rich Ti-Pd alloys, during cooling process.

Chapter 6

Effect of Aging on Martensitic Transformation in Near-Equiatomic Ti-Pd Shape Memory Alloys

6.1 Introduction

In the previous chapter the mechanism of successive transformation in near equiatomic Ti-rich Ti-Pd alloys was discussed in connection with the formation of fine Ti_2Pd precipitates with $C11_b$-type structure. Upon heating the first transformation step represents the reverse martensitic transformation of the TiPd matrix, while the second one is due to the reverse martensitic transformation of small neighboring volume of Ti_2Pd precipitate at which Pd concentration is higher than that of the matrix. Also, three precipitates variants were observed in furnace cooled specimens, while in the quenched ones after heating in DSC only two precipitate variants were observed. The number of variants seems to depend on the nucleation site of the precipitates, i. e. three precipitate variants were observed when nucleate in the parent phase and only two were observed when nucleated in martensitic phase.

Since the mechanism of successive transformation in Ti-rich near-equiatomic Ti-Pd alloys is connected with the nucleation and growth of Ti_2Pd precipitates which are controlled by diffusion process, both aging temperature and time will greatly affect the transformation behavior. Therefore, it is very interesting and useful to find out how transformation proceeds with different aging treatments.

In this chapter will be introduced the effect of aging on successive martensitic transformation in near-equiatomic Ti-rich Ti-Pd alloys investigated by means of DSC

measurements and TEM observations. Subsequently, the equilibrium phase boundary of TiPd compound in Ti-rich side will be estimated on the basis of transformation behavior. The change of transformation behavior with aging condition is discussed on the basis of phase equilibrium between TiPd matrix and Ti_2Pd precipitate.

6.2 Experimental Procedure

The transformation behavior of the near-equiatomic Ti-rich Ti-Pd alloys is essentially the same except for the transformation temperatures which are specific to each composition as was shown before. Therefore, we chose a Ti-47at.%Pd alloy for studying the effect of aging on martensitic transformation behavior.

The Ti-47at.%Pd alloy and DSC and TEM specimens were prepared in the same way as described in the previous chapters. The specimens for DSC measurements were heated and cooled at several rates from 3 to 25 K/min. The quenched Ti-47at.%Pd solution treated specimens were also cycled thermally between room temperature and 973K for 10 times and the transformation temperatures after each cycle were measured by DSC with a heating and cooling rate of 10K/min. After solution treatment the specimens for DSC measurements and for TEM observations were aged at different temperatures ranging from 873 K to 1273 K from various periods ranging from 1.8 ks to 720 ks. The specimens were introduced in the furnace after the setting temperature becomes stable. Thus, the heating time needed to reach the setting temperature was decreased to the smallest extent possible. After aging treatment the specimens were quenched into ice water. Some of the aged TEM specimens were subjected to the same thermal history of DSC measurement. In other words, they were heated up to prescribed temperatures with the rate of 10 K/min in a muffle furnace equipped with digital program controller, and then quenched into ice water. This operation was denote as DSC-like heat treatment. The DSC experiments and TEM observations were carried out in a Shimadzu DSC-50 calorimeter and a JEM-2000FX electron microscope, respectively.

6.3 Effect of Aging on the Martensitic Transformation Behavior

Figure 6.1 shows the DSC curves measured at different heating rates for Ti-47at.%Pd alloy. For relatively low heating rates (3 and 5 K/min) an intermediary sharp peak could be observed between A2* an A1* on the heating curve. The intermediate peak is denoted as A2-1*. The A2-1* peak could also be observed at heating rates higher than 5 K/min but it shrinks and the A2* peak develops with increasing the heating rate. In the same time, the position of A1* on the DSC heating curves is independent of the heating rate. The change of the DSC curve profile with the heating rate indicates that a diffusion process occurs in the specimen structure. The diffusion process is connected with nucleation and growth of Ti_2Pd precipitates in TiPd matrix, as discussed in previous chapters.

It seems that with decreasing the heating rate below 10 K/min the A2-1* peak develops on the expense of A2* peak. Therefore, it could be concluded that A2* and A2-1* peaks are connected by the same transformation process and this fact will be proved below by aging experiments. In the present work, the heating and cooling rate of 10 K/min was used.

Figure 6.2 shows the effect of aging time on the transformation behavior of the Ti-47at.%Pd alloy aged at 873 K after quenching from 1273 K. The successive transformation takes place only in the specimen aged for relatively short time (3.6 ks). The temperature range of the first reaction is shifted to high temperature region by increasing in aging time, and the A2* peak overlaps the A1* peak in the case of the specimens aged less than 180 ks. The transformation behavior is fairly identical and stable in the specimens aged for more than 180 ks, and the peak position of these specimens lie at the same temperature as the A1* peak of the specimen aged for 3.6 ks. It can be concluded that the quenched Ti-47 at.% Pd alloy aged at 873 K attains the stable state by aging for more than 180 ks.

Figures 6.3 to 6.9 show the DSC heating curves of the Ti-47at.%Pd alloy aged at 973 K, 1023 K, 1073 K, 1123 K, 1173 K, 1223 K and 1273 K for various periods indicated at the left hand

side of each figure. In all the cases, after relatively short aging period (3.6 ks), two endothermic peaks are observed along the DSC heating curve. The A2* shifts its position depending on the aging temperature. In the specimens aged below 1123 K the peak temperature first rises and then lowers with increasing aging temperature. On the other hand, in the specimens aged above 1123 K the A2* peak temperature is independent of aging temperature. The higher temperature peak denoted as A1* is unaffected by the aging temperature and lies at the same position within experimental errors. The A1* peak temperature is nearly identical with the reverse martensitic transformation peak temperature of the equiatomic Ti-Pd alloy, as discussed in Chapter 4. The variation of A2* peak indicates that compositional and/or structure changes occur during aging in the specimens aged below 1023 K.

The effect of aging conditions on the reverse transformation peak temperatures is summarized in Fig. 6.10. Here, the A1* and A2* peaks temperatures in the specimens aged at various temperatures for 3.6 ks and relatively prolonged period are plotted as function of aging temperature. The relatively prolonged period is defined as the aging time by which the transformation behavior has become stable. For instance, the relatively prolonged period is 180 ks or more in the specimen aged at 873 K as shown in Fig. 6.2. All the specimens aged for 3.6 ks show two endothermic peaks independently of the aging temperature as described above. In this case the A1* presents no significant variation with the aging temperature, while A2* firstly increases and then decreases with decreasing aging temperature below 1073 K, as pointed out before. The A2* peak shows almost constant temperature in the specimens aged above 1123 K for 3.6 ks. Only one endothermic peak appears in the specimen aged below 1023 K for relatively prolonged period. Although the A1* and A2* peaks temperatures in the specimens aged above 1073 K for prolonged period are slightly higher than those for 3.6 ks, essentially the same successive transformation takes place. As apparently from Fig. 6.10 the compositional and/or structural changes may occur during aging in the specimens aged below 1023 K.

The phase equilibrium is completed above 1073 K within aging for 3.6 ks and/or no diffusion process such as decomposition occurs during aging. Therefore, in this case the specimen is in the homogeneity range of TiPd compound at the prescribed temperature. The slight increase of A1* and A2* in the specimen aged above 1073 K for prolonged period is probably due to the decrease of Ti concentration by evaporation and/or oxidation during aging.

Fig. 6.11 shows the effect of thermal cycling on transformation behavior of the solution treated Ti-47at.%Pd alloy. The A2* peak temperature it is almost constant by increasing the number of cycles, while A1* shifts to higher temperatures until after the fourth thermo-cycling only one endothermic peak appear on DSC heating curve. The effect of thermal cycling on transformation temperatures is equivalent to the effect of aging at a temperature around 973K.

6.4 Microstructure of Aged Specimens

Figure 6.12(a) is a bright field image of the microstructure in the Ti-47at.%Pd alloy aged at 873 K for 3.6 ks that shows the successive transformation as described in Figs. 6.2 and 6.10. There are Ti_2Pd precipitates with $C11_b$-type structure in the B19 martensite matrix. Both phases were identified by electron diffraction experiment. Morphological and crystallographic characteristics of the precipitates will be described later in this chapter and in the next one. Only B19 martensite phase was observed in the specimen quenched from 1273 K before aging, as seen in Fig 5.1. Therefore, the Ti-47at.%Pd is without doubt in the two-phase region at 873 K. Figure 6.12(b) shows a bright field image of the microstructure in Ti-47at.%Pd alloy aged at 873 K for 3.6 ks and then quenched, and heated again to just above A1* with 10 K/min in an identical manner to the DSC specimens. The latter treatment is called DSC-like treatment hereinafter. Both bright field images in (a) and (b) are recorded from $[010]_{B19}$ orientation. The size and density of precipitates increase after DSC-like treatment, as shown in (b). It is easily supposed that some of precipitates grow and some others newly nucleate during DSC-like treatment.

The bright field image in Fig. 6.13(a) is the microstructure of the Ti-47at.%Pd alloy aged at 873 K for 360 ks which shows no successive transformation as can be observed from Fig. 6.2. The precipitate grows several hundreds nm in length and several tens nm in thickness. Figure 6.13(b) shows a bright field image of the microstructure in Ti-47at.%Pd alloy aged at 873 K for 360 ks and then DSC-like treated. There is no change in the microstructure between (a) and (b). In other words, no decomposition takes place during the DSC treatment.

Figure 6.14(a) is a bright field image of the microstructure in Ti-47at.%Pd alloy aged at 1073 K for 36 ks that shows the successive transformation as plotted in Figs. 6.5 and 6.10. Rather large precipitates are observed but their density is quite low. On the other hand, one can see fine precipitates together with large precipitate denoted as L in the martensite matrix of the Ti-47at.%Pd alloy aged at 1073 K for 36 ks and then DSC-like treated, as shown in Fig. 6.14(b). These observations indicate that the Ti-47at%Pd alloy is in TiPd + Ti_2Pd duplex phase region at 1073 K. Only B19 martensite with no Ti_2Pd precipitate is observed in the specimens aged at 1123 K and 1273 K for 36 ks, as shown in Fig. 6.15. This observation supports the hypothesis that the phase boundary of TiPd single and TiPd + Ti_2Pd duplex phases in the Ti-47at%Pd alloy is between 1073 and 1123 K.

From Figs. 6.12, 6.13 and 6.14 is concluded that when the specimen shows the successive transformation, fine precipitates are always observed in the martensite matrix. We have pointed out that the successive transformation is intimately related to the formation of fine precipitates of Ti_2Pd phase during heating in DSC measurement. Therefore, the present TEM observations are consistent with the results of the previous chapters.

6.5 Homogeneity Range of TiPd

When comparing Fig. 6.10 and Fig. 4.4, one can roughly estimate the homogeneity range of TiPd compound, as shown in Figs. 6.16 and 6.17. The A2* peak temperature of the Ti-47at.%Pd alloy aged at 873 K for prolonged period in Fig. 6.10 is about 853 K that can be extrapolated to the

A2* of Ti-49.6at.%Pd in Fig. 4.4. This indicates that the matrix composition of the specimen in equilibrium with Ti_2Pd phase is about Ti-49.4at.%Pd at 873 K. In the same way, the equilibrium compositions of matrix are estimated to be Ti-49.0, 48.8 and 48.2 at.%Pd at 973, 1023 and 1073 K, respectively. It is also noted that the phase boundary of TiPd single and TiPd + Ti_2Pd duplex phases in the Ti-47at.%Pd alloy is considered to be in the temperature range between 1073 and 1123 K. These results indicate that the phase boundary of the TiPd compound in Ti side extends from near-equiatomic composition of about 50.4 at.%Ti at around 873 K to about 51.8 at.%Ti at 1073 K. This result is consistent with the previous reports[1-3], as shown in Fig. 2.1.

6.6 Transformation Mechanism in Aged Near-Equiatomic Ti-Rich Ti-Pd Alloys

The transformation mechanism of the aged Ti-47at.%Pd alloy is explained consistently on the basis of experimental results and the homogeneity range of TiPd estimated above, as follows.

The successive transformation occurs irrespective of the aging period when the specimen is aged above 1123 K. The specimen is in homogeneity range of TiPd compound above 1123 K and the single TiPd phase is obtained by quenching. Therefore, the successive transformation takes place with the formation of fine Ti_2Pd precipitates during heating of DSC measurement as concluded in the previous chapters. The transformation behavior around 1073 K is independent of the aging period. However, the Ti-47at.%Pd alloy is in the duplex phase region, i. e., TiPd and Ti_2Pd phases, as shown in Fig. 6.13(a). The equilibrium between TiPd and Ti_2Pd phases is completed within 3.6 ks. After aging and then quenching from around 1073 K the supersaturated Ti in TiPd matrix is considered to be sufficient for the precipitation of Ti_2Pd during the heating for DSC measurement, since the homogeneity range of TiPd decreases from about 51.8 at.%Ti at 1073 K to about 50.4 at.%Ti at 873 K. It is likely that the supersaturated Ti further increases at room temperature. Therefore, the fine Ti_2Pd precipitates appear in the specimen aged at 1073 K for 36 ks and then subjected to DSC-like treatment as seen in Fig. 6.14(b). Consequently, DSC detects

inevitably the successive transformation. The successive transformation also takes place when the specimen is aged below 1023 K for short period. With lowering the aging temperature the prolonged period is required to establish the equilibrium between TiPd and Ti_2Pd. Therefore, the TiPd matrix still contains enough supersaturated Ti for the nucleation and/or growth of Ti_2Pd precipitates. This is confirmed by the TEM observations in Fig. 6.12. No decomposition occurs after prolonged aging, since the equilibrium between TiPd and Ti_2Pd is completed and there is no sufficient supersaturated Ti for the precipitation of Ti_2Pd in the TiPd matrix. Therefore, no fine precipitate is observed in the specimen aged at 873 K for 360 ks as shown in Fig. 6.13(b).

The present explanation, together with the conclusions of the previous chapters, gives the systematic understanding of the successive transformation mechanism in the near-equiatomic Ti-rich Ti-Pd alloys.

6.7 Conclusions

The effect of aging on successive martensitic transformation in the near-eqiatomic Ti-rich Ti-Pd alloys was investigated and discussed based on the experimental results of DSC measurements and TEM observations. Below are summarized the results of this chapter.

1) Transformation behavior is greatly affected by aging conditions. Successive transformation takes place in the Ti-47at.%Pd alloy after short time aging irrespective of aging temperature. On the other hand, only the specimen aged above 1073 K shows successive transformation after relatively prolonged period.

2) The homogeneity range of the TiPd compound in Ti-rich side is estimated to extends from the near-equiatomic composition of about 50.4 at.%Ti at around 873 K to about 51.8 at.%Ti at 1073 K.

3) The mechanism of transformation behavior in aged Ti-47at.%Pd alloy is explained based on the experimental results and the homogeneity range of TiPd compound, as follows:

- In the specimens aged above 1123 K successive transformations occur irrespective of aging period. Successive transformation behavior is connected to the formation of fine Ti_2Pd precipitates and takes place in the same way as in solution treated alloys. The first transformation step on heating represent the reverse transformation of the TiPd matrix, while the second one is due to the reverse martensitic transformation in small volumes around Ti_2Pd precipitates where Pd concentration is higher than in the matrix.
- The successive transformation behavior is independent of aging time in the specimens aged around 1073 K. Although the equilibrium between TiPd and Ti_2Pd is completed after short time aging, by cooling the specimens to the room temperature, the TiPd matrix become supersaturated in Ti as could be understood from the variation of the homogeneity range of TiPd compound. By heating, new precipitates will nucleate and grow in the matrix and therefore, the conditions for successive transformation are accomplished.
- After relatively prolonged period successive transformations do not appear in the specimens aged below 1023 K since the equilibrium between TiPd and Ti_2Pd is stable, and the matrix is not any more supersaturated in Ti for formation of new precipitates.

References

1) Y. Shugo and T. Honma: *J. Institute of Mineral - Dressing and Smelting in Tohoku Univ.*, **43** (1987) 128.
2) Y. Shugo: *Mater. Sci. Forum*, **56-58** (1990) 631.
3) M. Nishida, Y. Morizono, H. Kijima, A. Ikeya, H. Iwashita and K. Hiraga: *Materials for Smart Systems II, Symposium Proceedings Volume 459*, ed. by E. P. George, R. Gotthard, K. Otsuka, Susan T. McKinstry and Marilyn Wun-Fogle, Materials Research Society (1997) 375.

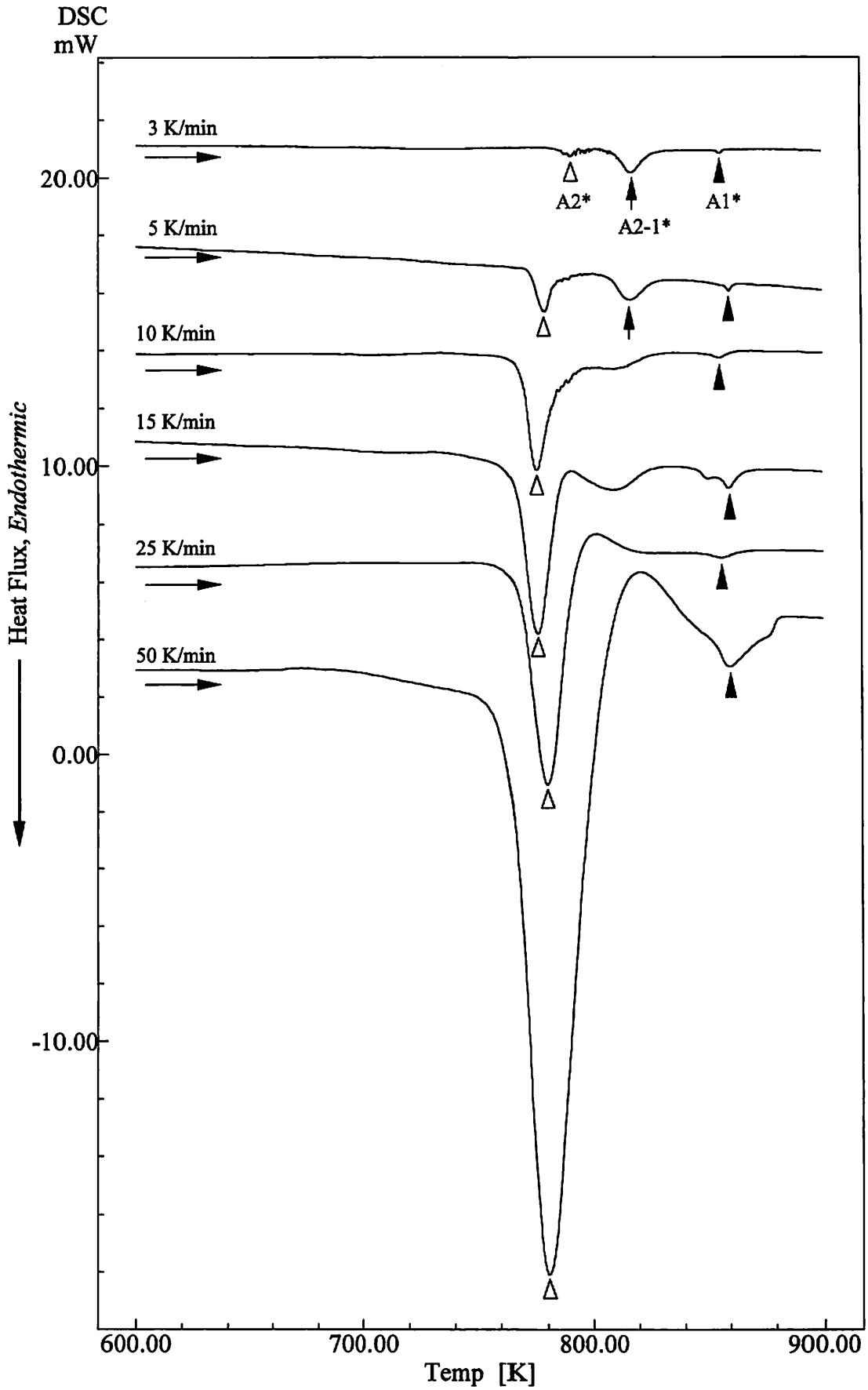

Fig. 6.1 DSC heating curves of the quenched Ti-47at.%Pd alloy solution treated at 1273 K for 3.6 ks, obtained with the different heating rates.

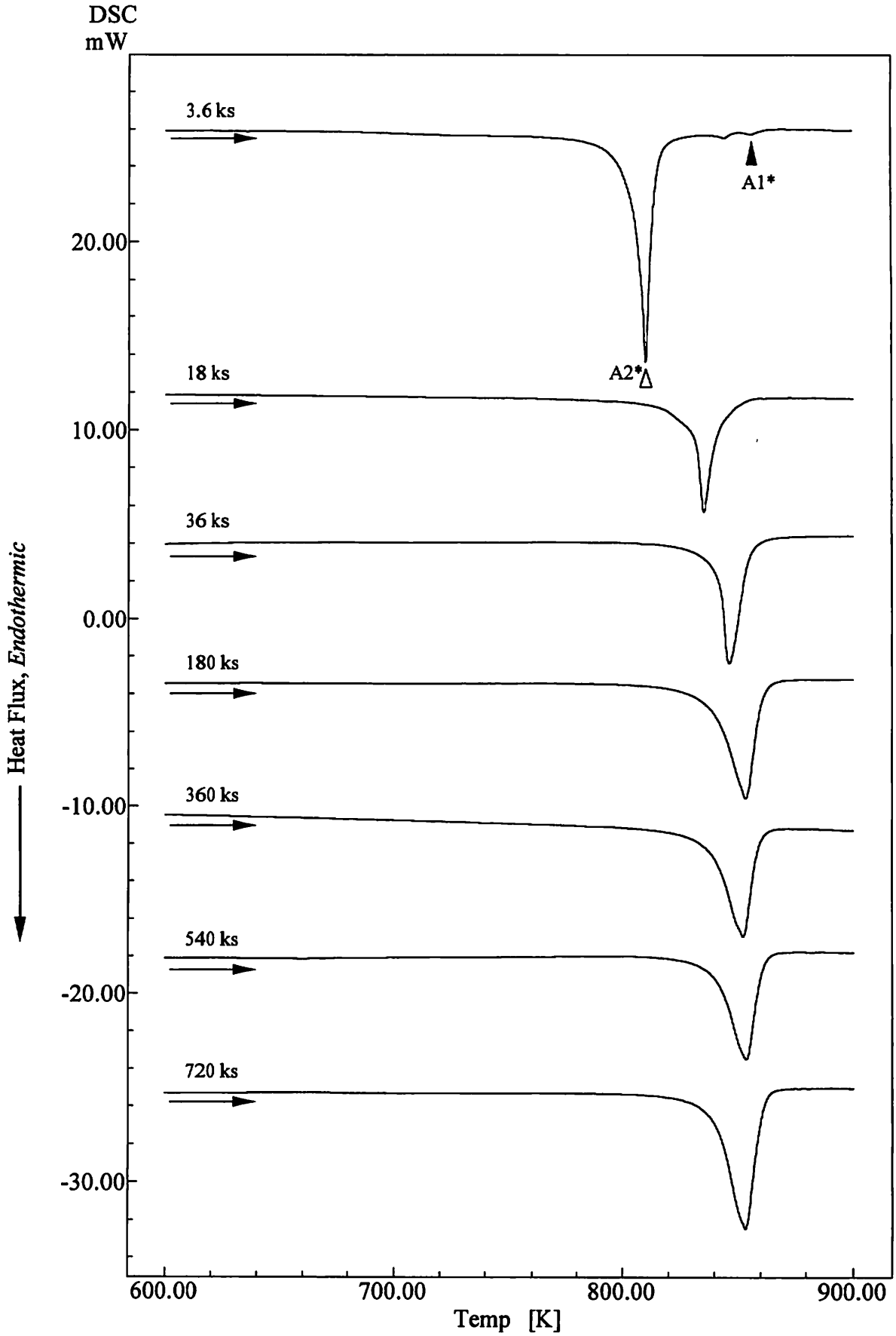

Fig. 6.2 DSC heating curves of the Ti-47at.%Pd alloy aged at 873 K for various periods, indicated at the left side of the figure.

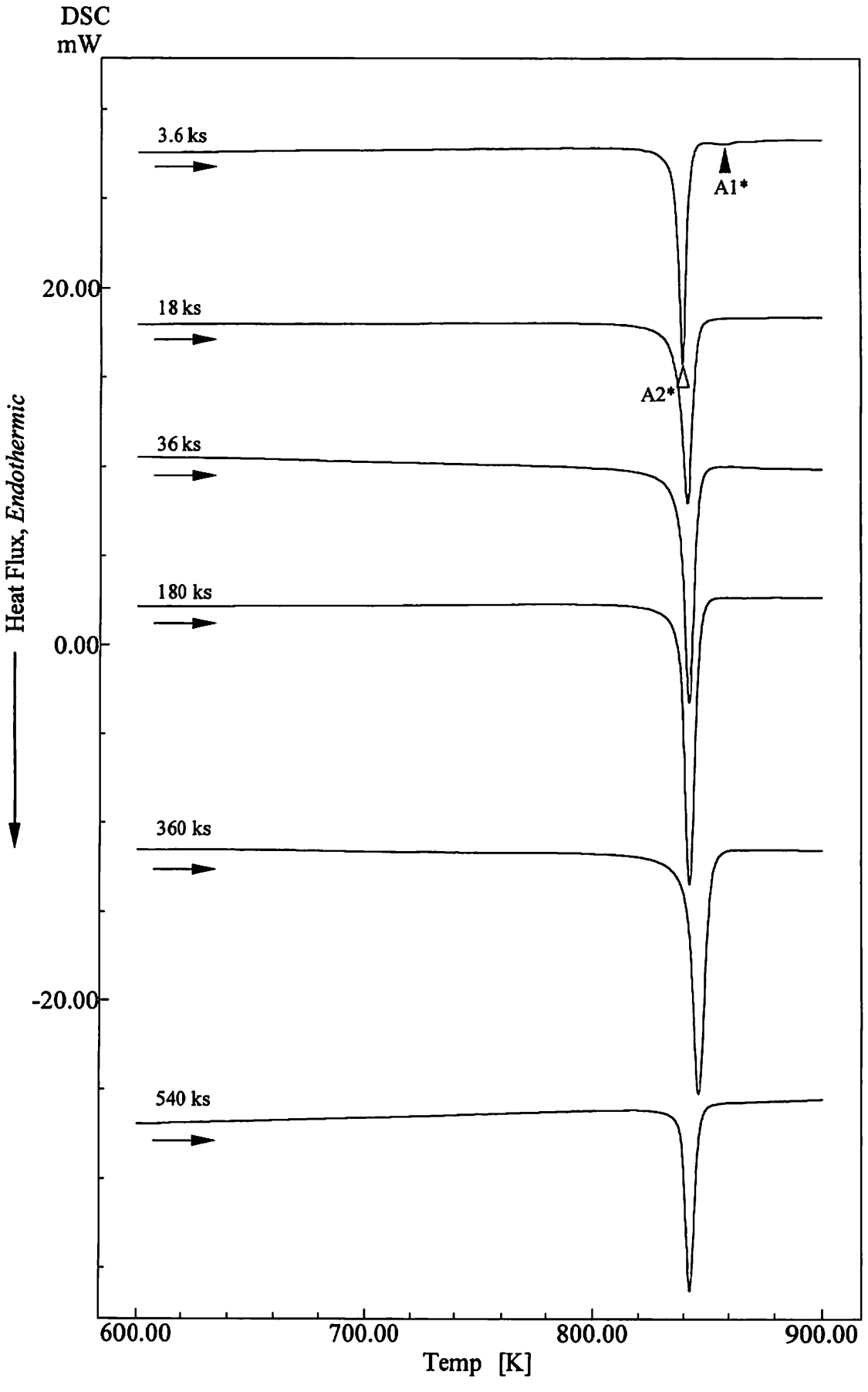

Fig.6.3 DSC heating curves of the Ti-47at.%Pd alloy aged at 973 K for various periods, indicated at the left side of the figure.

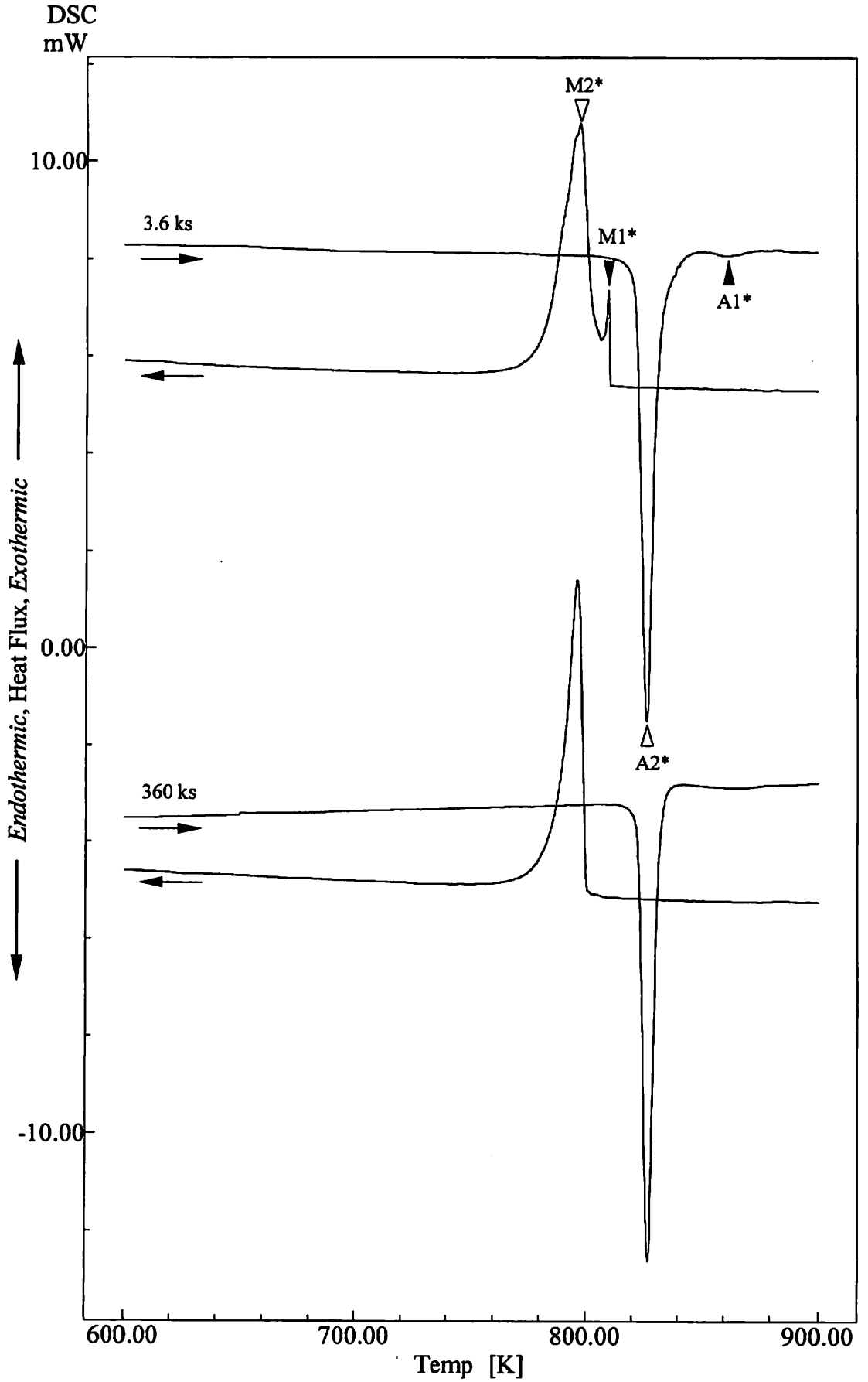

Fig. 6.4 DSC curves of the Ti-47at.%Pd alloy aged at 1023 K for various periods, indicated at the left side of the figure.

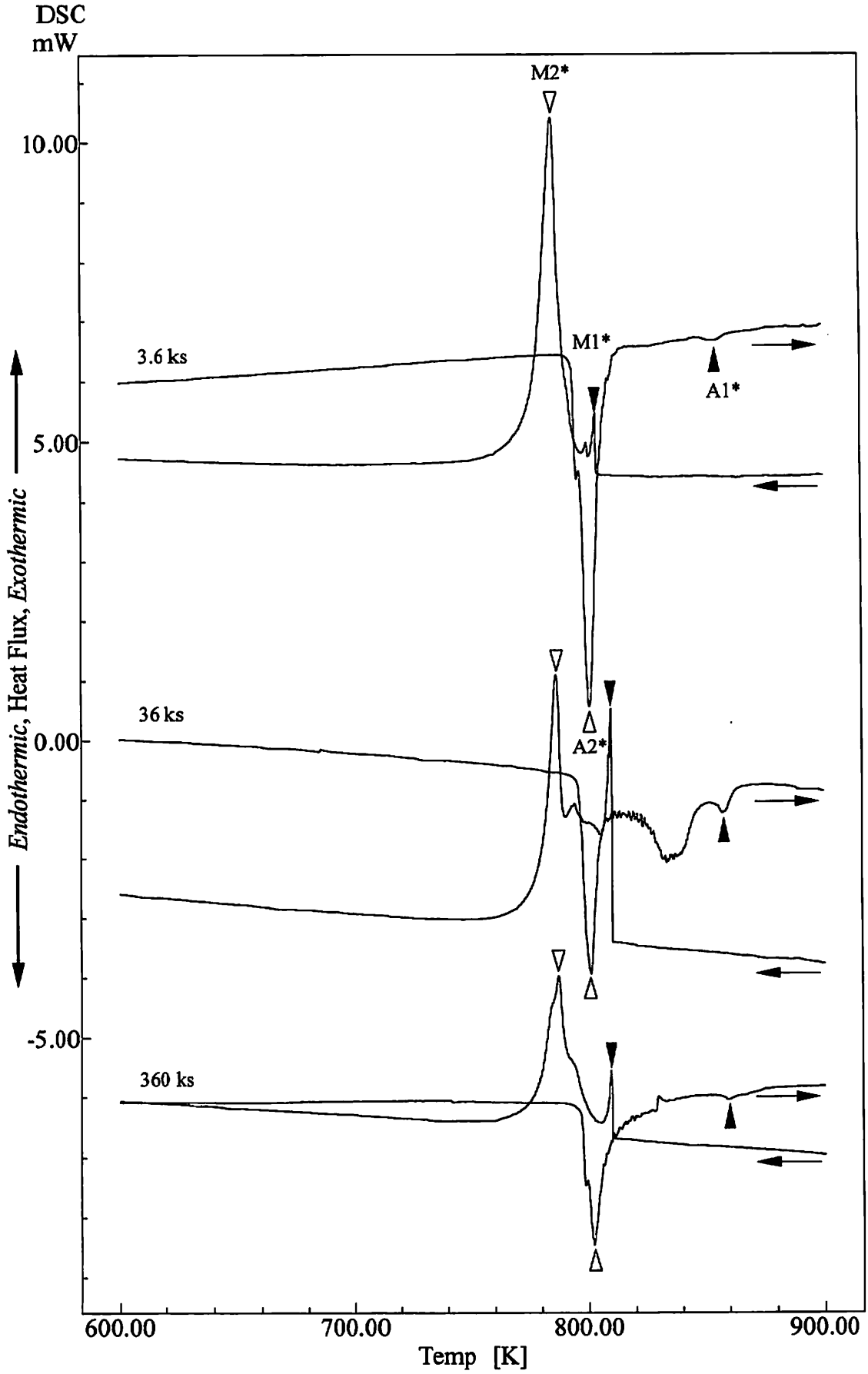

Fig. 6.5 DSC curves of the Ti-47at.%Pd alloy aged at 1073 K for various periods, indicated at the left side of the figure.

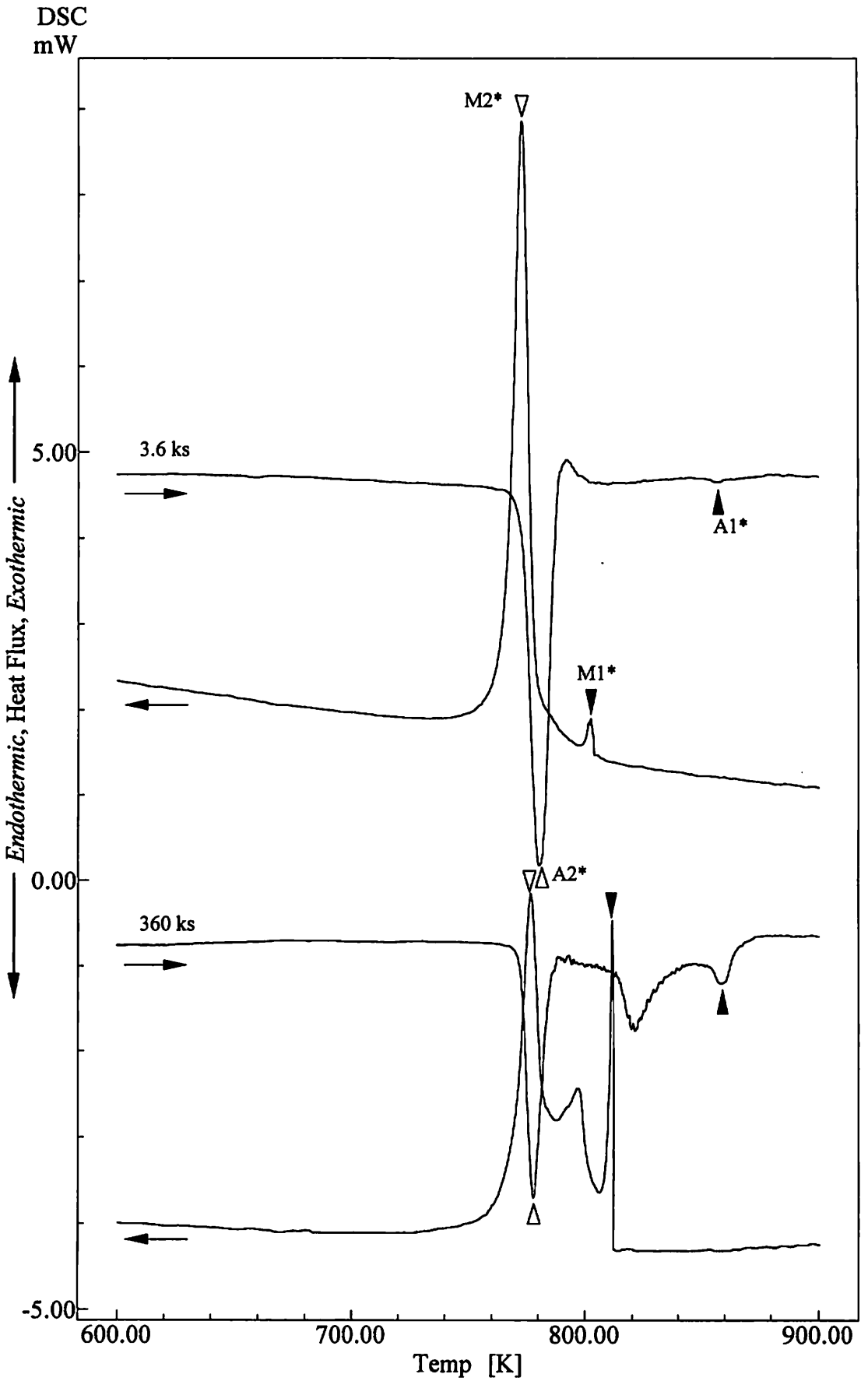

Fig. 6.6 DSC curves of the Ti-47at.%Pd alloy aged at 1123 K for various periods, indicated at the left side of the figure.

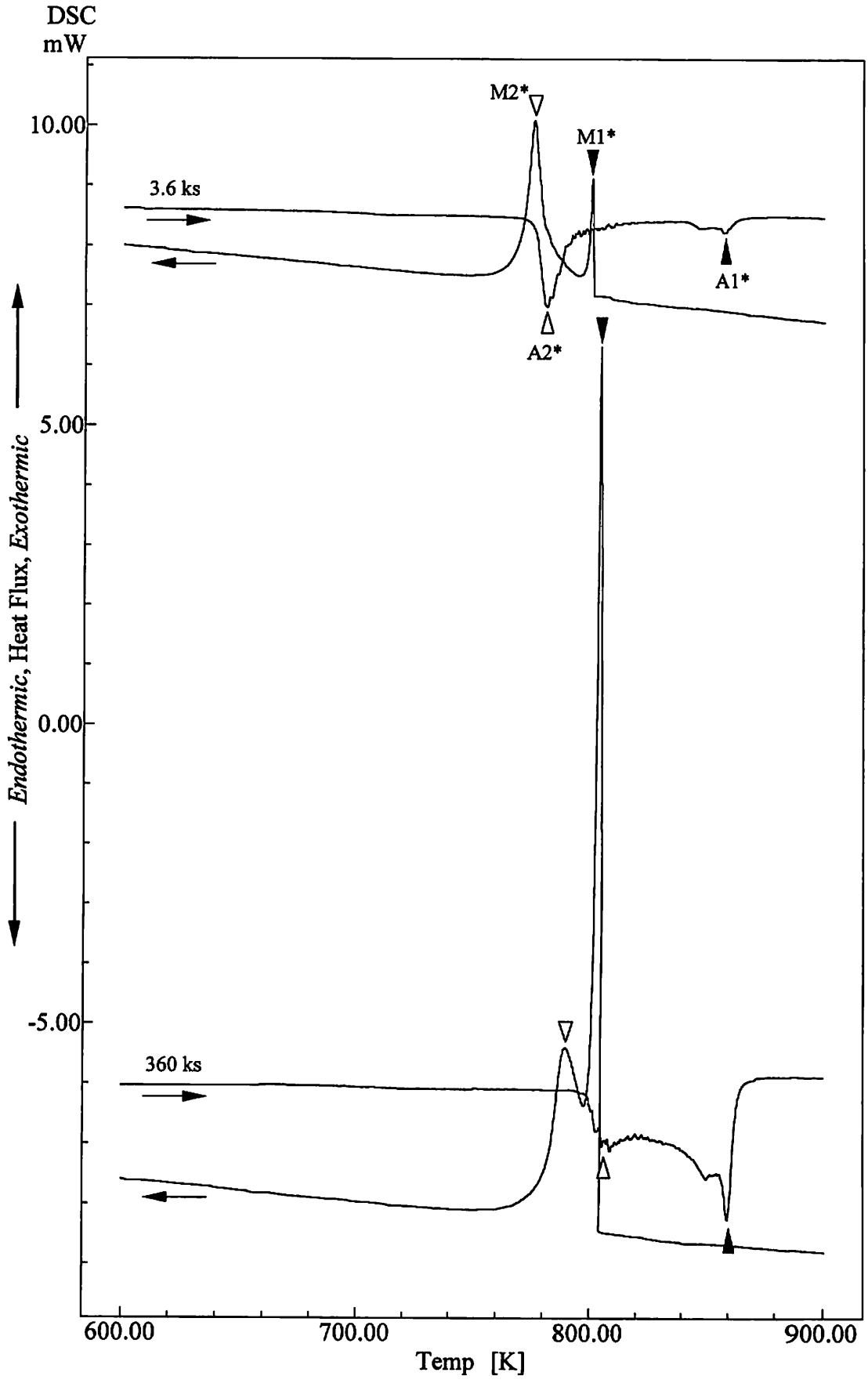

Fig. 6.7 DSC curves of the Ti-47at.%Pd alloy aged at 1173 K for various periods, indicated at the left side of the figure.

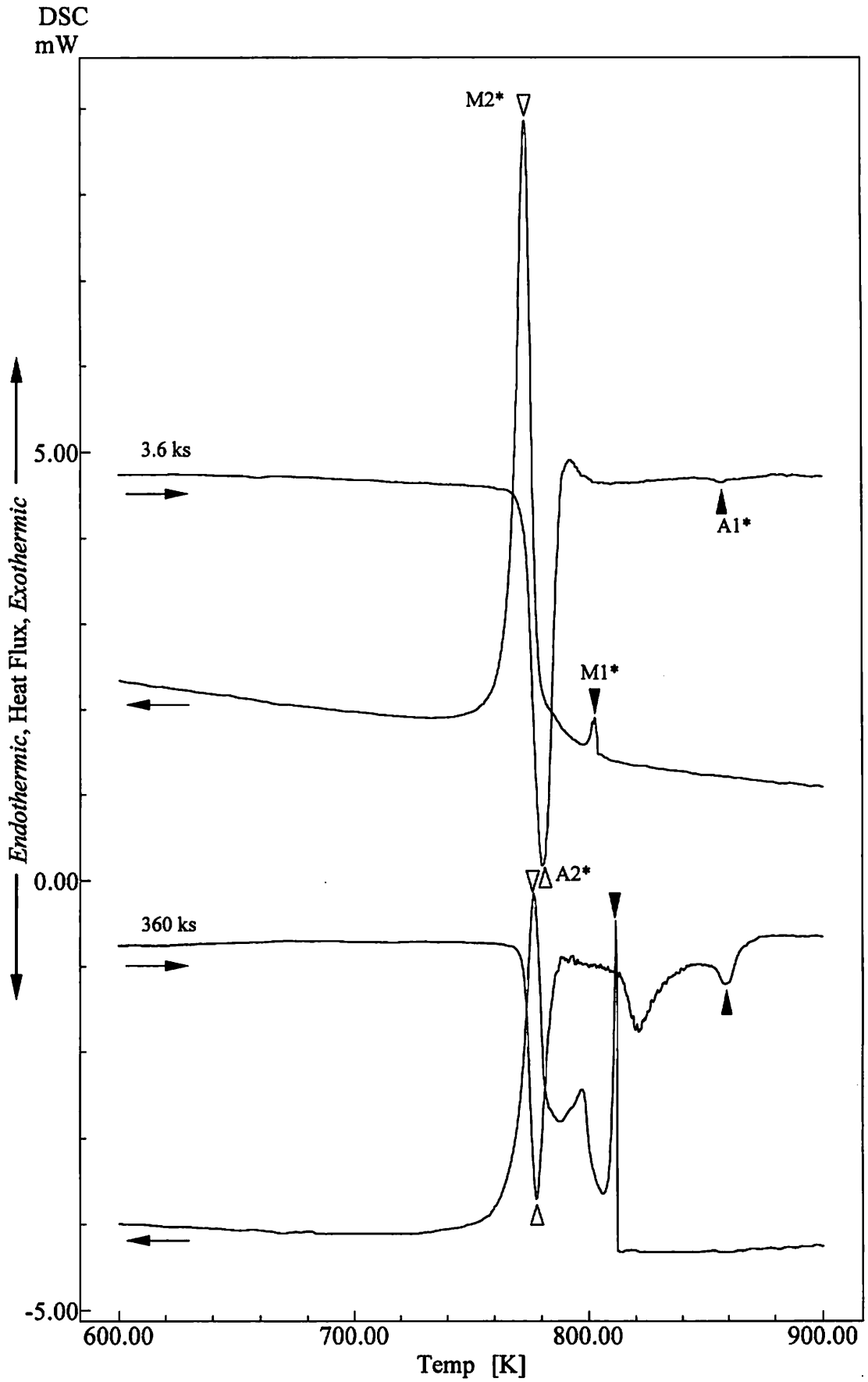

Fig. 6.8 DSC curves of the Ti-47at.%Pd alloy aged at 1123 K for various periods, indicated at the left side of the figure.

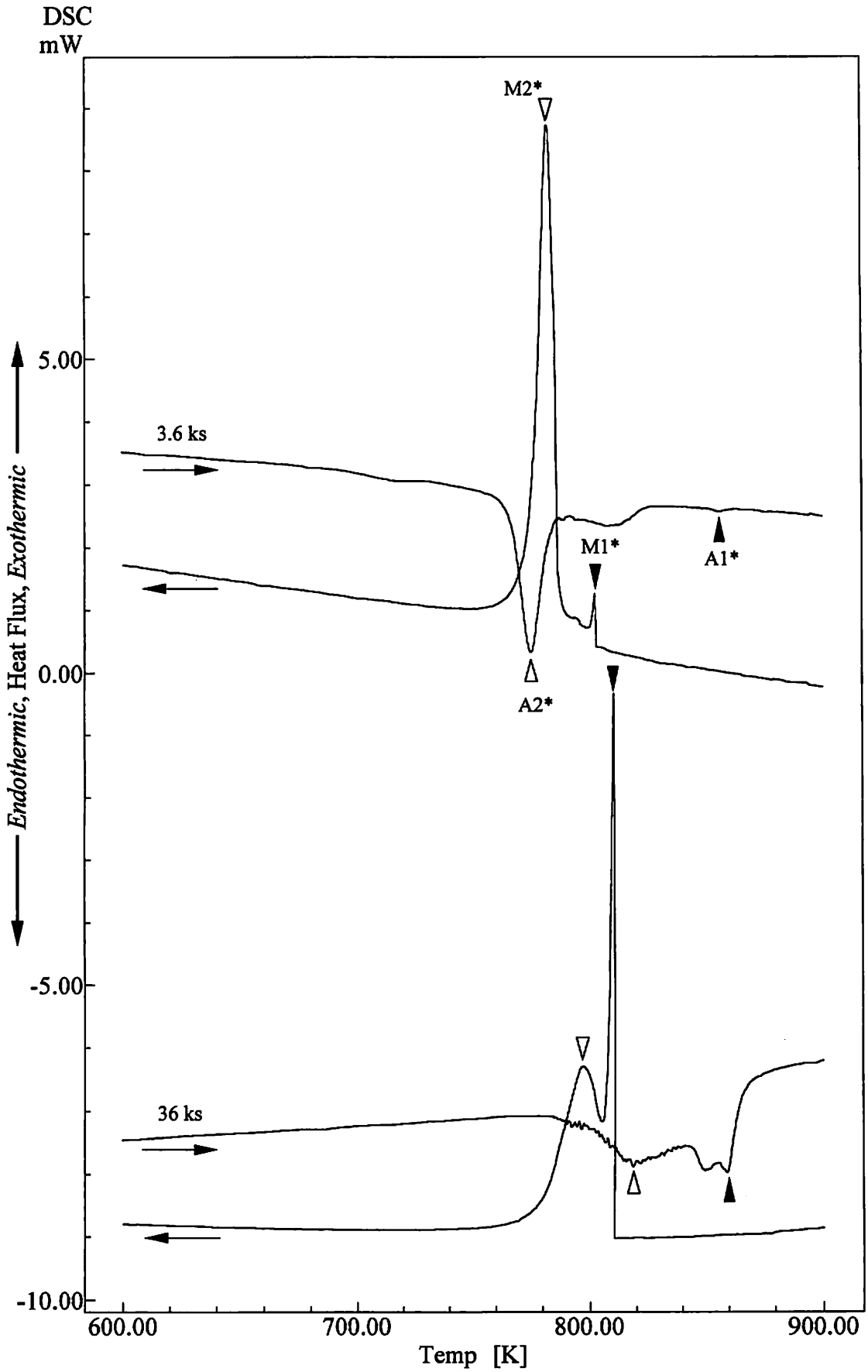

Fig. 6.9 DSC curves of the Ti-47at.%Pd alloy aged at 1273 K for various periods, indicated at the left side of the figure.

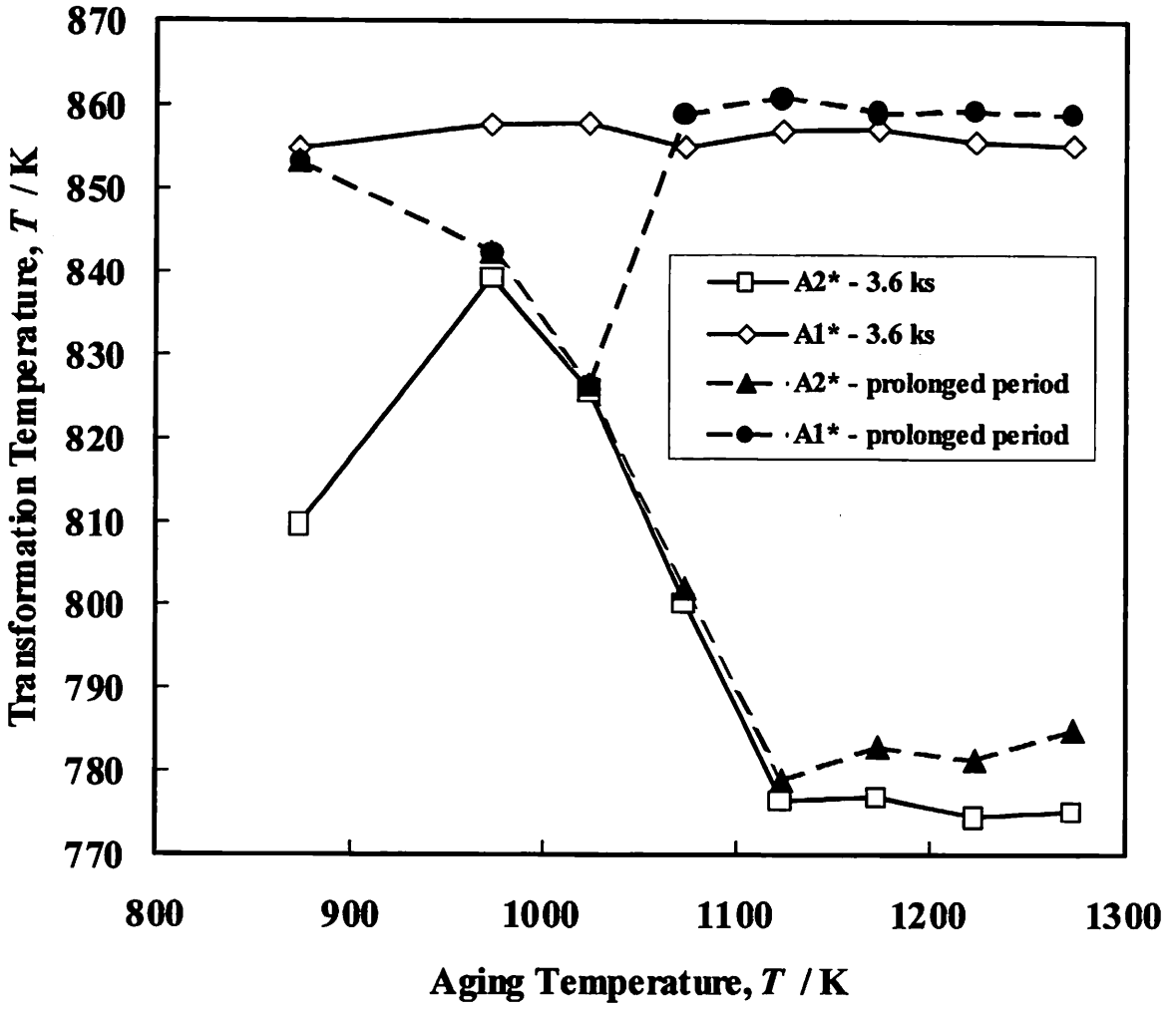

Fig. 6.10 Aging time and temperature dependence of transformation peak temperatures (A2* and A1*) for Ti-47at%Pd alloy. The prolonged periods are 720, 540, 360 and 36 ks at 873, 973, 1023 and 1073 - 1273 K, respectively. See text for details.

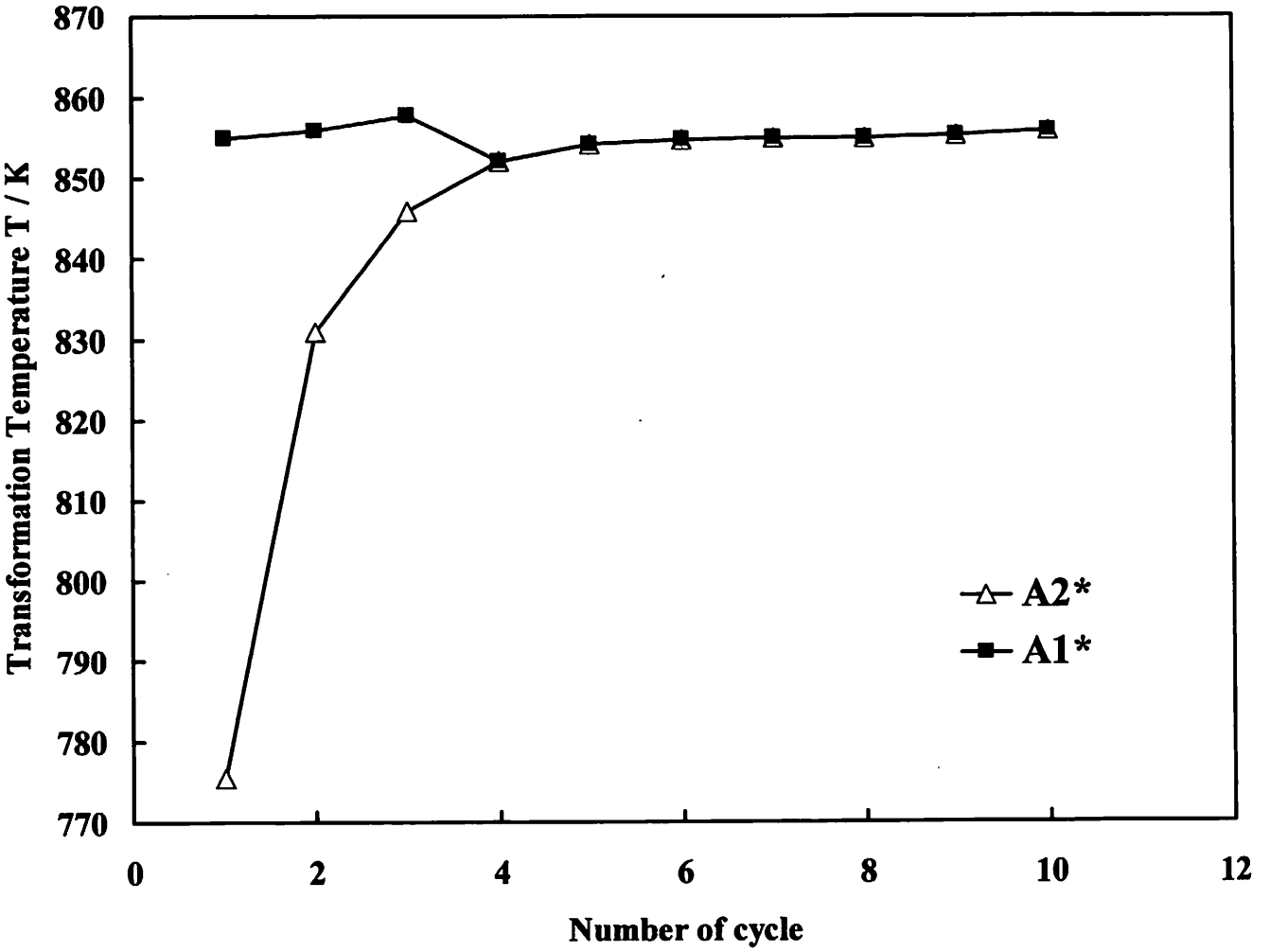

Fig. 6.11 Thermo-cycling dependence of the A2* and A1* transformation peaks temperatures for a Ti-47at%Pd solution treated alloy cycled in DSC between room temperature and 973 K.

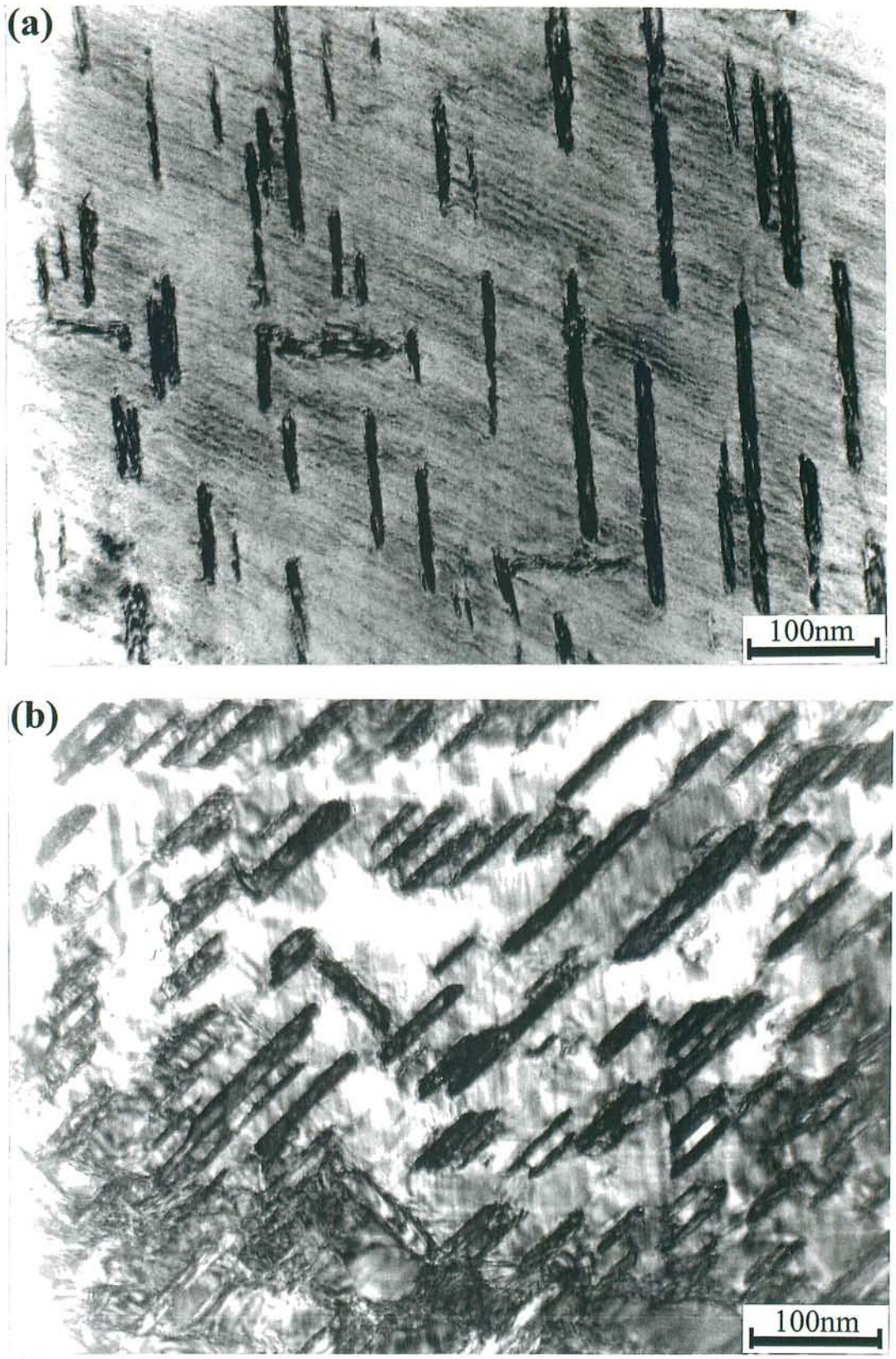

Fig. 6.12 The microstructure of Ti-47at.%Pd alloy aged at 873 K for 3.6 ks (a) before and (b) after DSC-like treatment.

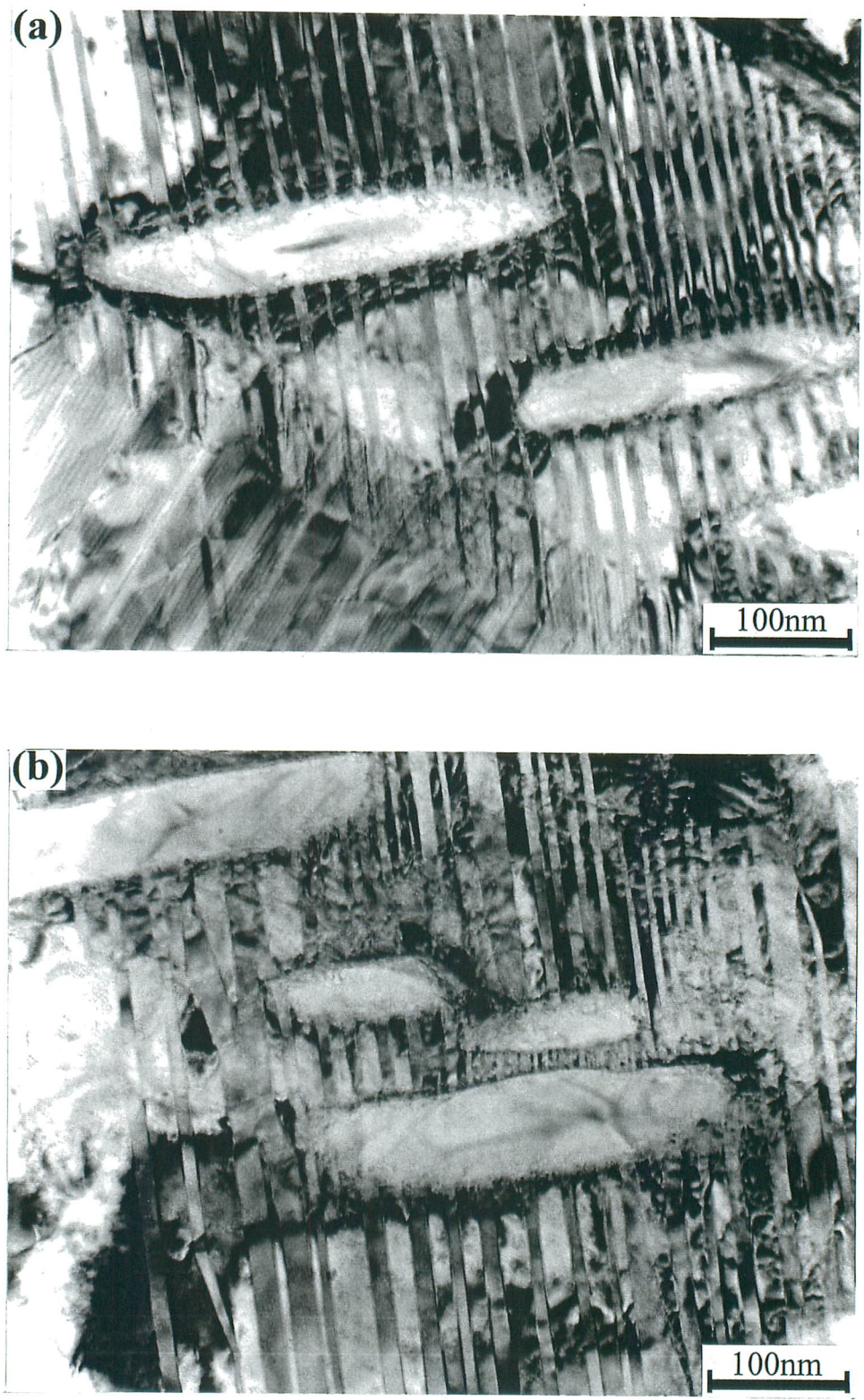

Fig. 6.13 The microstructure of Ti-47at.%Pd alloy aged at 873 K for 360 ks (a) before and (b) after DSC-like treatment.

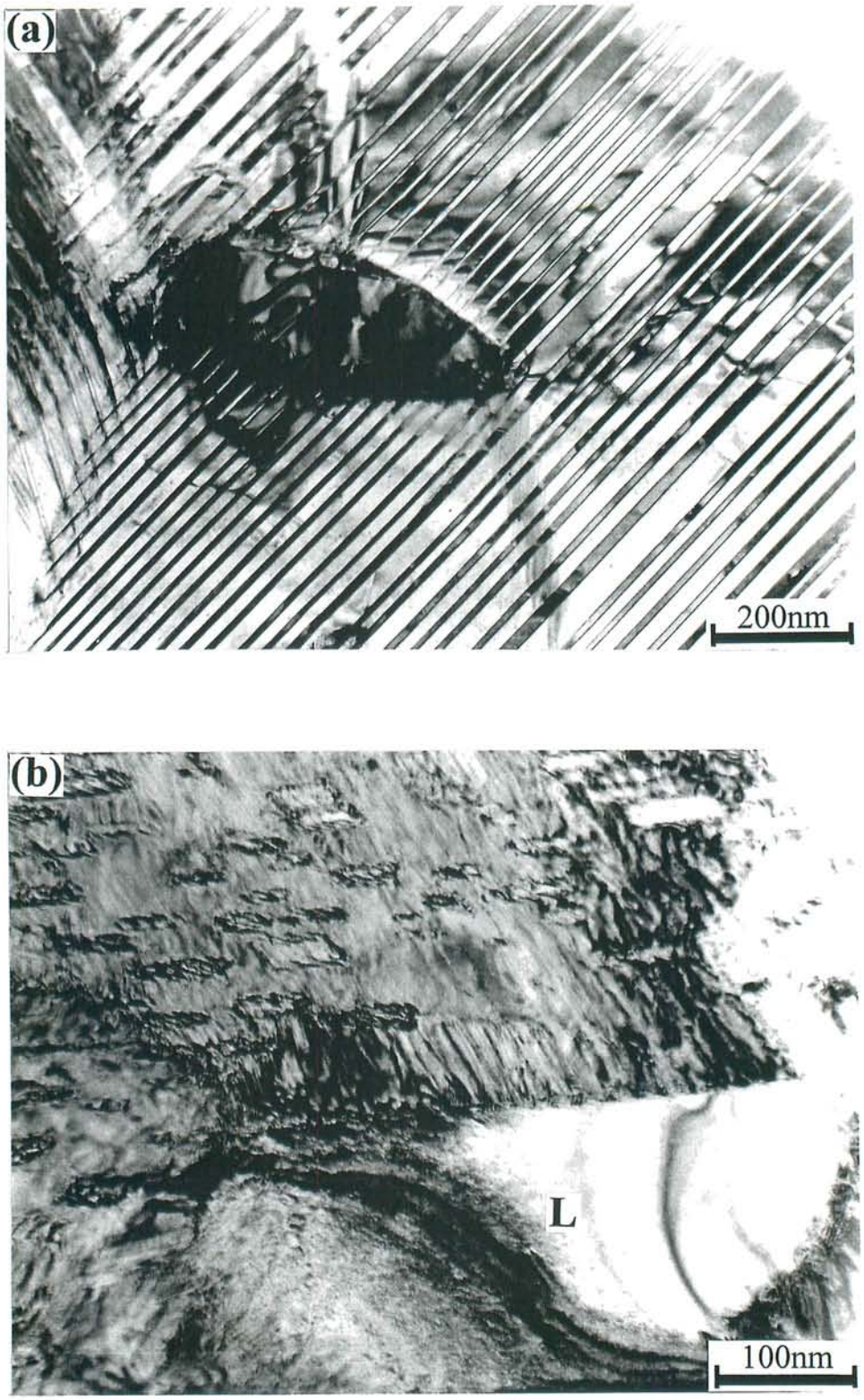

Fig. 6.14 The microstructure of Ti-47at.%Pd alloy aged at 1073 K for 36 ks (a) before and (b) after DSC-like treatment.

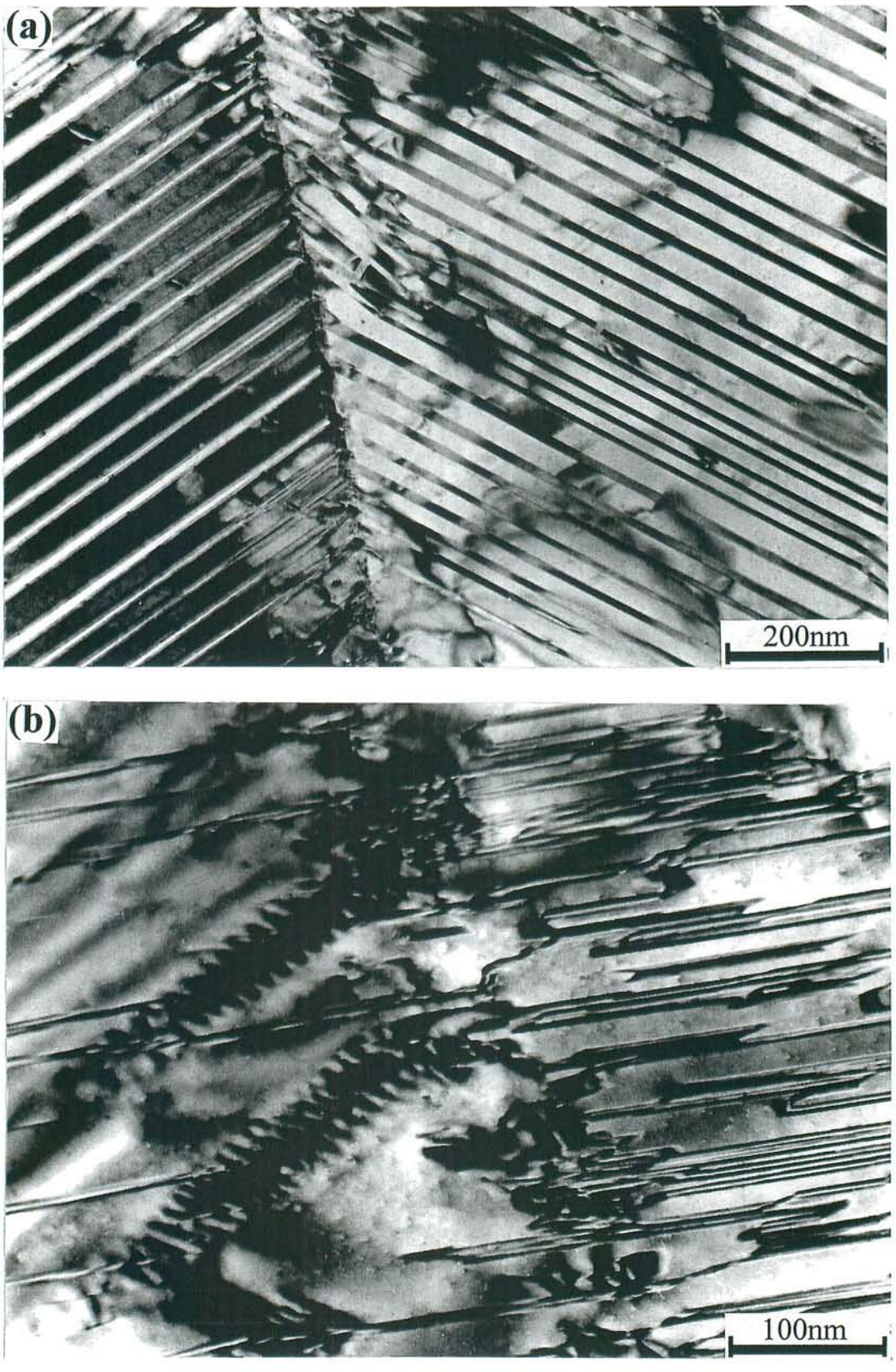

Fig. 6.15 The microstructure of Ti-47at.%Pd alloy aged at (a) 1123 K and (b) 1273 K for 36 ks.

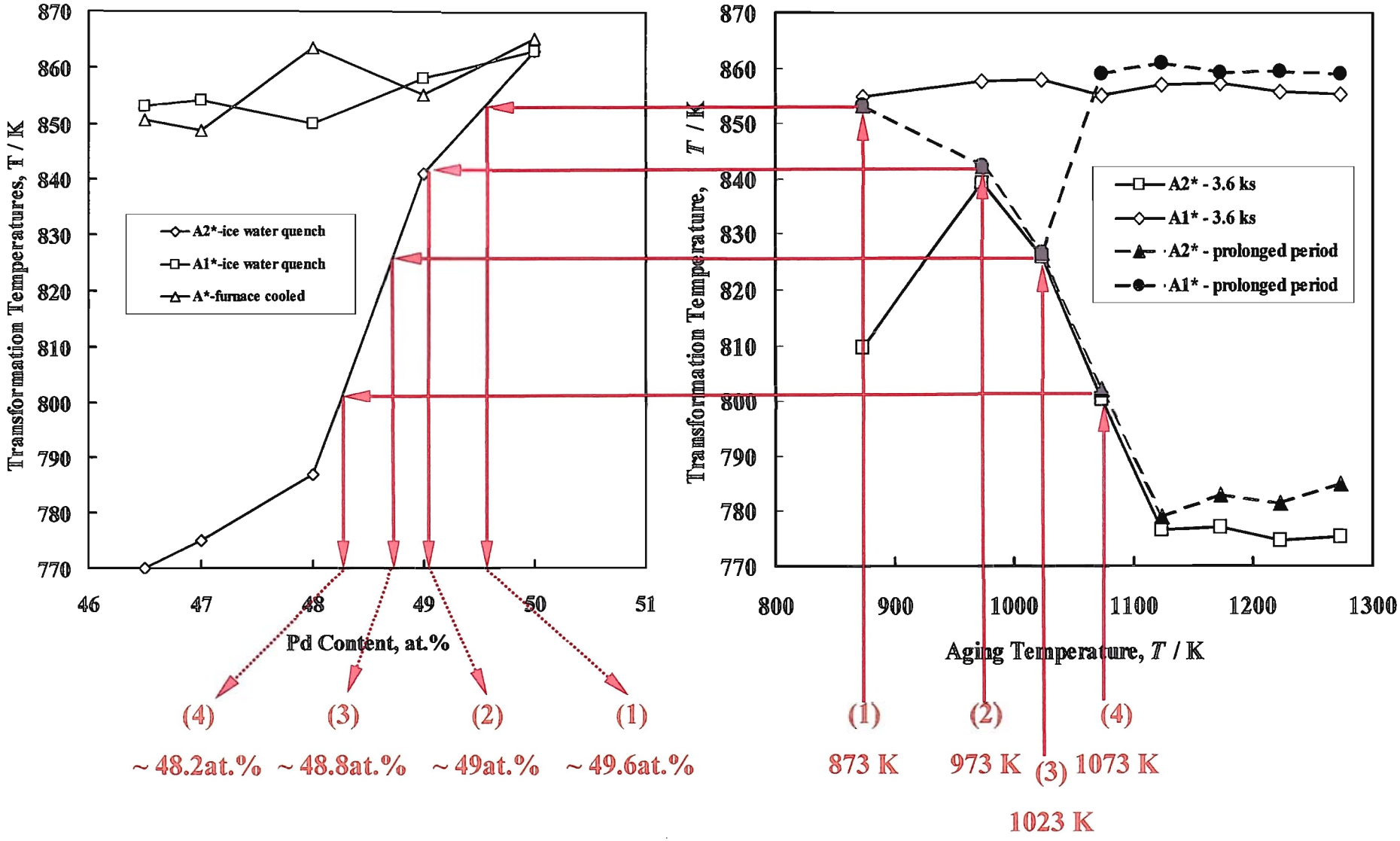

Fig. 6.16 Determination of the TiPd matrix equilibrium composition at different temperatures.

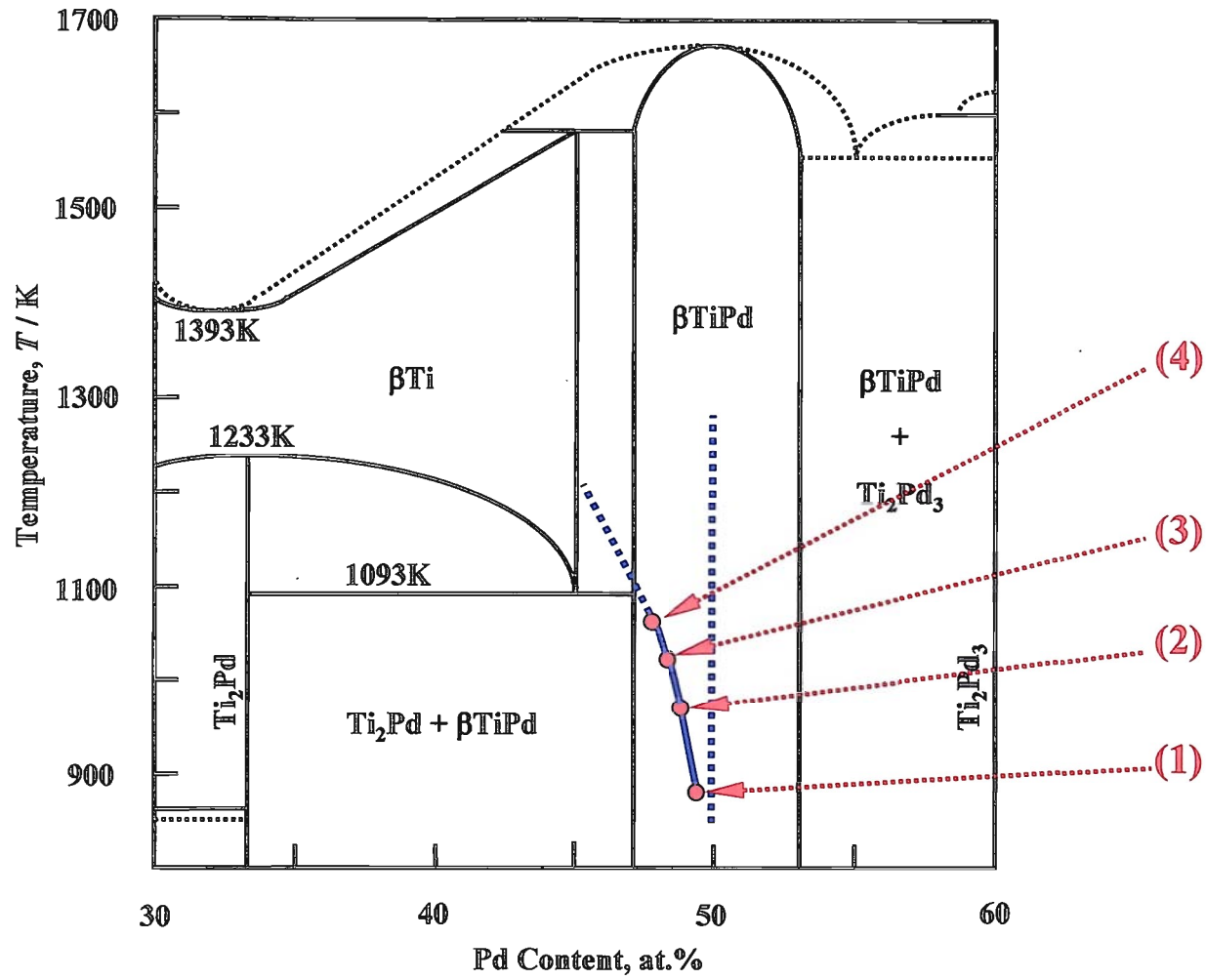

Fig. 6.17 Estimation of the homogeneity range of TiPd compound.

Chapter 7

Morphologic and Crystallographic Aspects of $C11_b$-Type Precipitates Nucleated in Martensitic and Parent Phase Matrices in Aged Ti-Rich Ti-Pd Shape Memory Alloys

7.1 Introduction

Ti-Pd alloys are well known as high-temperature shape memory material since they undergo a B2 $\rightarrow$ B19 thermoelastic martensitic transformation around 800 K upon cooling. Martensitic transformation temperatures in Ti-rich Ti-Pd alloys decrease with decreasing Pd content. For instance, reverse martensitic transformation start temperature A_s decreases from around 850 K in Ti-50at.%Pd alloy to nearly 700 K in Ti-45at.%Pd alloy. Martensitic transformation behavior in these alloys is greatly affected by the nucleation and growth of Ti_2Pd precipitates with $C11_b$ type structure. The major influence of the Ti_2Pd precipitates is the occurrence of martensitic transformation in successive steps. There are also several interesting phenomena in the alloy.

First, the number of Ti_2Pd precipitate variants depends on the aging temperature. Thus, if the Ti_2Pd precipitate phase nucleate in parent phase there have been observed three variants, while only one or two variants were observed if nucleate in martensitic state, as pointed out in Chapter 5. Following, for the understanding of this phenomenon extensive experiments were carried out in two directions. In order to assure that the precipitates are nucleated in parent phase several specimens were aged in parent phase. Other quenched specimens were aged for long time (3600 ks) in martensitic phase just below the A2* peak. At this temperature small precipitates exist in the martensite matrix, as could be understand from Figs. 5.8 and 5.9. Few tensile specimens consisting

of martensite variants with rather large twin platelets and/or without platelets were also aged in martensitic state.

Second, the martensite morphology, especially the width of twinning plates, drastically changes with the precipitates size and density.

The purpose of this chapter is to discuss the results of TEM investigations on morphologic and crystallographic aspects of $C11_b$-type precipitates nucleated in martensitic and parent phase matrices, as well as the influence of the precipitates size and density on martensite morphology in aged Ti-Rich Ti-Pd SMA's.

7.2 Experimental Procedure

The Ti-47, 47.5, 48 at.%Pd alloys were prepared from pure titanium and pure palladium by arc melting technique as described in the previous chapters. Several metallic sheets cut from the buttons were used for preparing tensile specimens by hot-rolling process. The as-cut metallic sheets with about 1.5 - 2 mm in thickness were hot-rolled into 0.25 - 0.35 mm thick sheets with 0.05 - 0.1 mm thick reduction per step. One "step" means one rolling operation effectuated between two intermediate anneals at 923 K. Tensile specimens, 5 mm in width, were spark-cut from as-rolled plates. Before the heat treatment the specimens were mechanically polished in order to remove the oxide layer. Tensile specimens encapsulated in evacuated quarts tubes were solution treated at 1273 K for 3.6 ks and than quenched into ice water. Following this heat treatment, the recovery and recrystallization process was complete and the structure was in martensitic state at room temperature, as observed by electron microscopy. After tensile deformation in martensitic state at preset strains of $\varepsilon = 4$ and 8 % from gauge length, disk-shaped specimens for TEM observations and DSC measurements were yield from deformed material by ultrasonic cutting. The specimens, encapsulated in evacuated quartz tubes, were aged in martensitic state at different temperatures just below the A2* transformation peak.

Other specimens punched from as-cut metallic sheets were aged in martensitic phase at different temperatures just below the A2* transformation peak for 3600 ks. The aging treatment was also carried out at 873 K, with the specimens in parent phase, for various periods.

TEM specimens were prepared and observed as described in the previous chapters. The lattice parameters of B2 parent phase and B19 martensite have been also described in the Chapter 2. The following introduce the crystallographic properties of Ti_2Pd intermediate phase.

7.3 Crystallographic Characteristics of Ti_2Pd Intermediate Phase

Nevitt and Downey[1] have reported for the first time that Ti_2Pd has a Si_2Mo-type ($C11_b$) structure. Their results obtained from XRD measurements show that Ti_2Pd has a large tetragonal unit cell containing 6 atoms. This $C11_b$ crystal structure was further confirmed, and the lattice parameters and other crystallographic data of Ti_2Pd phase determined by different authors are shown in Table 7.1. Hoshi *et al.*[5-7] using the TEM techniques shows that $C11_b$ structure (Si_2Mo-type, *I4/mmm*) has the unit cell thrice as larger as one of BCC structure, as shown in Fig. 7.1. Based on the Ti_2Pd phase stiochiometry may be reasonable to assume that the Ti atoms are on the sites denoted by open circles, and the Pd atoms occupy the sites denoted by solid one.

7.4 Precipitates Variant Selection in Ti-Rich Ti-Pd Alloys

Since the nucleation of precipitates must occur uniformly on three $\{001\}_{B2}$ planes in the parent phase there are three variants of Ti_2Pd precipitate in the furnace cooled Ti-47at.%Pd alloy as shown in a previous chapter, in Fig. 5.3.

The three variants are clearly observed in the Ti-47at.%Pd alloy aged at 873 K for 1.8 ks as shown in Fig. 7.2. The aging temperature is about 20 K higher than A1*. The nucleation of the precipitates takes place certainly in the parent phase and then the parent phase transforms to

martensitic phase upon quenching. In Fig. 7.2(a) there are observed two types of precipitates denoted as B and C with their apparent habit plane parallel to the incident beam direction. The third precipitate denoted as D in Fig. 7.2(a) is clearly seen in the enlarged micrograph in Fig. 7.2(b) which is slightly tilted from $[10\bar{1}]_{B19}$ zone axis in Fig. 7.2(c) to reveal the contrast. The pattern in Fig. 7.2(c) consists of five sets of reflections. The three of them are the same as those in Fig. 5.5(d), i. e., $(111)_{B19}$ twin pattern and $[001]_{C11b}$ zone axis. The two remained patterns are $[100]_{C11b}$ zone axes derived from the precipitates B and C. Since the apparent habit plane is parallel to the image plane of $(10\bar{1})_{B19}$ we can recognized without doubt that the precipitate D is the variant II. We cannot determine exactly the apparent habit plane of the other two precipitates from this incident beam direction because of the twinned martensite matrix. Therefore, the precipitates B and C are the variants I and III or vice versa. However, there is no doubt that the nucleation of precipitates occurs uniformly on three $\{001\}_{B2}$ planes in the parent phase.

Only one or two variants are seen in Fig. 7.3 (as well as in Figs. 5.6(a), (c) and 5.9 in Chapter 5) that shows the microstructure of the quenched Ti-47at.%Pd alloy after DSC. The observed variants correspond to the Variant I or/and II as it was discussed in Chapter 5. In their case, the nucleation of precipitates occurs in the martensitic phase. From the lattice parameters of both precipitate phase and B2 parent phase (a = 0.3180 nm[8]) and the orientation relationship between them, the difference between the corresponding interplanar spacing is roughly estimated to be:

$$[d(003)_{C11b} - d\{100\}_{B2}] / d\{100\}_{B2} = 5.4\ \% \qquad (7.1)$$

Similarly, in the case of precipitates nucleated in the B19 martensitic phase the corresponding interplanar spacing difference for Variants I and II is about:

$$[d(003)_{C11b} - d\{101\}_{B19}] / d\{101\}_{B19} = 0.9\ \% \qquad (7.2)$$

On the other hand, that of the Variant III is about:

$$[d(003)_{C11b} - d\{010\}_{B19}] / d\{010\}_{B19} = 20\ \% \qquad (7.3)$$

Therefore, within the martensitic phase the formation of the Variants I and II is more preferable than that of the Variant III. This preferential precipitation may be apparently cancelled by the presence of twin. Nevertheless, a single or two precipitate variants are observed throughout the present research as shown in Fig. 7.3. A geometrical illustration of the orientation relationship between Ti_2Pd precipitate variants and TiPd matrices with B2- and B19-type structures is shown in Fig. 7.4. All the data necessary for the calculation of the differences between the corresponding interplanar spacing of precipitate phase and both B2 parent phase and B19 martensitic phase are presented in Fig. 7.5.

One of difficulties of analysis is that the original twinned martensite disappears during heating and the observed martensite in Fig. 7.3 transforms from the parent phase containing densely dispersed fine precipitates. Details of interaction between the original twin structure and the preferential precipitation on the specimens aged in martensitic state for prolonged time will be reported in the following.

7.5 Effect of Long Time Aging in Martensitic State on Precipitates Morphology

Two types of TEM specimens have been aged for long time in martensitic phase. The specimens of the first type were prepared from quenched Ti-47.5at.%Pd alloy solution treated at 1273 K for 3.6 ks. These specimens were aged at 753 K for 3600 ks. The long aging time was chouse in order to obtain precipitates big enough for a proper determination of the orientation relationship with the matrix. For instance, the precipitates were too small and the orientation

relationship could not be obtained from SAD patterns in the specimens aged in martensitic state at 723 K for 1440 ks.

The specimens of the second type were prepared from tensile strain Ti-48at.%Pd alloy specimens, by aging at 788 K for 1620 ks. The tensile strain was $\varepsilon = 8$ %. These specimens were prepared in order to eliminate the influence of twins on Ti_2Pd precipitates nucleated and grown in martensitic state. The aging temperatures were below A_s temperatures of Ti-47.5at.%Pd and Ti-48at.%Pd alloys that have been presented in the Experimental procedure.

Figure 7.6 shows the microstructure of the Ti-47.5at.%Pd alloy aged in martensitic state at 753 K for 3600 ks. A bright field (BF) image in Fig. 7.6(a) and a dark field (DF) image in Fig. 7.6(b) taken along $[10\bar{1}]_{B19}$ direction show only one precipitate variant in the specimen structure which is in concordance to the previous results and conform to ours expectations. This is confirmed by the SAD pattern in Fig. 7.6(c) that shows three sets of diffraction spots: two from twins and one from precipitate. The diffraction spots from the precipitates can be indexed by assuming Ti_2Pd phase of $C11_b$-type structure. It is interesting to notice that from the same $[10\bar{1}]_{B19}$ direction the habit plane of Ti_2Pd precipitate in DSC-like specimen could be easily understood, as show in Fig. 7.3(c). The morphology of the precipitate as seen in Fig. 7.3(c) is disk-like. This is not the case in Fig 7.6 where the precipitate shape is different and the habit plane seems also to be different. However, the conditions of precipitate growing are different since the precipitates in Fig. 7.3 nucleated in martensitic phase and grew in parent phase, while the precipitates in Fig. 7.6 nucleated and grew in martensitic phase. Further researches are necessary to clarify this problem.

Figure 7.7 shows BF images of the Ti-48at.%Pd alloy where (a) and (b) are the micrographs after deformation with $\varepsilon = 4$ % and 8 %, respectively. The parallel thick bands in both images are deformation twins containing B19 martensite variants. The deformation twins were introduced as the result of tensile deformation of the specimen. In Fig. 7.7(a) the stripes appearing in every variant are internal twins. By increasing the strain, the morphology changes from (a) to (b), (b) showing martensite variants without any internal twins. Thus, by aging in martensitic state a Ti-48

at.% Pd specimen tensile strain with ε = 8 % it is possible to avoid the influence of twins on the formation of Ti_2Pd precipitates.

Figure 7.8(a) presents an enlarged area of Ti-48at.%Pd specimen tensile strain with ε = 8 % that shows two B19 martensite variants. From SAD pattern in Fig. 7.8(b) it was confirmed that no internal twins exist in martesite variant. The deformation twins in Fig. 7.8(a) are {101} compound twins, as could be understood from the diffraction pattern.

In the thermal stress cycled Ti-Pd alloys used as a stress relaxation layer of ceramics/metal joint the {101} compound twins with banded morphology were frequently observed[9]. Recently, the {101} twining mode having an isolated fashion in the martensite variant consisting of {111} Type I twins was also observed in solution treated Ti-50at.%Pd alloy[10]. It was reported that this twinning might be induced as a result of elastic interactions during the martensitic transformation.

Transformation temperatures of tensile strain specimens were determined by DSC measurements, as shown in Fig. 7.9. Two peaks denoted the same as in previous chapters with A2* and A1* was observed on DSC heating curves. By increasing the tensile strain the A2* peak is shifted toward high temperatures, while the temperature of A1* is almost constant. Increasing of reverse transformation temperatures in deformed martensite was reported before in Ti-Ni-Nb[11-18], Ti-Pd-Ni[19], Cu-Al-Ni and Ti-Ni[20] alloys, but this is the first observation of this phenomenon in binary near-equiatomic Ti-Pd alloys. The mechanism of increasing reverse transformation temperatures was explained by Piao *et al.*[20]. It was confirmed that the raise of reverse transformation temperature in thermoelastic alloys is due to the introduction of the permanent strain by pre-deformation, which relax the stored elastic energy in self-accommodating morphology of deformed martensite. Increase of A2* peak temperature for the present alloy was founded to be about 21 K.

Figure 7.10 shows the microstructure of a tensile strain (ε = 8 %) Ti-48at.%Pd alloy specimen after aged in martensite phase at 788 K for 1620 ks. From the DF images in Fig 7.10(a) and (d) and BF image in Fig 7.10(c) only one precipitate variant could be observed. This is

confirmed by the SAD pattern in Fig. 7.10(b) that was taken along the same direction as DF and BF images and shows only two sets of diffraction spots one from the matrix and the other one from the precipitate. From this diffraction pattern is also confirmed the existence of no internal twins in martensite matrix. Comparing Figs. 7.10 and 7.3(c) it is easy to discern the differences in precipitate morphology in this case and in DSC-like specimens. A preliminary experiment carried out in order to solve this problem show that martensite in deformed specimens has the 4H structure, which is different from the 2H structure of martensite in quenched Ti-Pd alloy. However, extensive researches are necessary in order to confirm the above hypothesis.

7.6 Effect of Precipitates Size and Density on Martensite Morphology

Another interesting phenomena was observed in the near-equiatomic Ti-Pd SMA's during researching the transformation behavior and phase equilibrium. The martensite morphology, namely twin width, changes significantly with precipitate size and density. The twin width ratio[21] or, a similar expression, relative twin width[22] (1-x):x is a critical value in the phenomenological crystallographic analysis of martensitic transformation since the invariant plane as a habit plane can be obtained only at a particular value of x[23-28].

The martensite morphology in a quenched Ti-47at.%Pd alloy after solution treatment at 1273 K for 3.6 ks is shown in Fig. 7.11(a). The relatively large twins are in {111} Type I relation as could be seen from Fig. 7.11(b) that shows a SAD pattern consisting of two sets of reflections that belong to $[10\bar{1}]_{B19}$ zone axis.

Figure 7.12(a) to (d) present BF images of Ti-47at.%Pd alloy aged at 873 K for 1.8, 3.6, 36 and 360 ks, respectively. All the images are taken along $[10\bar{1}]_{B19}$ direction. In Fig. 7.12(a) small and quite dense precipitates coexists with very narrow twins. By increasing the aging time the morphology changes from (a) to (d). Both, precipitate size and twin width, increase with aging time, but precipitates density decrease. Therefore, it can be concluded that when MT occur in a parent

phase containing small and dense precipitates, dense and narrow twins form in the structure. On the other hand, when MT takes place in a parent phase with large but rare precipitates, large twins appear in the structure.

The precipitates nucleated in martensitic phase do not affect the twin width. This could be seen in Fig. 7.13(a) that shows a BF image of a Ti-47at.%Pd alloy after DSC-like treatment at 743 K. Although small and dense precipitates were formed after DSC-like treatment the twin width is the same as in Fig. 7.11(a). The image in Fig. 7.13(a) is taken along $[10\bar{1}]_{B19}$ direction as well as SAD pattern in (b).

Variation of twin width with precipitate size in quenched and aged Ti-47at.%Pd alloy is plotted in Fig. 7.14. The twins' widths were measured from micrographs in Figs. 7.11 and 7.12 at least for 10 different plates and the average value was used in Fig. 7.14. The measured twin width ratio for quenched alloy was 2.185. It decreases at 1.053 in the specimen aged for 3.6 ks, and then increase with aging time to 2.187 in the specimen aged for 360 ks. It would be interesting to compare the measured value of twin width ratio with a theoretical one calculated with the aid of phenomenological theory but until now there is no report on this direction in Ti-Pd alloys. However, this work was done in other SMA as for example in Ti-Ni alloy where the theoretical twin width ratio was reported to be 2.42 for {011} Type I twins[29]. The reported measured value is 2.16[30].

The main factor that affect martensite morphology in aged near-equiatomic Ti-rich Ti-Pd alloys seem to be the precipitates density rather than precipitates size. Due to the high density of precipitates, in the short time aged specimens the martensite must accommodate in very small volume, and the only possibility is formation of very narrow twins. On the other hand, when precipitates are rare (and large) as in the case of relatively long time aging specimens, martensite must accommodate in a large volume and therefore is easy to do it by large twins.

7.7 Conclusions

The morphologic and crystallographic aspects of $C11_b$-type precipitates nucleated in martensitic and parent phase matrices in aged Ti-rich Ti-Pd SMA's were investigated with electron microscopy techniques. The results of the research presented in this chapter are summarized as follows.

1) Three precipitate variants with the apparent habit planes of $(101)_{B19}$, $(10\bar{1})_{B19}$ and $(010)_{B19}$ nucleated and grew in the B2 parent phase of the aged Ti-47at.%Pd alloy. On the other hand, only one or two variants were observed when precipitates nucleated in martensitic state. Since the difference between the lattice spacing $(010)_{B19}$ and $(001)/3_{C11b}$ is about 20%, the nucleation of the third variant in martensite matrix is energetically unfavorable.

2) By long time aging (3600 ks) in martensitic state only one variant of Ti_2Pd precipitate was observed in the structure of Ti-47at.%Pd alloys. However, the morphology and the habit plane of the precipitate are different from those of the precipitate observed in DSC-like specimens.

3) In tensile strain specimens aged in martensitic state also only one precipitate variant was observed. Again, the morphology and the habit plane of the precipitate are different from those of the precipitate observed in DSC-like specimens. However, in this case the deformed martensite was found to have a 4H structure, which is different from the 2H structure of martensite in quenched Ti-Pd alloy. The reverse transformation temperatures in deformed specimens were found to increase with tensile strain.

4) The morphology of B19 martensite in near-equiatomic Ti-rich Ti-Pd alloys drastically change with the precipitates size and density. The main factor affecting martensite morphology seems to be the precipitate density. Due to the high density of precipitates the martensite must accommodate in very small volume, and the only possibility is formation of very narrow twins. The measured twin width ratio for quenched alloy is 2.185.

References

1. M. V. Nevitt and J. W. Downey: *Trans. Metall. Soc. AIME,* **22** (1962) 195.
2. E. Raub and E. Röschel: *Z. Metallkde.,* **59** (1968) 113.
3. V. N. Eremenko and T. D. Shtepa: *Porosh. Metall.,* **111** (1972) 75 (in Russian); tr. *Sov. Powder Metall.,* (1972) 228.
4. E. Quandt, C. Halene, H. Holleck, K. Feith, M. Kohl, P. Schloßmacher, A. Skokan and K. D. Skronbanek: *Sensor and Actuators A,* **53** (1996) 434.
5. H. Hoshi, K. Takezawa and K. Marukawa: *J. Japan Inst. Metals,* **62** (1998) 783.
6. H. Hoshi, K. Takezawa and K. Marukawa: *J. Japan Inst. Metals,* **62** (1998) 925.
7. H. Hoshi, K. Takezawa and K. Marukawa: *J. Electron Microscopy,* **48(4)** (1999) 333.
8. H. C. Donkersloot and J. H. N. Van Vucht: *J. Less-Common Met.,* **20** (1970) 83.
9. Y. Morizono, M. Nishida and A. Chiba: *Advanced Materials III/B: Composites, Grain Boundaries and Nanophase Materials,* **16B,** ed. M. Sakai, M. Kobayashi, T. Suga, R. Watanabe, Y. Ishida and K. Niihara, Trans. Mat. Res. Soc. Japan (1994) 1151.
10. M. Nishida, T. Hara, Y. Morizono, A. Ikeya, H. Kijima and A. Chiba: *Acta Mater.,* **45** (1997) 4847.
11. K. N. Melton, J. Simpson and T. W. Duering: *Proc. Int. Conf. on Martensitic Transformations (ICOMAT-86),* Japan Inst. Metals (1986) 1053.
12. K. N. Melton, J. L. Proft and T. W. Duering: *Proc. MRS Int. Mtg. On Adv. Mats.,* Tokyo, **9** (1989) 165.
13. M. Piao, S. Miyazaki, K. Otsuka and N. Nishida: *Mater. Trans. JIM,* **33** (1992) 337.
14. M. Piao, S. Miyazaki and K. Otsuka: *Mater. Trans. JIM,* **33** (1992) 346.
15. L. C. Zaho, T. W. Duering and C. M. Wayman: *Proc. MRS Int. Mtg. On Adv. Mats.,* Tokyo, **9** (1989) 171.
16. L. C. Zaho, T. W. Duering, S. Justi, K. N. Melton, J. L. Proft, W. Yu and C. M. Wayman: *Scr. Metall.,* **24** (1990) 221.
17. C. S. Zhang, L. C. Zhao, T. W. Duering and C. M. Wayman: *Scr. Metall.,* **24** (1990) 1807.
18. T. W. Duering, K. N. Melton and J. L. Proft: *Engineering Aspects of Shape Memory Alloys,* (1990) 130.
19. D. Golberg, Ya Xu, Y. Murakami, K. Otsuka, T. Ueki and H. Horikawa: *Mater. Lett.,* **22** (1995) 241.
20. M. Piao, K. Otsuka, S. Miyazaki and H. Horikawa: *Mater. Trans. JIM,* **34** (1993) 919.
21. T. Onda, Y. Bando, T. Ohba and K. Otsuka: *Mat. Trans. JIM,* **33** (1992) 354.
22. K. Otsuka: *Materials Science Forum,* Trans Tech Publications, Switzerland, **56-58** (1990) 393.
23. M. S. Wechsler, D. S. Lieberman and T. A. Read: *Trans. AIME,* **197** (1953) 1503.
24. D. S. Lieberman, M. S. Wechsler and T. A. Read: *J. Appl. Phys.,* **26** (1955) 473.
25. J. S. Bowels and J. K. Mackenzie: *Acta Metal.,* **2** (1954) 129.
26. J. S. Bowels and J. K. Mackenzie: *Acta Metal.,* **2** (1954) 138.
27. J. S. Bowels and J. K. Mackenzie: *Acta Metal.,* **2** (1954) 224.
28. J. S. Bowels and J. K. Mackenzie: *Acta Metal.,* **5** (1957) 137.
29. K. M. Knowels and D. A. Smith: *Acta Metal.,* **29** (1981) 101.
30. M. Nishida, H. Ohgi, I. Itai, A. Chiba and K. Yamauchi: *Acta Metal.,* **43** (1995) 1219.

Table 7.1 Crystallographic data of Ti_2Pd phase

Phase	Structurebericht designation	Crystal structure	Space group	Prototype	Temp., [K]	Lattice parameters, [nm] a_t	Lattice parameters, [nm] c_t	Method	Reference
						0.3090 ± 0.0001	1.0054 ± 0.0008		Nevitt and Downey[1]
Ti_2Pd	$C11_b$	Tetragonal	*I4/mmm*	Si_2Mo	293	0.3090	1.00425	X-ray diffraction	Raub and Röschel[2]
						0.3095	1.0050		Eremenko and Sthepa[3]
						0.3078	1.0045	X-ray diffraction on thin-films	E. Quandt *et al.*[4]

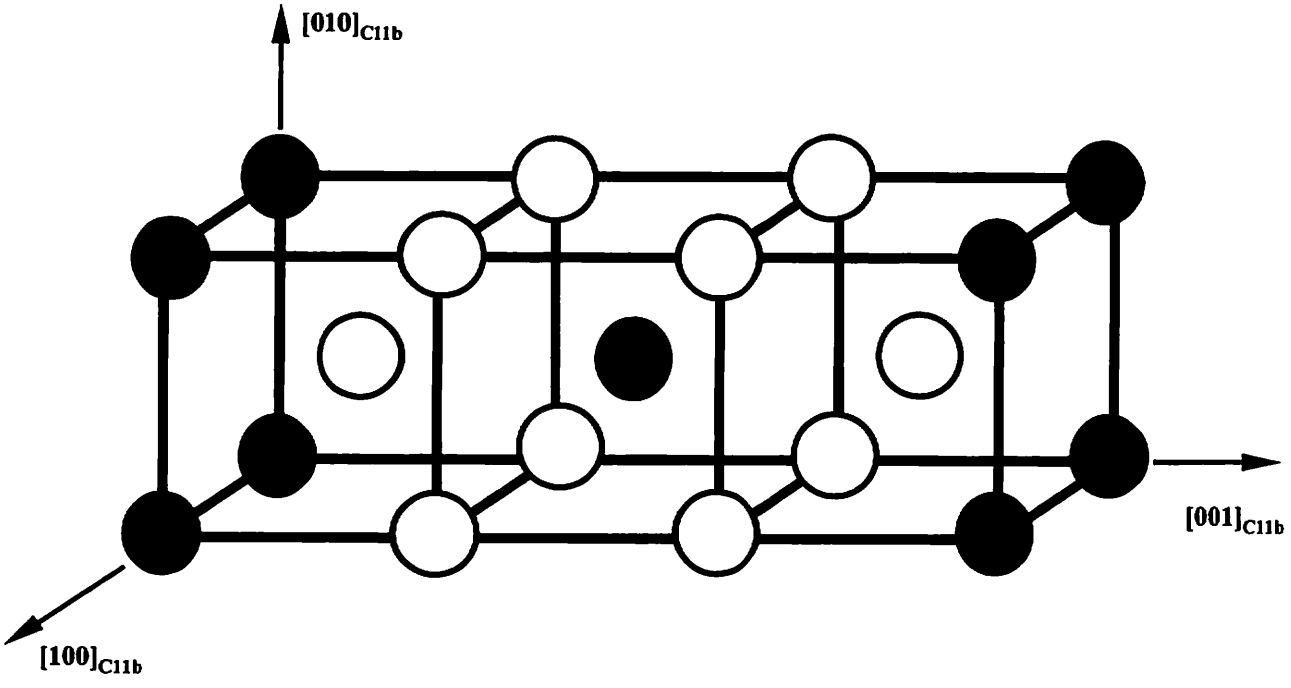

Fig. 7.1 The unit cell of the $C11_b$ structure. Open and solid circles denote different species of atoms[5-7].

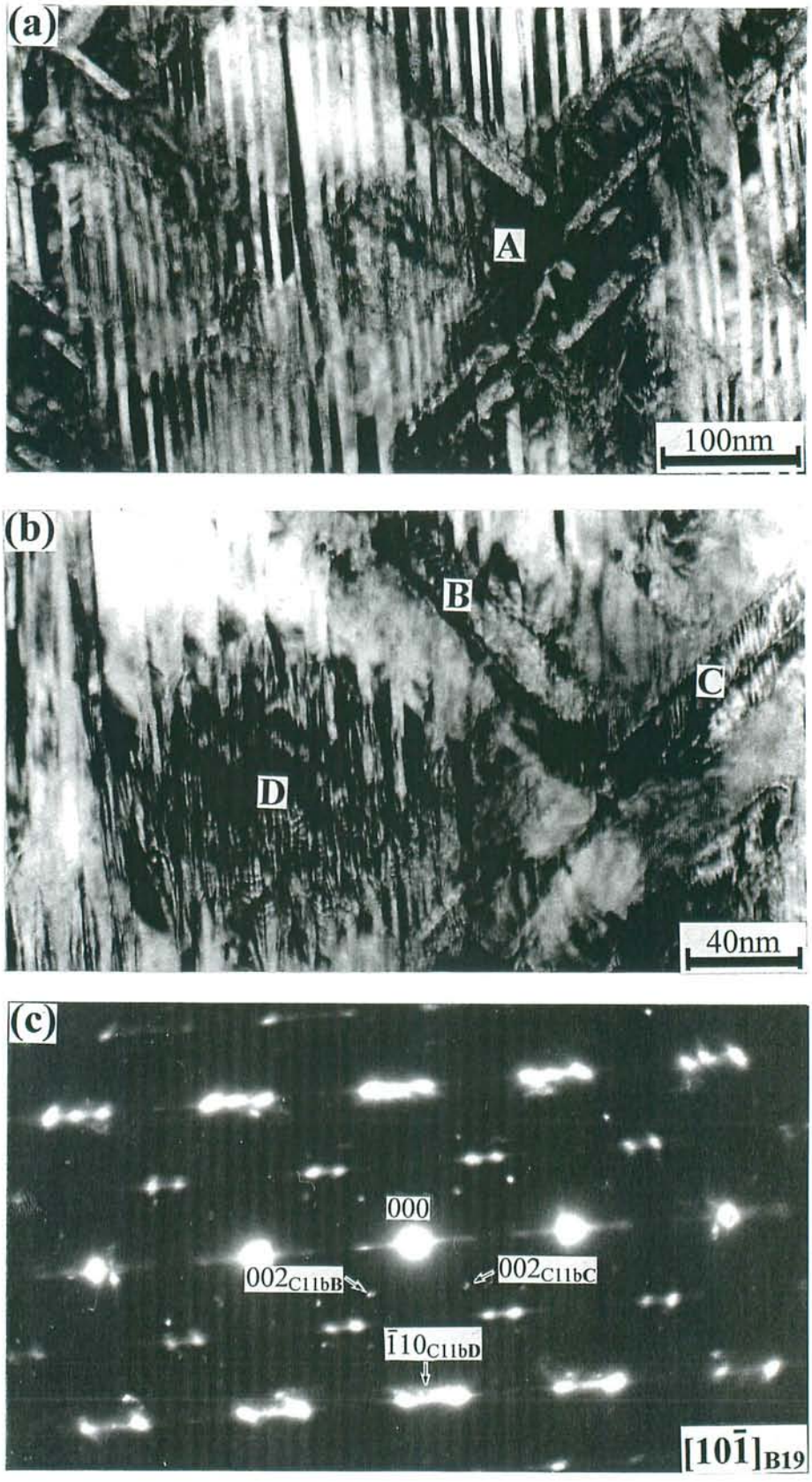

Fig. 7.2 (a) Bright field image of quenched Ti-47at%Pd alloy aged at 873 K for 1.8 ks. (b) Enlarged image of area A in (a). (c) Selected area diffraction pattern taken from area A in (a) showing $[10]_{B19}$ direction. See text for details.

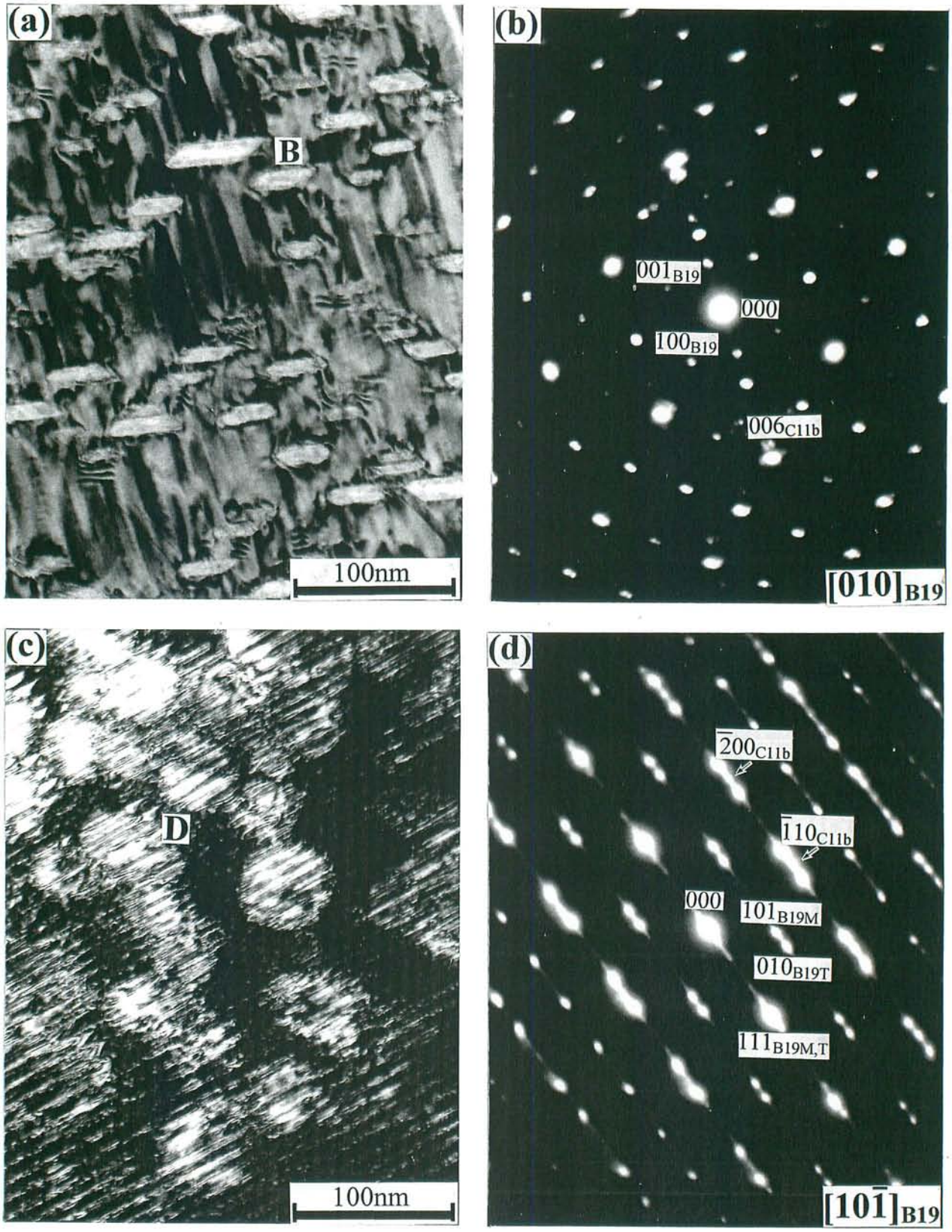

Fig. 7.3 (a) Bright field and (c) dark field images of water quenched Ti-47at%Pd alloy after heated up in DSC at 973 K and then quenched into ice water. (b), (d) Selected area electron diffraction patterns taken from (a) and (c) showing $[010]_{B19}$ and $[10\bar{1}]_{B19}$ zone axes, respectively.

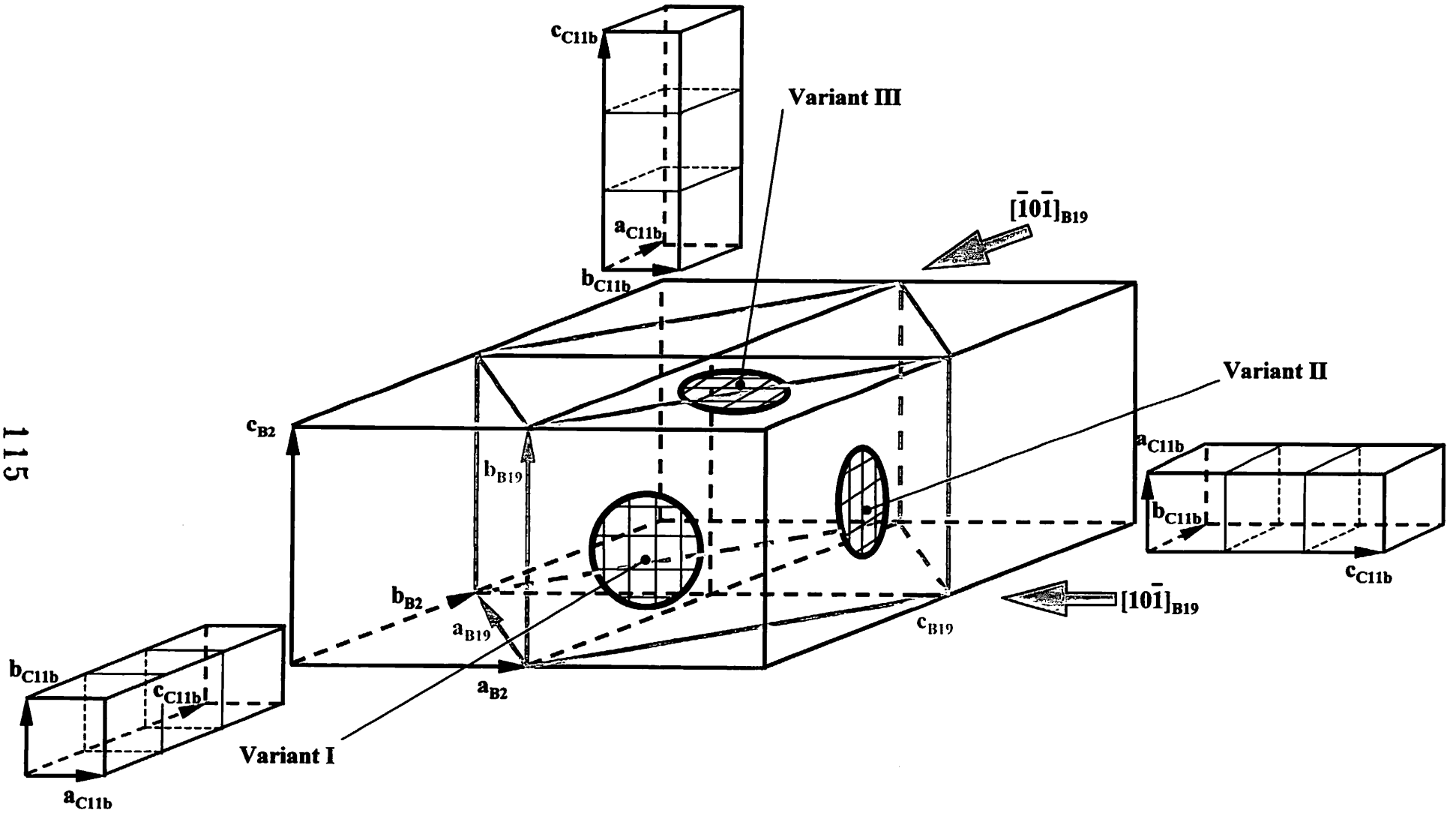

Fig. 7.4 Schematic illustration of the orientation relationships between Ti_2Pd precipitate variants ($C11_b$-type structure) and TiPd matrix with B2- and B19-type structures.

Lattice parameters of βTiPd, αTiPd and Ti_2Pd phases:

Phase	Strukturbericht symbol	Crystal structure	Lattice parameters, [nm]		
			a	b	c
βTiPd (parent phase)	B2	BCC	0.3180	0.3180	0.3180
αTiPd (martensitic phase)	B19	orthotombic	0.4560	0.2810	0.4890
Ti_2Pd	$C11_b$	tetragonal	0.3090	0.3090	1.0054

Beam direction in the present analysis:

Incident beam // $[001]_{B2}$ // $[010]_{B19}$ // Variant I $[010]_{C11b}$ // Variant II $[100]_{C11b}$ // Variant III $[001]_{C11b}$

Orientation relationship between precipitate variants and parent phase and martensitic phase matrices:

Variant I: $(001)_{C11b}$ // $(101)_{B19}$ // $(010)_{B2}$

Variant II: $(001)_{C11b}$ // $(10\bar{1})_{B19}$ // $(100)_{B2}$

Variant III: $(001)_{C11b}$ // $(010)_{B19}$ // $(001)_{B2}$

Precipitates nucleated in the parent phase:

Variant	Habit plane	Interplanar spacing, [nm]		Difference between the corresponding interplanar spacing $(d_{C11b} - d_{B2}) / d_{B2}$, [%]
		d_{C11b}	d_{B2}	
I	$(001)_{C11b}$ // $(010)_{B2}$	$d_{(003)C11b} = 0.3500$	$d_{(010)B2} = 0.3180$	5.4
II	$(001)_{C11b}$ // $(100)_{B2}$	$d_{(003)C11b} = 0.3500$	$d_{(100)B2} = 0.3180$	5.4
III	$(001)_{C11b}$ // $(001)_{B2}$	$d_{(003)C11b} = 0.3500$	$d_{(001)B2} = 0.3180$	5.4

Precipitates nucleated in the martensitic phase:

Variant	Habit plane	Interplanar spacing, [nm]		Difference between the corresponding interplanar spacing $(d_{C11b} - d_{B19}) / d_{B19}$, [%]
		d_{C11b}	d_{B19}	
I	$(001)_{C11b}$ // $(101)_{B19}$	$d_{(003)C11b} = 0.3500$	$d_{(101)B19} = 0.3335$	0.9
II	$(001)_{C11b}$ // $(10\bar{1})_{B19}$	$d_{(003)C11b} = 0.3500$	$d_{(101)B19} = 0.3335$	0.9
III	$(001)_{C11b}$ // $(010)_{B19}$	$d_{(003)C11b} = 0.3500$	$d_{(010)B19} = 0.2810$	**20**

Fig. 7.5 Calculation of the difference between the corresponding interplanar spacing of Ti_2Pd precipitate with $C11_b$-type structure and TiPd matrices with B2- and B19-type structures.

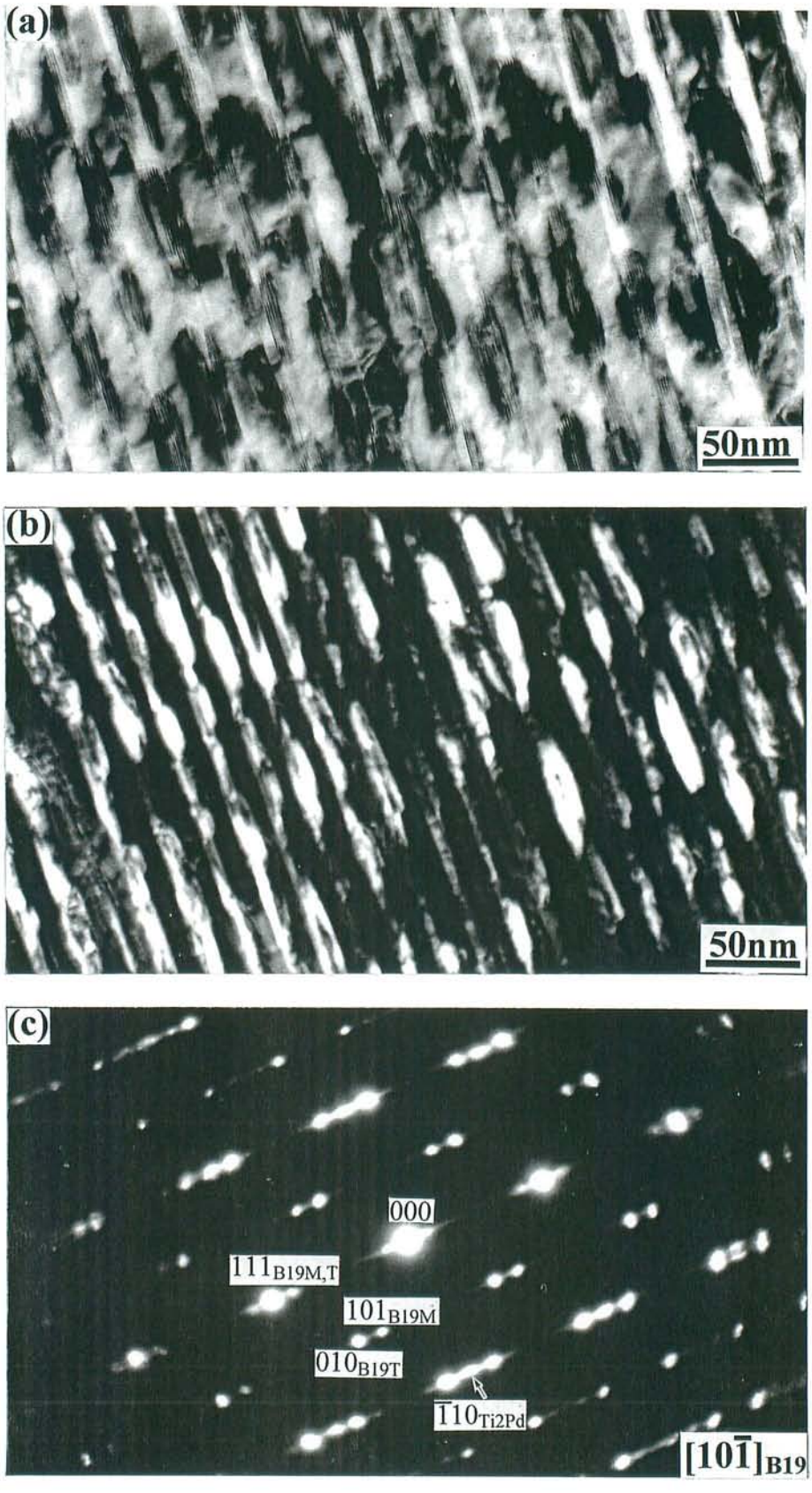

Fig. 7.6 (a) Bright field and (b) dark field images of Ti–47.5at.%Pd alloy aged in martensitic state at 753 K for 3600 ks. (c) Selected area electron diffraction pattern taken along $[10\bar{1}]_{B19}$ direction from the region shown in (a) and (b).

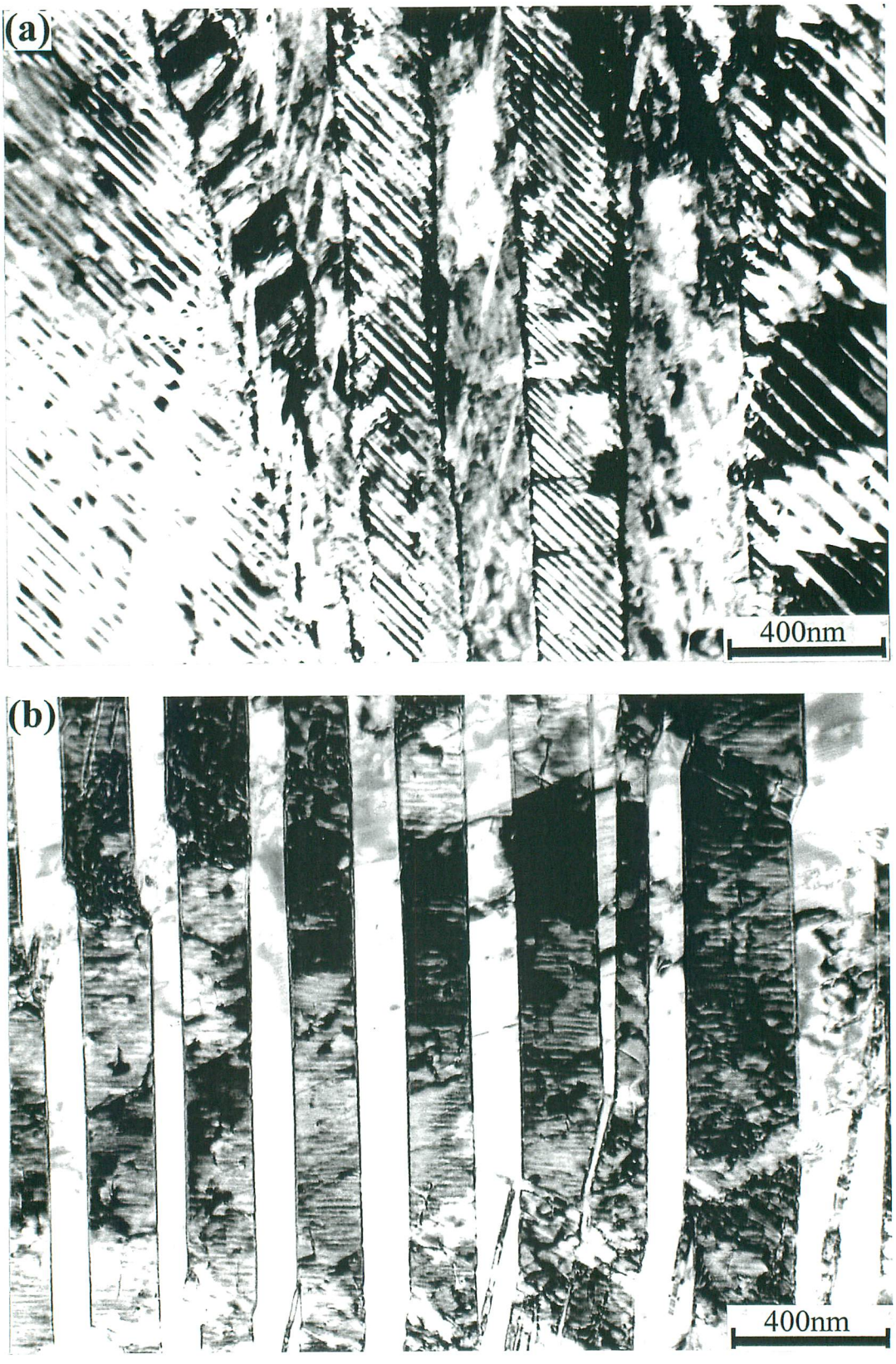

Fig. 7.7 Bright field micrographs of deformed Ti-48at.%Pd alloy. (a) $\varepsilon = 4\%$ and (b) $\varepsilon = 8\%$.

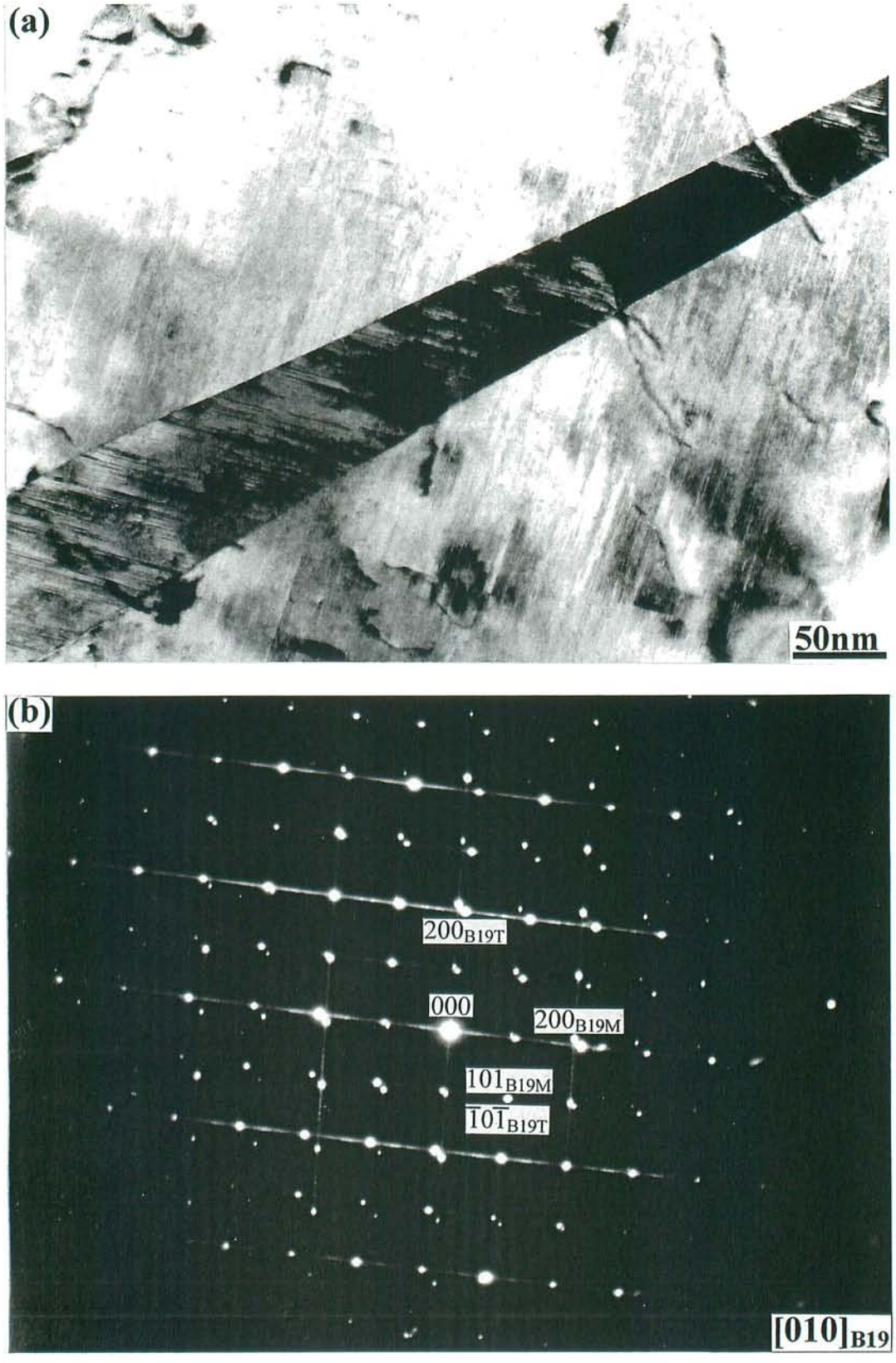

Fig. 7.8 (a) Bright field image from a quench Ti – 48at%Pd tensile test (ε = 8%) specimen. (b) Selected area electron diffraction pattern showing the (101) compound twin relation between the large martensite variants.

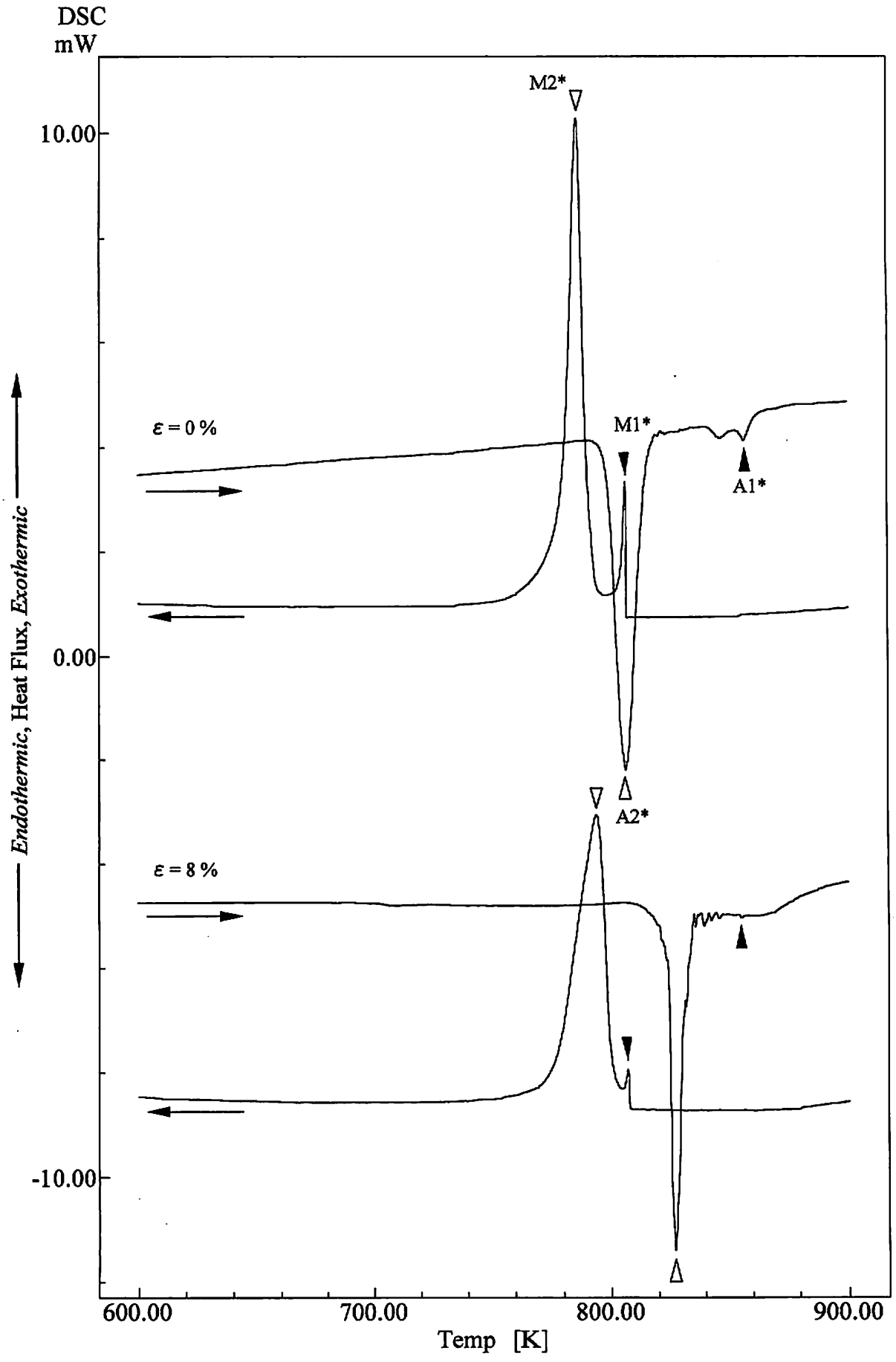

Fig. 7.9 DSC curves of the quenched Ti-48at.%Pd alloy solution treated at 1273 K for 3.6 ks ($\varepsilon = 0$ %) and tensile deformed at room temperature ($\varepsilon = 8$ %).

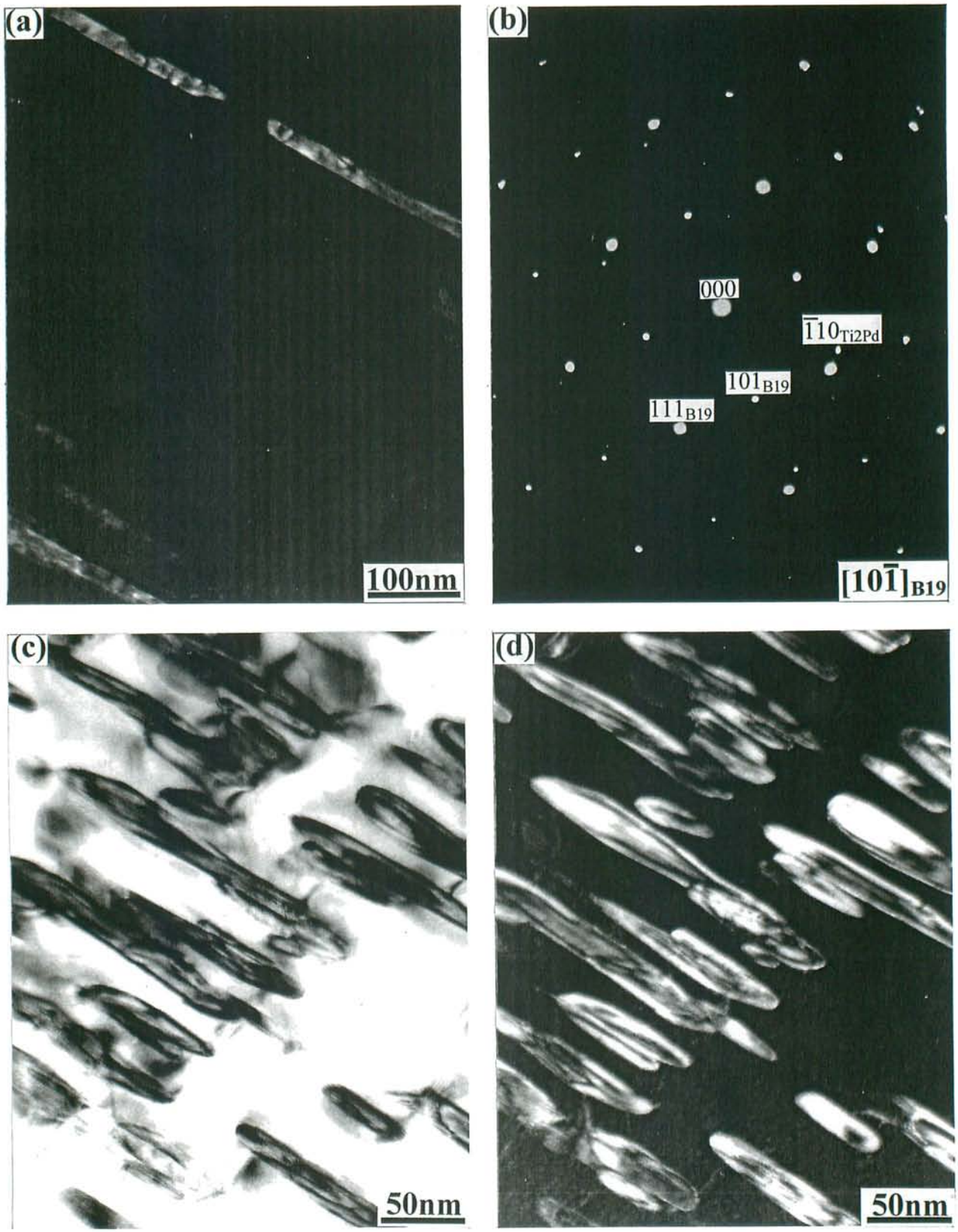

Fig. 7.10 (a), (d) Dark field images of tensile test (ε = 8%) Ti–48at.%Pd alloy aged in martensitic state at 788 K for 1620 ks. (b) Selected area electron diffraction pattern taken along $[10\bar{1}]_{B19}$ direction in (a). (c) Bright field image taken along $[10\bar{1}]_{B19}$ direction showing one precipitate variant.

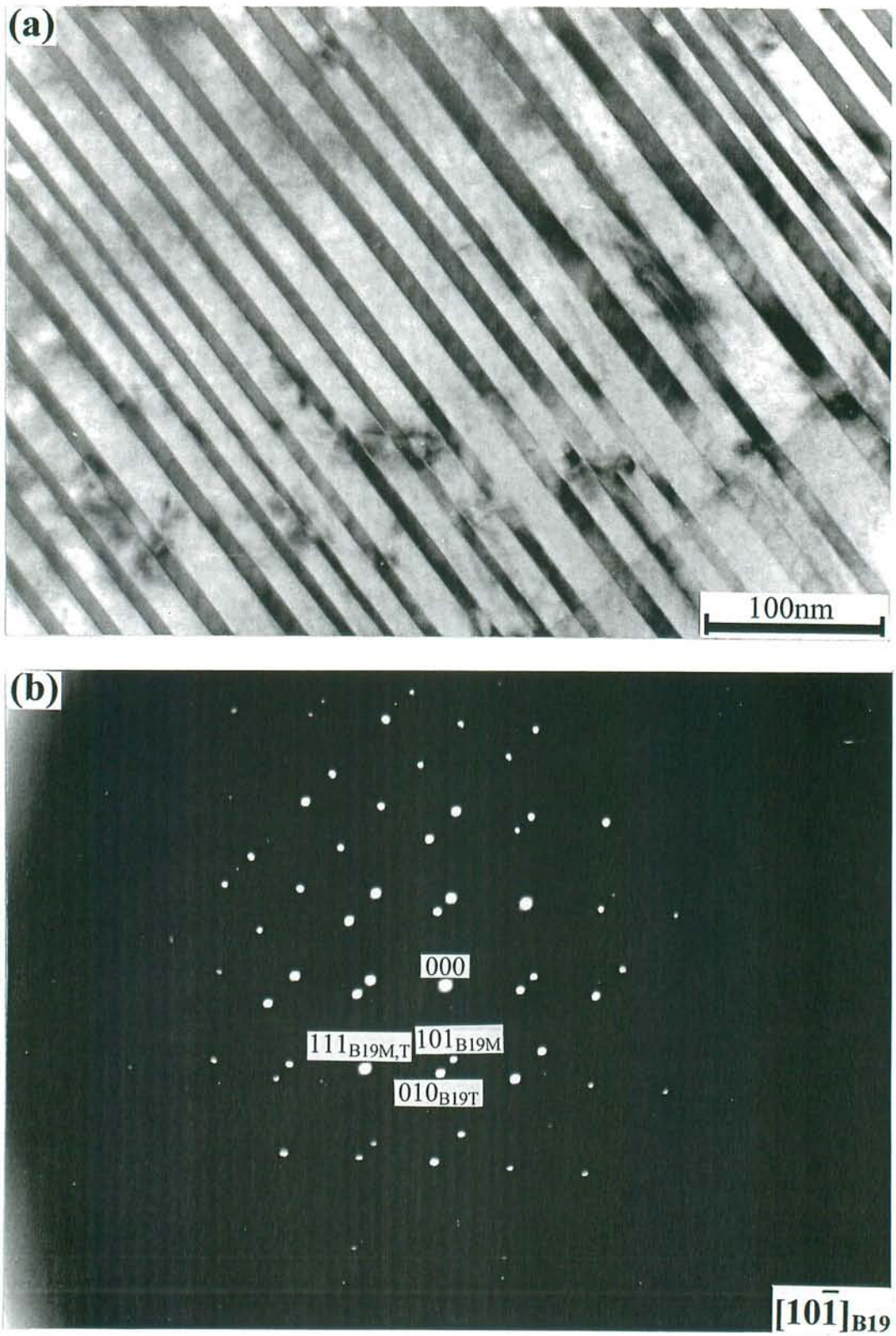

Fig. 7.11 (a) Bright field image of B19 martensite with large twins in a quenched Ti-47at.%Pd alloy solution treated at 1273 K for 3.6 ks. (b) Selected area diffraction pattern taken from (a), showing $[10\bar{1}]_{B19}$ zone axis.

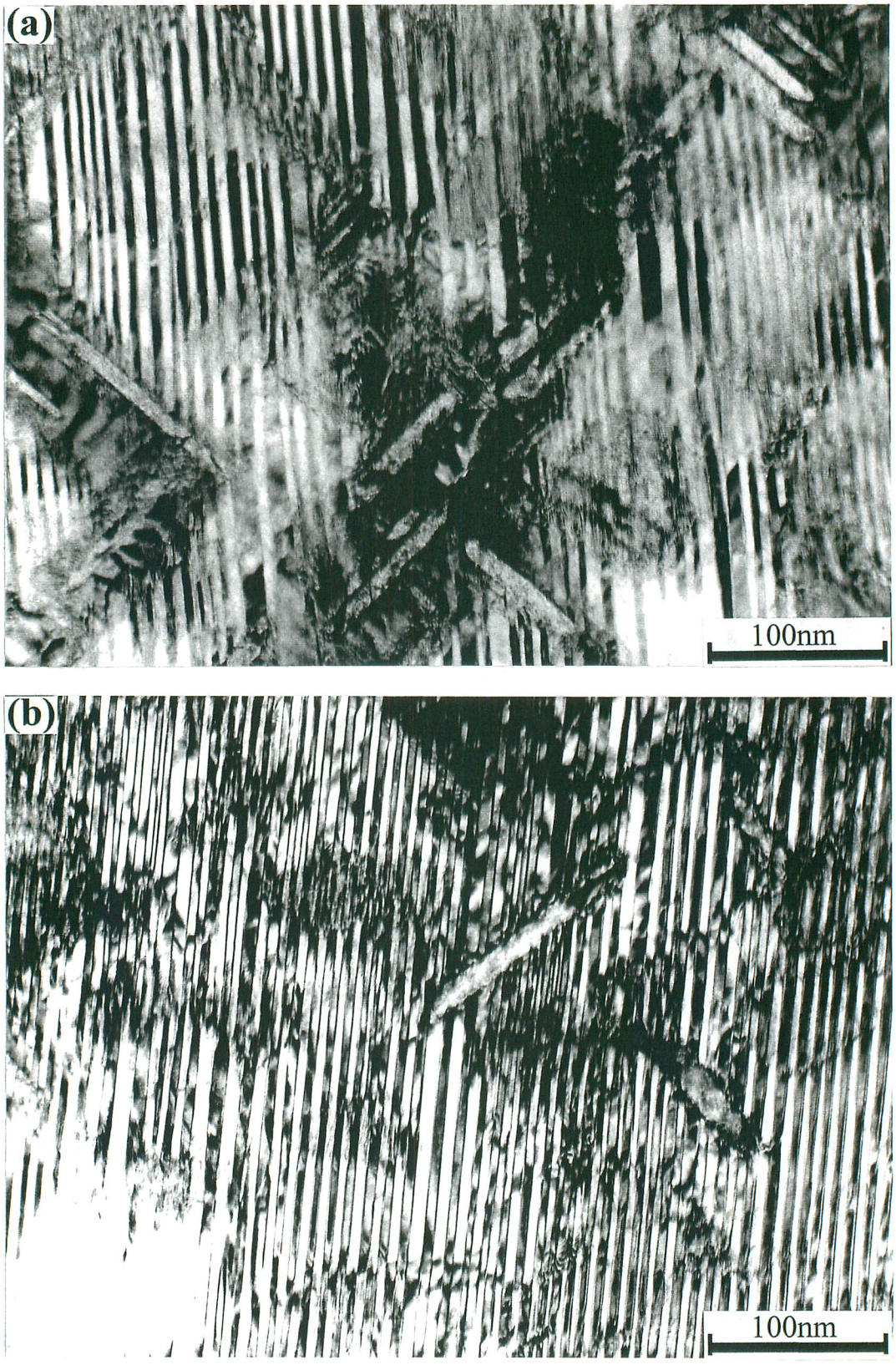

Fig. 7.12 The micrographs of a Ti-47at.%Pd alloy aged at 873 K for (a) 1.8 ks and (b) 3.6 ks showing the variation of both precipitates density and size and twins width with aging time.

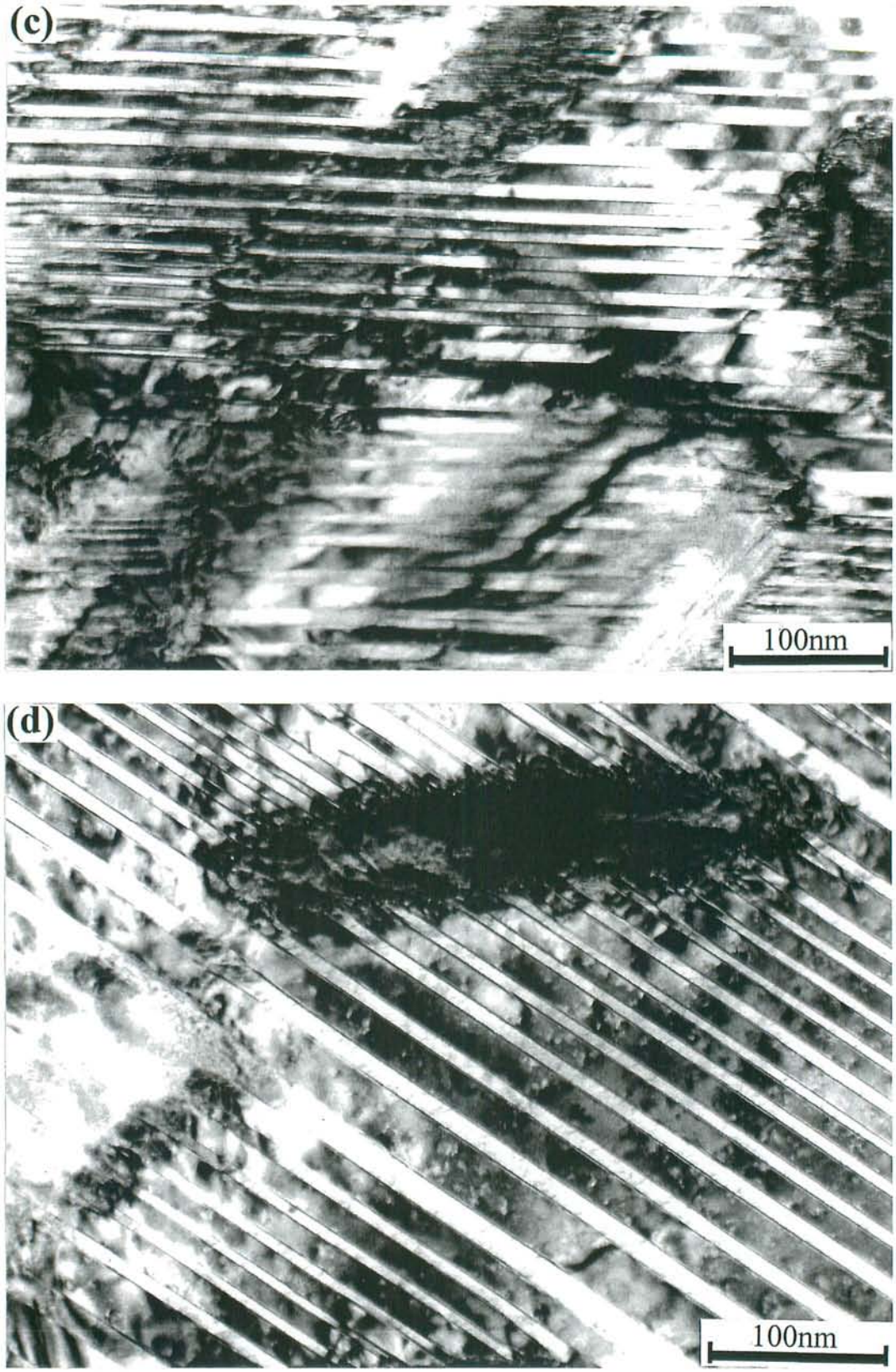

Fig. 7.12 (cont.) The micrographs of a Ti-47at.%Pd alloy aged at 873 K for (c) 36 ks and (d) 360 ks showing the variation of both precipitates density and size and twins width with aging time.

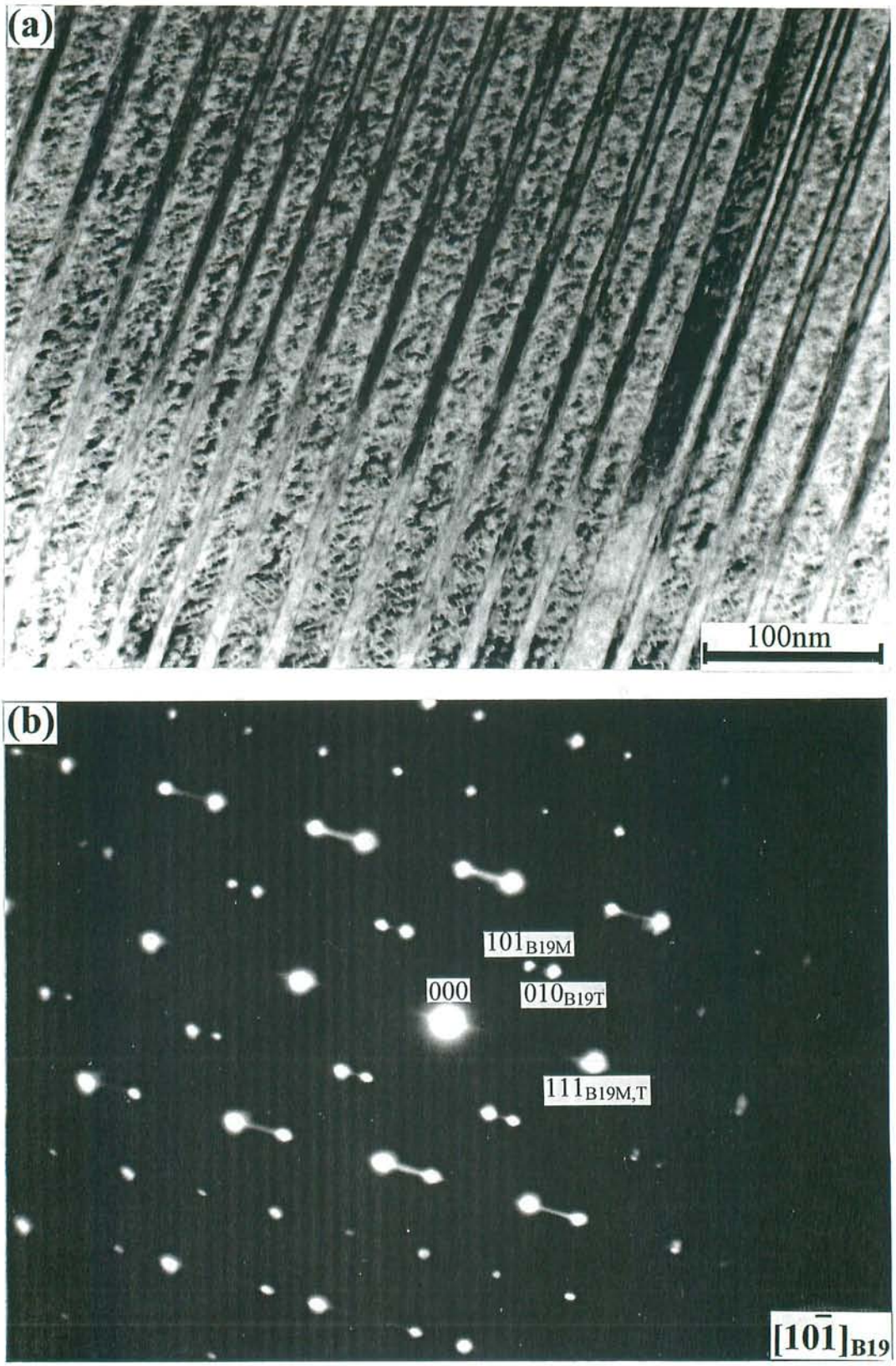

Fig. 7.13 (a) The micrograph of a Ti-47at.%Pd alloy after DSC-like treatment at 743 K. (b) Selected area diffraction pattern taken from (a) and showing $[10\bar{1}]_{B19}$ zone axis.

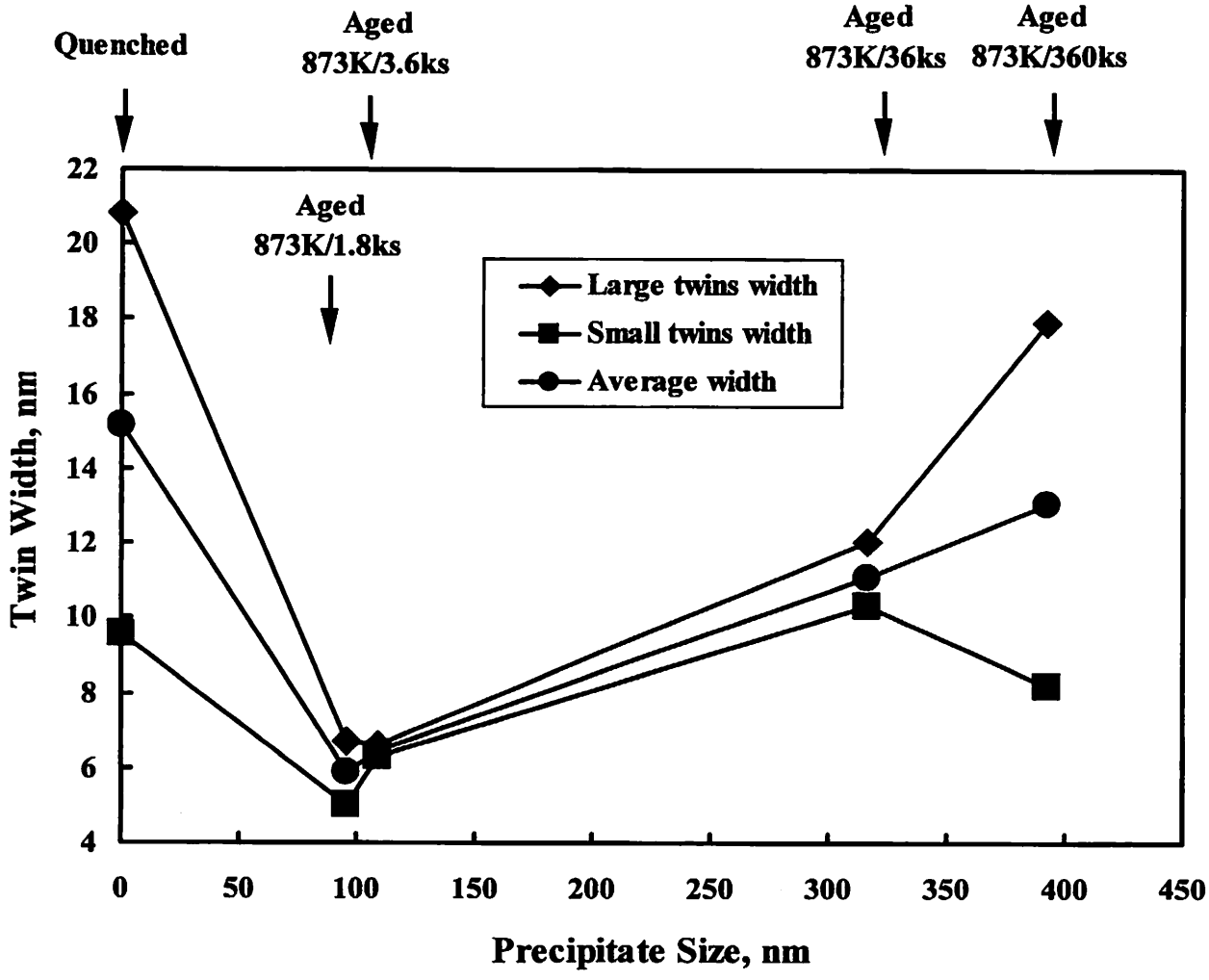

Fig. 7.14. Variation of twin width with precipitates size in Ti - 47at%Pd alloys aged at 873 K for 3.6, 36, 360 ks compared with twin width in quenched alloy.

Chapter 8

Concluding Remarks about Transformation Behavior and Related Phenomena in Near-Equiatomic Ti-Pd Shape Memory Alloys

The martensitic transformation behavior in near equiatomic Ti-Pd alloys has been studied by DSC and TEM techniques. The results obtained in the present work clarify the successive transformation mechanism, as well as effect of aging on successive transformation behavior. Other interesting phenomenon connected with martensitic transformation in Ti-Pd alloys, as for example precipitate variant selection and influence of precipitate density and size on martensite morphology was also researched and discussed. The phase boundary of TiPd intermetallic compound was reevaluated in the light of the obtained results. The main results of the present research are summarized in the following.

1) In Ti-rich alloys martensitic transformation takes place in two successive steps, while in Pd-rich alloy martensitic transformation occurs in only one step as indicated by the pairs of endothermic-exothermic peaks on DSC curves of those alloys.
2) The successive martensitic transformation behavior is closely related to the nucleation and growth of fine Ti_2Pd precipitates ($C11_b$-type structure) and its mechanism could be explained as follows. The first step represents the reverse martensitic transformation of the TiPd matrix and the second one is due to the reverse martensitic transformation in the local neighboring areas of the precipitates where Pd concentration is higher than that in matrix.
3) Three variants of the precipitates, with the apparent habit planes of $(101)_{B19}$, $(10\bar{1})_{B19}$ and $(010)_{B19}$, nucleated and grew in the B2 parent phase.

4) Transformation behavior is greatly affected by aging conditions. Successive transformation takes place in the Ti-47at.%Pd alloy after short time aging irrespective of aging temperature. On the contrary, only the specimen aged above 1073 K shows successive transformation after relatively prolonged period.

5) From the obtained experimental data the homogeneity range of the TiPd compound in Ti-rich side is estimated to extends from the near-equiatomic composition of about 50.4 at.%Ti at around 873 K to about 51.8 at.%Ti at 1073 K.

6) The mechanism of transformation behavior in aged Ti-47at.%Pd alloy is explained based on the experimental results and the homogeneity range of TiPd compound, as follows:

- In the specimens aged above 1123 K successive transformations occur irrespective of aging period. Successive transformation behavior is connected to the formation of fine Ti_2Pd precipitates and takes place in the same way as in solution treated alloys. The first transformation step on heating represent the reverse transformation of the TiPd matrix, while the second one is due to the reverse martensitic transformation in small volumes around Ti_2Pd precipitates where Pd concentration is higher than in the matrix.
- In the specimens aged around 1073 K the successive transformation behavior is independent of aging time. Although the equilibrium between TiPd and Ti_2Pd is completed after short time aging, by cooling the specimens to the room temperature, the TiPd matrix become supersaturated in Ti as could be understood from the variation of the homogeneity range of TiPd compound. By heating, new precipitates will nucleate and grow in the matrix and therefore, the conditions for successive transformations are accomplished.
- After relatively prolonged period successive transformations do not appear in the specimens aged below 1023 K since the equilibrium between TiPd and Ti_2Pd is stable, and the matrix is not any more supersaturated in Ti for formation of new

precipitates.

7) Three precipitate variants with the apparent habit planes of $(101)_{B19}$, $(10\bar{1})_{B19}$ and $(010)_{B19}$ nucleated and grew in the B2 parent phase of the aged Ti-47at.%Pd alloy. On the other hand, only one or two variants were observed when precipitates nucleated in martensitic state. Since the difference between the lattice spacing $(010)_{B19}$ and $(001)/3_{C11b}$ is about 20%, the nucleation of the third variant in martensite matrix is energetically unfavorable.

8) By long time aging (3600 ks) in martensitic state only one variant of Ti_2Pd precipitate was observed in the structure of Ti-47at.%Pd alloys. However, the morphology and the habit plane of the precipitate are different from those of the precipitate observed in DSC-like specimens.

9) In tensile strain specimens aged in martensitic state also only one precipitate variant was observed. Again, the morphology and the habit plane of the precipitate are different from those of the precipitate observed in DSC-like specimens. However, in this case the deformed martensite was found to have a 4H structure, which is different from the 2H structure of martensite in quenched Ti-Pd alloy. The reverse transformation temperatures in deformed specimens were found to increase with tensile strain.

10) The morphology of B19 martensite in near-equiatomic Ti-rich Ti-Pd alloys drastically changes with the precipitates size and density. The main factor affecting martensite morphology seems to be the precipitate density. Due to the high density of precipitates the martensite must accommodate in very small volume, and the only possibility is formation of very narrow twins. The measured twin width ratio for quenched alloy is 2.185.

Based on the above-obtained results the potential of the Ti-Pd high temperature shape memory alloys for different practical applications can be significantly improved.

Appendix

High Temperature Shape Memory Alloys

Current commercial SMA's have the transformation temperatures below 473 K. However, if SMA's with martensitic transformation temperatures above 573 K are developed, it will became possible that applications of these materials to be much widened such as in automobiles engines, rocket engines, air planes turbines, fire protection, safety control of high temperature chemical reactions, nuclear reactor environments etc. There are few metallic materials that might be used as high temperature shape memory alloys (HTSMA's): Cu-Al-Ni-Mn, Ni-Al (Fe, Mn), Ti-Ni (Zr, Hf), Zr-Cu (Ni, Co), Ni-Mn (Ti, Al), Nb-Ru, Ta-Ru and Ti-noble metals (Au, Pt, Pd) alloys.

Cu-Al-Ni-based alloys show the transformation temperatures up to 723 K. However, these alloys have problems of ductility and phase stability that do not allow to observe SME at high temperatures. Addition of Mn can help, but the transformation temperatures are decreased to around 473 K.

Ni-Al alloys are attractive, since they are not expensive and the martensitic transformation start temperature (M_s) may be raised up to 1200 K, depending upon the composition. The major problems of these alloys are their brittleness and the fact that the martensite tends to transform into the Ni_5Al_3 phase instead of reverse transforming into the parent phase upon heating. The mechanical properties can be improved by precipitating a ductile face-centered cubic (FCC) phase by the addition of Fe or Mn as a ternary element.

In Ti-Ni (Zr, Hf) alloys transformation temperatures up to 723 K were reported. However, depending upon the composition a brittle phase appears and thus is not certain whether they can be used for practical applications or not.

Zr-Cu (Ni, Co) alloys have the maximum transformation temperatures around 1323 K. The problem with these alloys is the large transformation hysteresis (373 – 473 K) and non-thermoelastic transformation behavior. By alloying with Co the hysteresis is reduced but transformation temperatures decreases.

Ni-Mn based HTSMA's exhibit transformation temperatures between 373 K and 973 K depending upon composition and alloying elements. The problems with these alloys are identical with those of Ni-Al based alloys: poor ductility and phase decomposition.

Nb-Ru and Ta-Ru alloys have been recently discovered as potential materials for high temperature shape memory applications. These alloys have shape memory transition temperatures in excess of 1273 K. Although they exhibited significant strain recovery, limited ductility was reported due to the average grain size larger than 1 mm.

Finally, Ti-noble metals (Au, Pt, Pd) alloys have fairly high transformation temperatures. The main problem is that these alloys are quite expensive, Ti-Pd being the less expensive among them. The M_s temperature in a Ti-50 at.%Pd alloy is about 823 K and can be changed widely by replacing Pd with a ternary element such as Ni, Fe, Cr, Co, V. Crystal structures, transformation temperatures, shape memory characteristics and references of/about the presently known HTSMA's are described in Table A.1.

References

1. J. Gui, W. H. Zou, R. Wang, D. Zhang, C. H. Tang, M. Z. Xiang and D. Z. Yang: *Scr. Materl.*, **35** (1996) 435.
2. Y. Itsumi, Y. Miyamoto, T. Takashima, K. Kamei and K. Sugimoto: *Proc. Int. Conf. on Martensitic Transformations (ICOMAT-89),* Sydney, Australia, *Materials Science Forum Vols. 56 – 58,* Trans Tech Publications, Switzerland (1990) 469.
3. S. Stanciu, Ph. D. Thesis, "Gh. Asachi" Technical University of Iasi, Romania (1998).
4. K. Sugimoto, K. Kamei and M. Nakaniwa: *Proc. In.l Conf. on Engineering Aspects of Shape Memory Alloys,* Butterworth-Heineman, London (1990) 89.
5. K. Sugimoto, K. Kamei, H. Matsumoto, S. Komatsu and T. Sugimoto: *Proc. Int. Conf. on Martensitic Transformations (ICOMAT-82),* Leuven, Belgium, *J. de Phys.*, **43** (Suppl. 4) (1982) C4-761.
6. M. Qi, C. Y. Chung and D. Z. Yang: *Proc. Int. Conf. on Martensitic Transformations (ICOMAT-95),* Lausanne, Switzerland, *J. de Phys. IV,* Colloque C8 (Suppl. J. de Phys. III, no. 12) (1995) C8-931.
7. P. Olier, J. C. Brachet, J. L. Bechade, C. Foucher and G. Guenin: *Proc. Int. Conf. on Martensitic Transformations (ICOMAT-95),* Lausanne, Switzerland, *J. de Phys. IV,* Colloque C8 (Suppl. J. de Phys. III, no. 12) (1995) C8-741.
8. L. Meisner and V. Sivokha: *Proc. Int. Conf. on Martensitic Transformations (ICOMAT-95),* Lausanne, Switzerland, *J. de Phys. IV,* Colloque C8 (Suppl. J. de Phys. III, no. 12) (1995) C8-765.
9. Krupp GmbH, Essen., Patentschrift DE 4006076. CI. Fried (1990).

10. D. R. Angst, P. E. Thoma and M. Y. Kao: *Proc. Int. Conf. on Martensitic Transformations (ICOMAT-95),* Lausanne, Switzerland, *J. de Phys. IV,* Colloque C8 (Suppl. J. de Phys. III, no. 12) (1995) C8-747.
11. G. Airoldi, S. Piredda, M. Pozzi and A. V. Shelyakov: *Proc. Int. Symp. on Shape Memory Materials (SMM'99),* Kanazawa, Japan, *Materials Science Forum Vols. 327–328,* Trans Tech Publications (2000) 135.
12. H. C. Donkersloot and J. H. N. Van Vucht: *J. Less-Common Metals,* **20** (1970) 83.
13. K. Otsuka, K. Oda, Y. Ueno, Min Piao, T. Ueki and H. Horikawa: *Scr. Metall. Mater.,* **29** (1993) 1355.
14. P. G. Lindquist and C. M. Wayman: *Proc. Int. Conf. on Engineering Aspects of Shape Memory Alloys,* Butterworth-Heineman, London (1990) 58.
15. D. Golberg, Y. Xu, Y. Murakami, S. Morito, K. Otsuka, T. Ueki and H. Horikawa: *Scr. Metal. Mater.,* **30** (1994) 1349.
16. D. Golberg, Y. Xu, Y. Murakami, K. Otsuka, T. Ueki and H. Horikawa: *Mater. Lett.,* **22** (1995) 241.
17. K. Otsuka and X. Ren: *Intermetallics,* 7 (1999) 511.
18. K. Otsuka, *Materia Japan,* **37** (1998) 125.
19. Y. Suzuki, Y. Xa, S. Morito, K. Otsuka and K. Mitose: *Mater. Lett.,* **36** (1998) 85.
20. K. Enami, Y. Kitano and K. Horii: *Proc. MRS Int. Meeting on Advanced Materials,* **9** (1989) 117.
21. K. Enami, K. Horii and J. Takahashi: *ISIJ International,* **29** (1989) 430.
22. K. Otsuka and D. Golberg: *Intelligent Materials and Systems,* Ed. P. Vincenzini, Techna Srl, (1995) 55.
23. K. Enami, T. Yoshida and S. Nenno: *Proc. Int. Conf. on Martensitic Transformations (ICOMAT-86),* Nara, Japan, The Japan Institute of Metals, (1986) 103.
24. K. Enami, H. Seki and S. Nenno: *Tetsu to Hagane,* **72** (1986) 563.
25. K. Enami, K. Morota, M. Hisa and K. Inue: *Proc. Int. Symp. on Shape Memory Materials (SMM'99),* Kanazawa, Japan, *Materials Science Forum Vols. 327–328,* Trans Tech Publications (2000) 287.
26. V. V. Martynov, K. Enami, L. G. Khandros, S. Nenno and A. V. Tkachenko: *Proc. Int. Conf. on Martensitic Transformations (ICOMAT-82),* Leuven, Belgium, *J. de Phys.,* **43** (Suppl. 12) (1982) C4-659.
27. V. V. Martynov, K. Enami, L. G. Khandros, A. V. Tkachenko and S. Nenno: *Phys. Met. Metallography,* **55** (1983) 136.
28. J. L. Smialek and R. F. Hehemann: *Metall. Trans.,* **4** (1973) 1571.
29. Y. D. Kim and C. M. Wayman: *Scr. Metall. Mater.,* **24** (1990) 245.
30. P. L. Potapov, N. A. Poliakova and V. A. Udovenko: *Scr. Mater.,* **35** (1996) 423.
31. P. L. Potapov, P. Ochin, J. Pons and D. Schryvers: *Acta Mater.,* **48** (2000) 3833.
32. R. Kaniuma, H. Ohtani and K. Ishida: *Metall. Mater. Trans. A,* **27A** (1996) 2445.
33. R. Kaniuma, H. Nakano and K. Ishida: *Metall. Mater. Trans. A,* **27A** (1996) 4153.
34. P. L. Potapov, N. A. Polyakova, V. A. Udovenko and E. L. Svistunova: *Z. Metallk.,* **87** (1996) 33.
35. P. L. Potapov: *Metal Science and Heat Treatment,* **35** (1993) 520.
36. K. K. Lee, P. L. Potapov, S. Y. Song and M. C. Shin: *Scr. Mater.,* **36** (1997) 207.
37. V. A. Udovenko, P. L. Potapov, N. A. Poliakova and V. Prieb: *Z. Metallk.,* **86** (1995) 345.
38. Y. N. koval, G. S. Firstov, J. V. Humbeeck, L. Delaey and W. Y. Jang: *Proc. Int. Conf. on Martensitic Transformations (ICOMAT-95),* Lausanne, Switzerland, *J. de Phys. IV,* Colloque C8 (Suppl. J. de Phys. III, no. 12) (1995) C8-1103.
39. V. V. Nemoshkalenko, A. V. Zhalko-Titarenko and Y. N. Koval: *Proc. Int. Conf. on Martensitic Transformations (ICOMAT-95),* Lausanne, Switzerland, *J. de Phys. IV,* Colloque C8 (Suppl. J. de Phys. III, no. 12) (1995) C8-1151.
40. R. W. Fonda, H. N. Jones and R. A. Vandermeer: *Scr. Mater.,* **39** (1998) 1031.
41. R. W. Fonda and H. N. Jones: *Mater. Sci. Eng. A,* **273-275** (1999) 275.

Table A.1. Crystal structure, transformation temperatures and shape memory characteristics of the presently known HTSMA's.

Alloy system	Composition	Crystal structure		Transformation temperatures, K				Last step of the thermal history	ε_{SME}, %	Def. mode	Ref.	Observations
		Parent phase	Martensitic phase	A_s	A_f	M_s	M_f					
Cu-based alloys	Cu-(11-13.6)Al-5Ni-(1.6-2)Mn-1Ti, (wt.%)	$L2_1$	$M18R_1$	approx. 455 K	approx. 510 K	approx. 440 K	approx. 420 K	Quenched from 1173 K		Compres-sion	[1] [2]	- Transformation temperatures can increase by different aging treatments; - Better SME by rapid thermal cycling between RT and 510 K; - Alloys with eutectoid composition had the best thermal resistance for SME (eutectoid composition ~ 12.7 wt.% Al).
	Cu-(12.5-13.5)Al-(3.7-4)Ni-(0.3-0.6)Fe, (wt.%)			max. 587 K	max. 698 K	max. 651 K	max. 556 K	Quenched from 1173 K	?	Bending	[3]	- Applied deformation completely recovered by SME.
	?											- Other references about Cu-based HTSMA's: [4]-[6].
Ti-Ni-based alloys	Ti-(48.5-50)Ni-(1-20)Zr, (at.%)	B2	B19'	approx. 470 K	approx. 491 K	approx. 436 K	approx. 403 K	Heat treated above 1123 K	4.5	Torsion	[7] [8]	- Transformation temperatures rise with increasing Zr content.
	Ti-Ni-Zr-Cu										[8] [9]	
	Ti-49Ni-(3-30)Hf, (at.%)			Endothermic peak temperature max. 895 K		Exothermic peak temperature max. 798 K					[10]	
	Ti-50Ni-(12-15)Hf, (at.%)			max. 474 K	max. 491 K	max. 436 K	max. 403 K	Homogenized at 1153 K for 259.2 ks	4	Tensile	[7]	- Improving of SME when the pre-strain is performed in the austenitic state.
	Ni-30Ti-20Hf			503 K	520 K	438 K	433 K	Melt-spun ribbons heat treated at 833 K for 300 s			[11]	
	?											
Ti-noble metals alloys	Ti-(45-55)Pd, (at.%)	B2	B19	approx. 847 K	approx. 865 K	approx. 820 K	approx. 812 K	Quenched from 1173 K	1 (at RT)	Tensile	[12] - [14]	- No SME in the specimens deformed at high temperature.

Table A.1. *Continued*

Alloy system	Composition	Crystal structure		Transformation temperatures				Last step of the thermal history	ε_{SME}, %	Def. mode	Ref.	Observations
		Parent phase	Martensitic phase	A_s	A_f	M_s	M_f					
	Ti-(45-52.6)Au, (at.%)	B2	B19	min. 808 K	min. 858 K	min. 848 K	min. 793 K	Rapid quenched			[12]	
	Ti-(45-52.5)Pt, (at.%)	B2	B19	min. 1268 K	min. 1293 K	min. 1273 K	min. 1253 K	Rapid quenched			[12]	
	?											
Ti-Pd-based alloys	Ti-(50-x)Pd-xNi $10<x\leq30$, (at.%)	B2	B19	max. 847 K	max. 865 K	max. 820 K	max. 812 K	Quenched from above 1123 K	>2	Tensile	[15] - [18]	- Transformation temperatures varies significantly with Ni content; - Deformation recovered by SME increases to 5.5% if the specimen is annealed at 673 K for 3.6 ks after cold working.
	Ti-30Pd-19.8Ni-0.2B, (at.%)	B2	B19	494 K	506 K	489 K	482K	Quenched from 1173 K	~5	Tensile	[19]	- Addition of B is beneficial to high temperature ductility and strength of Ti-30Pd-20Ni.
	Ti-(50-x)Pd-xCr $2\leq x\leq7$, (at.%)	B2	B19(2H) (+9R+IC)	min. 416 K	min. 440 K	min. 429 K	min. 406 K	Quenched from 1373 K	<2	Tensile	[20] - [22]	
	Ti-(46-x)Pd-xCr $2\leq x\leq3$, (at.%)	B2	B19+9R	min. 419 K	min. 444 K	min. 434 K		Quenched from 1373 K			[21]	
	Ti-(50-x)Pd-xFe $6\leq x\leq10$, (at.%)	B2	B19(2H)+ 9R (or IC)	min. 451 K	min. 463 K	min. 446 K	min. 434 K	Quenched from 1373 K			[23]	
	Ti-(46-x)Pd-xFe $4\leq x\leq6$, (at.%)	B2	B19(2H)+ 9R	min. 397 K	min. 442 K	min. 392 K	min. 375 K	Quenched from 1373 K	~1	Tensile	[23] [24]	- Recoverable pseudoelastic strain of 3%.
	Ti-(50-x)Pd-xV $4\leq x\leq8$, (at.%)	B2	B19(2H)+ 9R (or IC)			min. 407 K		Quenched from 1373 K			[20]	
	(50-x)Ti-50Pd-xV, $6\leq x\leq10$, (mol.%)	B2	B19(2H)	min. 723 K	min. 755 K	min. 704 K	min. 682 K	Quenched from 1273 K	?	Bending	[25]	
	Ti-(50-x)Pd-xCo, $12\leq x\leq16$, (at.%)	B2	B19(2H)+ 9R			min. 400 K		Quenched from 1373 K			[20]	
	?											

Table A.1. *Continued*

Alloy system	Composition	Crystal structure		Transformation temperatures				Last step of the thermal history	ε_{SME}, %	Def. mode	Ref.	Observations
		Parent phase	Martensitic phase	A_s	A_f	M_s	M_f					
Ni-Al-based alloys	Ni-(31-40)Al, (at.%)	B2	$L1_0$ when Al<37at.% And 14M when Al>37at.%			max. 1200 K		Homogenized at 1670 K for 72 ks	≤0.7	Compres-sion	[26] - [30]	- Whether or not the 14 M structure should be considered as an independent structure or simply a variation of $L1_0$ is still under discussion [31].
	$(Ni_{64}Al_{36})$-xCu 0.43≤x≤1.21, (at.%)	B2	$L1_0$(3R)	min. 402 K	min. 426 k	min. 404 K	min. 382 K	Quenched from 1573 K			[32]	
	?											
Ni-Mn-based alloys	Ni-(50-x)Mn-xAl, 0<x≤16, (at.%)	B2	$L1_0$(+14M)	min, 407 K	min. 465 K	min. 464 K	min. 401 K	Quenched from 1273 K-1373 K			[33]	- The 14 M martensite appear in the Ni-Al-Mn alloys with Mn content larger than 30 at.% [32].
	(40-60)Ni-(50-15)Mn-(10-25)Al, (at.%)	B2	$L1_0$(+14M)	min. 459 K	min. 472 K	min. 461 K	min. 434 K	Quenched from 1273 K-1373 K			[33]	
	39.7Ni-50.3Mn-10Al, (at.%)	B2	$L1_0$(+14M)					Aged at 723 K for 3.6 ks in air	~1.5	Bending	[34]	- Small two-way SME was also observed.
	40.3Ni-50.1Mn-9.6Ti, (at.%)	B2	$L1_0$					Aged at 723 K for 3.6 ks in air	~0.5	Bending	[34]	- Transformation temperatures higher than 373 K; - Deformations of 3.5 % completely recovered by SME was also reported [35].
	(37.9-49.9)Ni-(54.5-42.4)Mn-(13.8-2.6)Ti	B2	8M(24R), 10M(15R), 4O(4H)	max. 808 K	max. 895 K	max. 820 K	max. 770 K	Quenched from 1173 K	~3	Compres-sion	[36] [37]	
	?											
Zr-based alloys	ZrRh compound	B2	B19'	823 K	923 K	723 K	623 K				[38] [39]	- Complete SME.
	Zr_2CuNi	$L2_1$	B19'	963 K	1063 K	883 K	783 K		~0.3	Bending	[38]	
	Zr_2CoNi		B19'?	973 K	1223 K	893 K	973 K				[38]	- Incomplete SME (only 90% of the initial strain recovered by SME).

Table A.1. *Continued*

Alloy system	Composition	Crystal structure		Transformation temperatures				Last step of the thermal history	ε_{SME}, %	Def. mode	Ref.	Observations
		Parent phase	Maretnsitic phase	A_s	A_f	M_s	M_f					
	ZrIr	B2	B19'	1163 K	1263 K	1023 K	973 K				[38]	- Incomplete SME (only 90% of the initial strain recovered by SME).
	?											
Ru-based alloys	Ru-50Ta, (at.%)	B2	monoclinic	approx. 1088 K	approx. 1393 K	approx. 1393 K	approx. 1088 K	Heat Treated at 1873 K for 144 ks and then at 1773 K for 684 ks	5	Bending	[40] [41]	- Deformation recovered by SME was measured at tensile surface of bent samples.
	Ru-50Nb, (at.%)	B2	monoclinic	approx. 1008 K	approx. 1158 K	approx. 1158 K	approx. 1008 K		4	Bending	[41]	- Deformation recovered by SME was measured at tensile surface of bent samples.
	?											
?												

Acknowledgements

The present work has been accomplished with the invaluable help of many friends. I would like to thank all of them. I would especially like to express my deep gratitude to the following:

•

Ministry of Education, Science, Sports and Culture (MONBUSHO), Japan for the chance to study at Kumamoto University;

Prof. M. Nishida for his effort to admit me to the Department of Material Science and Engineering as Ph. D. student, for his supervision of the present work, for intensive discussions and for all the things I have learned from him;

All members of the Chiba and Nishida laboratory. They have always shown interest in my work and tried to help me. Particularly, Prof. A. Chiba and Prof. Y. Morizono for many discussions, concern about my investigations and friendly advises;

Prof. K. Imamura, former professor of our laboratory, for all his help during these years and for his kind advises on preparing specimens for the tensile test;

Mr. T. Aoki (Arizona State University), former graduate student of the Prof. Nishida group for many discussions on different topics of materials science, for his help on studying electron microscopy and for his friendship;

Prof. S. Miura and Mr. M. Koushima (Sojo University, Kumamoto) for their valuable discussion and suggestions and for their help on mechanical testing;

Former and present graduate students of Chiba-Nishida laboratory, especially Dr. S. Ii., Mr. Y. Matsuoka, Mr. S. Kimura and Miss Masako Fukunaga for their help whenever was necessary;